UNIVERSITY OF CAMBRIDGE
Department of Plant Sciences

Energetics of maize C_4 physiology under light limiting conditions

Chandra Bellasio

Clare College

This dissertation is submitted for a PhD in Plant Sciences

Dedicated to Myself

Preface

This dissertation is my own work and contains nothing which is the outcome of work done in collaboration with others, except as specified in the text and acknowledgements. No part of this thesis has been submitted for qualification at any other university.

The dissertation does not exceed the word limit set by the Degree Committee for the Faculty of Biology.

Summary

C_4 plants have a biochemical carbon concentrating mechanism (CCM) that increases CO_2 concentration around Rubisco in the bundle sheath (BS). Maize CCM has two CO_2 delivery pathways to the Bundle Sheath (BS) (respectively via malate, MAL or aspartate, ASP); rates of PGA reduction, carbohydrate synthesis and PEP regeneration vary between BS and Mesophyll (M) cells. For these anatomical and biochemical complexities, C_4 plants are highly sensitive to light conditions. Under limiting light, the activity of the CCM generally decreases, causing an increase in leakiness, (Φ), the ratio of CO_2 retrodiffusing from the BS relative to C_4 carboxylation processes. This increase in Φ had been theoretically associated with a decrease in biochemical operating efficiency (expressed as ATP cost of gross assimilation, ATP / *GA*) under low light and, because a proportion of canopy photosynthesis is carried out by shaded leaves, to potential productivity losses at field scale. In C_4 leaves, because of the concentric anatomy, light reaches M cells before the deeper BS (Evans ***et al.***, 2007), and could alter the energetic partitioning balance between BS and M and potentially cause efficiency losses. In this experimental programme I investigated strategies deployed by C_4 plants to adjust operating efficiency under different illumination conditions.

Firstly, maize plants were grown under high and low light regimes (respectively HL, 600 vs LL, 100 $\mu E\ m^{-2}\ s^{-1}$). Short term acclimation of Φ was compared from isotopic discrimination (Δ), gas exchange and photochemistry using an improved modelling approach which does not suffer from elements of circularity. Long term acclimation to low light intensities brought about physiological changes which could potentially increase the operating efficiency under limiting ATP supplies.

Secondly, profiles of light penetration across a leaf were used to derive the potential ATP supply for M and BS cells induced by changing light quality. Empirical measurements of net CO_2 uptake, ATP production rate and carbon isotope discrimination were made on plants under a low light intensity. The overall conversion efficiency was not affected by light quality. A comprehensive metabolic model highlighted the importance of both CO_2 delivery pathways in maize. Further, metabolic plasticity allowed the balancing of ATP and NADPH requirements between BS and M.

Finally, I tested the hypothesis that plants can modify their physiology so as to reach a status of higher operating efficiency when exposed to high light ***and then*** to low light, so as to mimic the transition which leaves undergo when shaded by newly emerging leaves in a crop canopy. Plants were grown under high light and low light for three weeks, ***then***, HL plants were transferred to low light for a further three weeks. Re-acclimation was very effective in reducing ATP cost of ***net*** assimilation under low light intensities. In addition, the hyperbolic leakiness increase observed under low light intensities was not associated to operating efficiency loss.

Overall, in the three experimental Chapters I showed compelling theoretical and empirical evidence proving the hypothesis that C_4 plants deal with low light conditions and with different light qualities without losing operating efficiency.

Table of Contents

List of Tables

List of Figures

List of acronyms, symbols and abbreviations*

Symbol	Definition	Units
A	Net assimilation	µmol m^{-2} s^{-1}
AB	Absorbed light	
AB BS / M	Partitioning of absorbed light	dimensionless
ALA	Alanine	
ASP	Aspartate	
ATP	Adenosine 5’ triphosphate	
ATP / GA	Predicted ATP demand for gross assimilation, i.e. predicted biochemical operating efficiency	µmol m^{-2} s^{-1}
ATP_{BS}	ATP demand in BS	µmol m^{-2} s^{-1}
ATP_{M}	ATP demand in M	µmol m^{-2} s^{-1}
B	Blue	
BS	Bundle sheath	
C_{BS}	CO_2 concentration in BS	µmol mol^{-1}
C_{BS}	CO_2 concentration in BS	µmol mol^{-1}
CCM	Carbon concentrating mechanism	
CEF	Cyclic electron flow	
C_i	CO_2 concentration in the intercellular spaces as calculated by the IRGA.	µmol mol^{-1}
C_M	CO_2 concentration in the mesophyll $C_M = C_i - \frac{A}{g_M}$	µmol mol^{-1}
DHAP	Dihydroxyacetone phosphate	
ETR	Electron transport rate	µmol m^{-2} s^{-1}
G3P	glyceraldehyde 3-phosphate	
G	Green	
GA	Gross assimilation ($A + R_{LIGHT}$)	µmol m^{-2} s^{-1}
g_{BS}	Bundle sheath conductance to CO_2	mol m^2 s^{-1}
GLA	Glycolic acid	
g_M	Mesophyll conductance to CO_2	mol m^2 s^{-1} bar^{-1}
g_s	Stomatal conductance to CO_2	mol m^2 s^{-1}
IRGA	Infra-red gas analyzer	
IVD	Inter veinal distance	µm
J_{ATP}	Total ATP production rate	µmol m^{-2} s^{-1}
J_{ATP} / A	ATP production rate relative to net assimilation	dimensionless
J_{ATP} / GA	ATP production rate relative to gross assimilation	dimensionless
J_{ATPBS}	ATP production rate in BS	µmol m^{-2} s^{-1}
J_{ATPM}	ATP production rate in M	µmol m^{-2} s^{-1}
J_{MOD}	Modelled ATP production rate	µmol m^{-2} s^{-1}

LEF	Linear electron flow	
LCP	Light compensation point	µE m^{-2} s^{-1}
M	Mesophyll	
MAL	Malic acid	
MDH	Malate dehydrogenase	
MDH_{BS}	Malate dehydrogenase reaction rate in BS	µmol m^{-2} s^{-1}
MDH_{M}	Malate dehydrogenase reaction rate in M	µmol m^{-2} s^{-1}
ME	Malic enzyme	
ME	Malic enzyme reaction rate	µmol m^{-2} s^{-1}
NADPH	Nicotinamide adenine dinucleotide phosphate	
$NADPH_{BS}$	NADPH demand in BS	µmol m^{-2} s^{-1}
$NADPH_{TOT}$	Total NADPH demand	µmol m^{-2} s^{-1}
OAA	Oxaloacetic acid	
O_{BS}	O_2 mol fraction in the bundle sheath cells (in air at equilibrium)	µmol mol^{-1}
O_{M}	O_2 mol fraction in the mesophyll cells (in air at equilibrium)	µmol mol^{-1}
PAR	Photosynthetically active radiation	µE m^{-2} s^{-1}
PEP	Phosphoenolpyruvate	
PEPC	Phosphoenolpyruvate carboxylase	
PEPCK	Phosphoenolpyruvate carboxykinase	
PEPCK	PEPCK reaction rate	µmol m^{-2} s^{-1}
PGA	3-phosphoglyceric acid	
PGA	3-phosphoglyceric acid	
PGLA	2-phosphoglycolic acid	
PPDK	Pyruvate phosphate dikinase	
PPDK	PPDK reaction rate	µmol m^{-2} s^{-1}
PR	PGA reduction	
PR_{BS}	PGA reduction rate in BS	µmol m^{-2} s^{-1}
PR_{M}	PGA reduction rate in M	µmol m^{-2} s^{-1}
PSI	Photosystem I	
PSII	Photosystem II	
PYR	Pyruvic acid	
R	Red	
RB	Red-Blue	
R_{BS}	Respiration in the light in BS	µmol m^{-2} s^{-1}
RGB	Red-Green-Blue	
R_{LIGHT}	Respiration in the light	µmol m^{-2} s^{-1}
R_{LIGHT}	Respiration in the light	µmol m^{-2} s^{-1}
R_{M}	Mesophyll non photorespiratory CO_2 production in the light R_M = 0.5 R_{LIGHT}	µmol m^{-2} s^{-1}
RPP	Reductive pentose phosphate	
Rubisco	Ribulose bisphosphate carboxylase oxygenase	
RuBP	Ribulose-1,5-bisphosphate	
RuP	Ribulose-5-phosphate	
s	Fractionation during leakage of CO_2 out of the bundle sheath cells	‰

SS	Carbohydrate synthesis	
SS_{BS}	Carbohydrate synthesis rate in BS	μmol m^{-2} s^{-1}
SS_M	Carbohydrate synthesis rate in M	μmol m^{-2} s^{-1}
SS_{TOT}	Total Carbohydrate synthesis rate	μmol m^{-2} s^{-1}
t	Ternary effects	‰
T	Transamination	
T	Transamination rate	μmol m^{-2} s^{-1}
V_C	Rubisco carboxylation rate	μmol m^{-2} s^{-1}
V_O	Rubisco oxygenation rate	μmol m^{-2} s^{-1}
V_P	PEP Carboxylation rate	
x	J_{ATP} partitioning factor between C_4 activity (V_P) and C_3 activity V_C+V_O (RPP pathway and photerespiratory cycle)	dimensionless
$Y(II)$	Yield of photosystem II	dimensionless
α	Fraction of PSII active in BS cells	dimensionless
γ^*	Half of the reciprocal of the Rubisco specificity	dimensionless
Δ	^{13}C Isotopic discrimination	‰
Δ	^{13}C Isotopic discrimination	‰
$\delta^{13}C$	^{13}C isotopic composition relative to Pee dee belemnite	‰
Δ_{MOD}	Modelled carbon Isotope discrimination against ^{13}C	‰
Δ_{OBS}	Observed carbon Isotope discrimination against ^{13}C	‰
Φ	Leakiness	dimensionless
Φ_{id}	Leakiness estimated with the isotope method including respiratory and photorespiratory fractionation and calculating C_{BS} Eqn 2.3 (Ubierna *et al.*, 2011)	dimensionless
Φ_{MOD}	Leakiness estimated with the C_4 light limited photosynthesis equations Eqn 2.11	dimensionless

* Values for variables and references are given in each experimental Chapter.

1 General Introduction

1.1 Reading guide

This dissertation is formed of five Chapters. The first is a general introduction, presents the general background, and the rationale for the research I have conducted. The central Chapters (2, 3, and 4) have been written specifically to be published in peer-review journals, therefore they are generally self-contained, including specific introduction, material and methods, results, discussion, figures and tables. The last Chapter forms a synthesis of the conclusions of the research, presents wider implications (at field, ecosystem and at agro-ecosystem scale) and the outlook for possible future developments. Since the first and the last Chapters are not intended to be submitted to a journal, I offer a personal view on the motivation that oriented the overall programme of work and the future perspectives for research.

1.2 Photosynthesis and photorespiration

Photosynthesis is a process used by plants and other organisms to convert light, normally from the sun, into chemical energy that can be later released to fuel the organisms' activities. This chemical energy is stored in carbohydrate molecules, such as sugars, which are synthesized from carbon dioxide and water. Photosynthesis is arguably the most complicated process known and it is often divided in two phases: the light reactions and the dark reactions. Light reactions occur in the thylakoid membranes of the chloroplasts and use light to drive the synthesis of the high energy intermediate metabolites ATP and NADPH. Light is initially captured by pigments (chlorophyll and auxiliary pigments), which, upon absorption of a photon are excited to an excited electron state. This excited state is eventually transferred to a ‘reaction centre’ where a special pigment undergoes a primary charge separation: it donates an electron to an acceptor and subsequently restore neutrality by extracting an electron from a donor. In oxygenic organisms (such as algae and plants) these electrons are indirectly extracted from water, a reaction which produces a potentially dangerous by-product: oxygen. The electrons extracted from water are shuttled through an electron transport chain which has the twofold function of generating a chemiosmotic potential across the thylakoid membrane (which drives ATP photophosphorylation) and using the electrons to regenerate a strong reductant: NADPH.

In the dark reactions (which, in spite of the name, also occur only in the light), the high-energy intermediate metabolites are converted into carbohydrates which are storable and transportable and are used to sustain the organism. This process starts with the fixation of CO_2, whereby carbon dioxide combines with a five-carbon sugar, ribulose 1,5-bisphosphate (RuBP), to yield two molecules of a three-carbon compound, 3-phosphoglycerate (PGA). This reaction is catalysed by an enzyme called Ribulose bisphosphate carboxylase oxygenase (Rubisco). PGA, is then reduced to glyceraldehyde 3-phosphate (G3P) using the ATP and NADPH produced in the light reactions. Most (5 out of 6 molecules) of the G3P produced is used to regenerate RuBP so that CO_2 fixation can continue, hence forming a cyclic pathway which is called reductive pentose phosphate (RPP) pathway, for it is used for reductive assimilation and 5 carbon sugar phosphates are key intermediates. The rest of G3P is rapidly interconverted to dihydroxyacetone phosphate (DHAP), a short sugar, precursor of heavier carbohydrates (glucose, fructose, sucrose, starch, cellulose).

Chemically, the reaction between RuBP and CO_2 catalysed by Rubisco is an addition whereby RuBP is converted into an enediol, and an electron pair from the enediol attacks the electron-poor carbon of CO_2. Unfortunately, the enediol electron pair can react also with molecular oxygen (Andersson, 2008) which competes for Rubisco catalytic sites, giving rise to atmospheric oxygen fixation. The final products of this RuBP oxygenation are one PGA molecule and a two-carbon molecule, phosphoglycolic acid (PGLA). PGLA has no known value to the plant and is toxic if allowed to accumulate to high concentration in the cell. Plants metabolize PGLA back to PGA in a series of reactions termed the glyoxylate cycle, or the photosynthetic carbon oxidative cycle (PCO cycle). Commonly, the oxygenation of RuBP and the metabolism of PGLA to PGA are called photorespiration (Moroney ***et al.***, 2013).

In photorespiration, PGLA is converted to glycine in the peroxisomes of leaves, and the glycine is converted to serine, ammonia, and CO_2 in the mitochondria. The serine is metabolized to PGA in a reaction that consumes ATP, while the ammonia must be reassimilated using ATP and reducing power (ferredoxin or NADPH, see Table 3.5). The CO_2 produced by glycine decarboxylation can diffuse out of the cell and remix with atmospheric air and because carbohydrates are oxidised with ambient O_2 and previously fixed CO_2 is given off, this process is called photorespiration. Since energy is consumed in the

photorespiratory cycle, conditions promoting Rubisco oxygenation reduce photosynthetic capacity and efficiency (Sharkey, 1988).

1.3 Carbon concentrating mechanisms and C_4 photosynthesis

Because of the strong inhibition on Rubisco exerted by O_2, evolution favoured the rise of mechanisms that reduced Rubisco oxygenase activity. These have resulted in optimised catalytic properties (increased Rubisco specificity for CO_2 versus O_2), which I will not address in this dissertation, and in mechanisms whereby CO_2 is concentrated around Rubisco, called carbon concentrating mechanisms (CCMs), which increase the CO_2 / O_2 ratio at the catalytic site. These CCMs evolved from C_3 photosynthesis under declining ambient CO_2 and increasing transpiration demand in semi-arid environments (Griffiths *et al.*, 2013; Meyer and Griffiths, 2013; Osborne and Beerling, 2006; Osborne and Sack, 2012) and consists of structural and biochemical modifications of the ancestry C_3 photosynthesis. So called 'C_3-C_4' species operate the simplest of these mechanism, thought to be an early stages terrestrial CCM evolution (Gandin *et al.*, 2014; Lundgren *et al.*, 2014; Monson and Moore, 1989; Sage *et al.*, 2012; Schulze *et al.*, 2013). In these species the leaf parenchyma is organised in two concentric layers of cells centred on vascular bundles [this anatomy is called 'Kranz', Figure 1.1, (Sage *et al.*, 2014)]: an outer layer called mesophyll (M) and an inner layer called bundle sheath (BS). BS cells constitute a small fraction of the total leaf volume and are generally isolated from the surroundings by the deposition of a gas tight suberized cell wall. Further, glycine decarboxylase (GDC) is exclusively localised within BS mitochondria. This biochemical compartmentalization is generally associated with numerous mitochondria, peroxisomes and chloroplasts arranged in a centripetal position within the BS cells. This allows the operation of a 'C_2 cycle' where glycolate is shuttled from the mesophyll to the BS cells and decarboxylated via GDC to increase the refixation of photorespired CO_2 (Brown and Hattersley, 1989; Rawsthorne, 1992; Rawsthorne *et al.*, 1988). The operation of the C_2 cycle brings considerable advantages as, compared to C_3 plants, the C_3-C_4 species have reduced rates of photorespiration and lower CO_2 compensation points (Γ), particularly under high temperatures (Lundgren *et al.*, 2014; Monson and Moore, 1989).

A more complex type of CCM involves a dedicated biochemical suite operating purposely to increase CO_2 around Rubisco in BS: C_4 photosynthesis. CO_2 concentration in BS results

from the establishment of a carboxylation / decarboxylation cycle, so that CO_2 is initially fixed into a four-carbon (C_4) organic acid in M and then shuttled to BS where Rubisco is localized [Figure 1.2, for an introductory overview see (Sage *et al.*, 2013) details are reported in 1.5 and in Chapter 3]. The released CO_2 accumulates to concentrations that are 10- to 20-fold greater than those present within the chloroplasts of C_3 plants, thereby suppressing the oxygenation reaction of Rubisco and allowing it to operate near CO_2 saturation (von Caemmerer and Furbank, 2003) even in hot conditions of low atmospheric CO_2 (Pearcy and Ehleringer, 1984). C_4 Rubisco catalytic properties are different from C_3, Rubisco has lower affinity for CO_2 and therefore higher V_{CMAX}. As a consequence, high photosynthetic rates can be sustained by a comparatively low amount of Rubisco, and a lower investment in leaf protein is required (Sage, 2002).

Figure 1.1. Cross section of a maize leaf

This drawing schematises a section of a maize leaf. Between the upper epidermis (yellow, some stomata are present but not shown in this picture) and the lower epidermis (yellow, with stomata in blue), there is the photosynthetic leaf parenchyma and the vascular bundles. The parenchyma is organized concentrically around the bundle and differentiated in mesophyll cells (shown in blue-green), and bundle sheath cells (shown in purple). This concentric anatomy is called 'Kranz'. Courtesy of Cambridge University Plant Sciences Department.

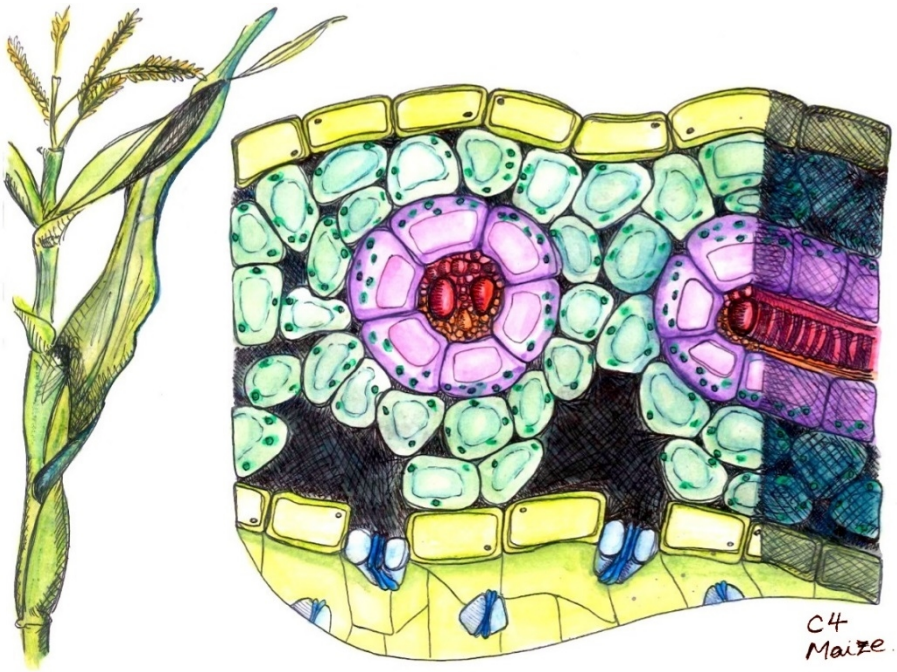

Figure 1.2. Simplified Biochemistry of C_4 photosynthesis

Micrograph showing a magnification of a NADP-ME C_4 plant. CO_2 enters the stomata and reaches mesophyll (M) cells where it is initially fixed by PEP carboxylase (P) into C_4 intermediates (here simplified to 'malate'). Malate diffuses to bundle sheath (BS) cells where it is decarboxylated to relase the initially fixed CO_2. This operation results in an increased CO_2 concentration in BS also because the BS volume is small compared to M. Rubisco (R) is located in BS and operates under CO_2 saturation. The PGA produced by Rubisco is reduced to carbohydrates (C_3 cycle, which occurs in BS and M, but simplified here) which are ultimately uploaded in the phloem. For a detailed description see the scheme in Figure 3.1. From (Sage *et al.*, 2013).

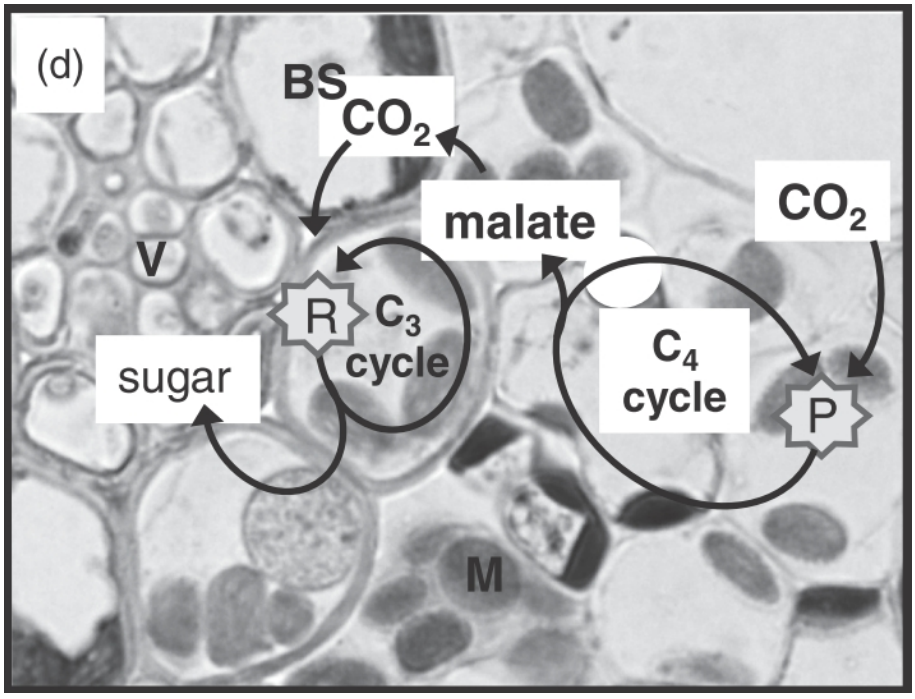

1.4 Agronomic and ecological importance of C_4 plants

C_4 plants are widely noted for the high productive potential e.g. (Sheehy, 2007). This is reflected in their contribution to global primary productivity: despite representing only 3% of the world terrestrial plant species [about 7500 (Sage *et al.*, 2011)] C_4 plants collectively account for close to a fourth of the global primary productivity on the terrestrial Earth. They dominate tropical and subtropical grasslands and savannah and are important elements in temperate grasslands (Beerling and Osborne, 2006). Half of the C_4 species are grasses, a fourth are sedges, and the other quarter are various eudicot species. Most tropical forage grasses and sedges are C_4, and most of the new bioenergy crops under development for warm climates are C_4 species e.g. (Petrasovits *et al.*, 2012; Sheehy, 2007). C_4 plants also make up the world's worst weeds (Brown, 1999). There are, however, no canopy-forming C_4 trees, such that the forests and woodlands of the Earth consist largely of C_3 species (Sage et al. 1999). As a result, in warmer environments where C_4 photosynthesis is advantageous, the major C_3 to C_4 interaction is between C_3 woodlands and C_4 grasslands (Beerling and Berner, 2005; Beerling and Osborne, 2006). The failure of the C_4 pathway to occur in canopy-forming trees has considerable consequences for the biomes across the warmer regions of the planet and has been linked to the C_4 susceptibility to light conditions [see Paragraph 1.7 below and (Sage, 2014)].

From an agronomic point of view, C_4 photosynthesis leads to high productive potential in crop species. Notable C_4 species include maize, sugarcane, sorghum, and millet. Under ideal conditions, C_4 agronomic species exhibit maximum growth rates that are 30 to 60% greater than C_3 species (Monteith, 1978). All species at low latitude producing over 60 tonnes dry biomass ha^{-1} per year are C_4 plants, while peak yields of C_3 species are generally below 40 dry tonnes ha^{-1} $year^{-1}$ (Snaydon, 1991).

1.5 Evolution of C_4 photosynthesis

The C_4 pathway is a very complex syndrome encompassing particular biochemical and anatomical traits and dedicated gene regulation. Several intermediate stages have been observed in nature, A likely path of C_4 evolution was recently hypothesized (Christin *et al.*, 2013; Sage *et al.*, 2012), and examples of the occurrence of C_4 traits in different taxa was presented. These included gene duplications, C_4 anatomical traits, the enhanced presence of

bundle sheath organelles, the specific expression of photorespiratory enzymes in the bundle sheath cells, and increased expression of PEPC in mesophyll. The occurrence in nature of these intermediates suggests that each of these traits conferred specific evolutionary advantage under particular environmental conditions. For instance, segregation of glycine decarboxylase in the BS conferred an advantage in photorespiratory conditions because it results in a photorespiratory CO_2 pump (also known as C_2 photosynthesis, see Paragraphs 1.2 and 1.3) which concentrates CO_2 in the BS (Sage *et al.*, 2012; Schulze *et al.*, 2013).

It was recently pointed out that the key step in C_4 evolution was the acquisition of C_4 anatomical traits, that are, the reduction in the distance between BS (Christin *et al.*, 2013), and an increase in the fraction of BS volume (Griffiths *et al.*, 2013). These large BS cells conferred key advantages in environmental conditions characterized by alternation of arid and humid seasons (Leegood, 2008). These include: i) the capacity to reduce water flow to the leaf in response to reduced water availability, effectively preventing cavitation. This function appear to be mediated by aquaporins that can open and close in response to various local and systemic signals (Pantin *et al.*, 2013); ii) water storage (Griffiths *et al.*, 2013); and iii) water excretion (guttation). Guttation is of critical importance to avoid the saturation of the parenchyma whilst sustaining a flow of nutrients from the roots in conditions of water excess (Feild *et al.*, 2005; Griffiths *et al.*, 2013). Despite this complexity, C_4 photosynthesis evolved more than 62 times independently in distantly related groups of flowering plants (Sage *et al.*, 2011). These recurrent C_4 origins were probably facilitated by the existence in most C_3 plants of metabolic modules suitable for the C_4 pathway and could be recruited for this new function through rearrangements of regulatory elements (Brown *et al.*, 2011; Hibberd and Quick, 2002).

1.6 Biochemical diversity of C_4 photosynthesis

Because of the polyphyletic origins of C_4 photosynthesis, substantial variation can be expected, although, surprisingly, there is recurrent emergence of similar biochemical patterns. In this way all C_4 species have been traditionally grouped in only three subtypes, according to the decarboxylating enzyme with the higher activity: the NADP-ME, the NAD-ME and the PEPCK subtypes (Hatch, 1987). Recently, it has been argued that the boundaries between the three subtypes may be much less defined than it was previously thought (Furbank, 2011;

Wang *et al.*, 2014a; Wang *et al.*, 2014b). Congruently, a meta-analysis of different comparative transcriptomics experiments in monocots and dicots has recently suggested a reduction from three to two C_4 photosynthetic subtypes (NADP-ME and NAD-ME) (Bräutigam *et al.*, 2011; Gowik *et al.*, 2011; John *et al.*, 2014; Wang *et al.*, 2014a). Within these two subtypes PEPCK may increasingly contribute to decarboxylation (Wang *et al.*, 2014a; Wang *et al.*, 2014b). For instance in NADP-ME subgroups, PEPCK is virtually nil in sorghum, intermediate in *Flaveria* and higher in maize (Furbank, 2011; Gutierrez *et al.*, 1974; Wang *et al.*, 2014a; Wang *et al.*, 2014b). A similar progression was proposed for the NAD-ME subtype with *Cleome* about midway along the progression (Wang *et al.*, 2014a; Wang *et al.*, 2014b). However, definitive justification for the role of PEPCK in C_4 photosynthesis has not been shown (a hypothesis is presented in Chapter 3).

This study focuses on the NADP-ME subtype, which includes all C_4 crops of primary economic importance (such as maize, sugarcane, sorghum), and in particular on maize, the world leading grain production crop (FAO, 2012).

1.7 Maize C_4 photosynthesis

Maize operates NADP-ME C_4 photosynthesis, which is a complex biochemical and anatomical modification of C_3 photosynthesis. At the anatomical level, mesophyll (M) cells surround bundle sheath (BS) cells forming two circular concentric layers of cells arranged around the vascular bundle (the so-called 'Kranz' anatomy, Figure 1.1). The two compartments are linked by plasmodesmata to allow the exchange of diffusive metabolites. At a biochemical level (Figure 1.2 and the overall scheme in Figure 3.1), two distinct carboxylation reactions occur: a first carboxylation occurs in the cytosol of M cells and a second carboxylation reaction in the BS cells. The first carboxylation reaction is mediated by PEP carboxylase (PEPC) which converts bicarbonate and PEP to form a C_4 compound, oxaloacetate (OAA). As opposed to the mechanism of action of Rubisco, that of PEPC does not give rise to auxiliary reactions, in fact the substrate of PEPC is bicarbonate and not CO_2 and no reaction intermediate state tends to react with molecular O_2. The product OAA is unstable and tends to decompose in pyruvate and CO_2, therefore it is stabilised and modified either by reduction to malate (MAL) or transamination to aspartate (ASP) [(Furbank, 2011; Pick *et al.*, 2011) and references therein]. Unfortunately, no suitable cyclic pathway can

utilize directly these C_4 intermediates to produce a stable photosynthetic product which the plant can use for storage and growth. For this reason the initially fixed CO_2 is then released and delivered to Rubisco. MAL or ASP are small molecules that diffuse through plasmodesmata and reach the BS, then they may follow different pathways, which may involve transamination, or reduction and are still to be completely clarified, probably also for a grat plasticity in the engagement of different pathways (Eprintsev ***et al.***, 2011; Ivanishchev and Kurganov, 1992). These will ultimately result in the release of CO_2. The decarboxylation of the C_4 intermediate is localized in a small compartment (BS), and results in a substantial increase of CO_2 concentration in BS, which can reach up to 3000 μmol / mol (von Caemmerer and Furbank, 2003). Rubisco is exclusively expressed in the BS, so as to benefit from the increased CO_2 concentration (see Paragraph 1.2 Photosynthesis and photorespiration). For this reason, the combined biochemical activity of M and BS is also referred as a biochemical carbon concentrating mechanism (CCM). C_4 intermediates are decarboxylated either by malic enzyme or by PEP carboxykinase (PEPCK, Figure 3.1).

The high CO_2 concentration in BS has a great influence on the carboxylation reaction catalysed by Rubisco. C_4 Rubisco is exclusively expressed in BS and has higher turnover rate and lower specificity for CO_2 than the homologous C_3 enzyme (Sage, 2002). Because of the high CO_2 concentration in BS C_4 Rubisco is generally CO_2-saturated, therefore it catalyses very low oxygenation rates. CO_2 is then fixed into a C_3 acid, phosphoglyceric acid (PGA). PGA can be utilized by a cyclic pathway (the reductive pentose phosphate, RPP pathway) which is unique because it produces sugar, which is the 'fuel' of metabolism (used for storage, maintenance and growth) and, at the same time, it regenerates Rubisco substrate, RuBP.

Following the RPP pathway, which is the same as for C_3 plants, PGA is reduced to triose phosphate (DHAP) which is in turn used to regenerate RuBP. The peculiarity in C_4 plants is the spatial localization of the biochemical reactions: PGA reduction is mainly located in M, so as to benefit from the NADPH produced in the light reactions at thylakoid level, while RuBP regeneration is exclusively located in BS (Majeran ***et al.***, 2005; Majeran and van Wijk, 2009). For this reason a substantial fraction of the PGA diffuses to M, it enters the RPP pathway in M and once converted to DHAP, it diffuses back to BS (a smaller fraction can supply carbohydrate synthesis in BS) [Chapter 3, see also (Wang ***et al.***, 2014a; Wang ***et al.***,

2014b). This flux is an exchange of C_3 intermediates of the RPP pathway and should not be confused with the exchange of metabolites resulting from CCM activity. However, both BS and M appear to have the enzymes to catalyse substantial rates of PGA reduction, carbohydrate synthesis and PEP recycling (Friso *et al.*, 2010; Kanai and Edwards, 1999; Majeran *et al.*, 2010). A satisfactory explanation of the reason underpinning the extensive overlap between M and BS functions and the two different decarboxylase systems had not been presented (I will provide extensive justification in Chapter 3). Further, the complexity of C_4 metabolism has been extensively simplified when describing C_4 photosynthesis. For instance, although ASP metabolism has long known to occur in maize, a common simplification neglects ASP metabolism in NADP-ME C_4 subtype [e.g. compare Figure 3 and Table II in (Hatch, 1987)]. Another common assumption involves a fixed proportion of PGA (50%) exported for reduction in M e.g. (Laisk and Edwards, 2009; Laisk and Edwards, 2000). Apart from the educational purposes, these simplifications were functional to develop working models of C_4 photosynthesis. In Chapter 3 definitive justification of the biochemical complexity of C_4 photosynthesis will be presented, and the metabolic plasticity will be directly related to efficiency of C_4 photosynthesis.

1.8 C_4 susceptibility to shade and light spectral quality

There are anatomical, biochemical and ecological constraints which make C_4 photosynthesis, as compared to C_3, more prone to shade, and limitations associated with light spectral quality. Concerning light quantity, biochemically, C_4 photosynthesis is energetically more expensive than C_3 photosynthesis in the absence of photorespiration, requiring 5 ATP per CO_2 assimilated relative to 3 ATP per CO_2 in C_3 species; however, when photorespiration occurs in C_3 species, the energy cost of CO_2 fixation can be greater, depending on factors such as atmospheric CO_2 supply, temperature and the C_4 subtype (Ehleringer and Pearcy, 1983). Further, the two main carboxylating enzymes are generally not CO_2 limited under ambient conditions, because Rubisco operates in a CO_2-saturated compartment whereas PEPC is abundant and has a very low Km. As a consequence, C_4 biochemistry is generally limited by ATP and NADPH supply produced in light reactions, and hence C_4 photosynthesis is generally limited by light (von Caemmerer, 2000). This is thought to explain the preferential C_4 distribution in open environments, with a higher light availability, a relative

lack of C_4 species in shaded environments, and why the C_4 pathway never evolved into canopy-forming trees (Sage, 2014). These hypotheses were backed by an observed increase in BS leakiness (which was thought to reflect a decreased efficiency of C_4 biochemistry see Paragraph 1.10 and Chapter 4) observed both at leaf and field level under low light intensities (Kromdijk, 2010; Kromdijk *et al.*, 2010; Kromdijk *et al.*, 2008; Pengelly *et al.*, 2010; Tazoe *et al.*, 2006; Ubierna *et al.*, 2011), which was taken in support of the idea that C_4 plants perform poorly under low light intensity. I will show in Chapter 2 and 4 that C_4 plants have effective mechanisms to acclimate to low light intensity thereby reaching a status of biochemical efficiency comparable to that of high-light plants.

Concerning changing light spectral quality, a minor effect on photosynthetic efficiency is exerted by the different relative quantum yield of PSI vs. PSII in harvesting different wavelengths. This imbalance is generally countered by adjusting the relative rate of cyclic electron flow, both in C_3 and C_4 plants (Kramer and Evans, 2011). A stronger limitation depends on the preferential absorption light by leaf pigments (blue light is absorbed more strongly than red or green). This involves that the light penetration profile within the leaf will differ under changing light qualities (Brodersen and Vogelmann, 2010; Gorton *et al.*, 2010; Vogelmann, 1989; Vogelmann and Evans, 2002; Vogelmann *et al.*, 1996). In C_3 plants light quality mainly pose an issue of energy distribution within the leaf. Under blue light superficial chloroplasts receive more excitation pressure (and PSII yield is therefore strongly quenched) while lower chloroplast are mostly entirely shaded (Han and Vogelmann, 1999; Terashima *et al.*, 2009; Vogelmann *et al.*, 1996). C_3 plants counteract by moving chloroplasts so as to regulate light penetration in the mesophyll (Banaś *et al.*, 2012; Wada, 2013) and modulate PSII quenching. By doing so they regulate the availability of ATP and NADPH produced in light reactions to match the demand exerted by assimilation. It is worth noting that biochemical capacity also follows a decreasing pattern down the leaf profile (Terashima *et al.*, 2009). However, because the NADPH and ATP sinks are localised within the C_3 chloroplasts, supply and demand are always locally balanced and optimisation to changing light quality is generally a matter of redistributing quantum yield in the leaf profile. In C_4 plants light quality poses completely different rebalancing pressures. In C_4 leaves, because of the concentric anatomy, light reaches M cells before the deeper BS (Evans *et al.*, 2007), and different profiles of light penetration alter the balance between light harvesting and energetic

partitioning between BS and M. Theoretical considerations have associated this imbalance to potential C_4 efficiency losses (Evans *et al.*, 2007). Because assimilation is a shared process between M and BS, these unbalances cannot be countered locally, within the single C_4 chloroplasts. Sun and colleagues observed that light quality does not alter C_4 efficiency under high light intensities. Following this observation, in Chapter 3, I hypothesized that C_4 plants have a complex suite of biochemical mechanisms which adjust the demand of ATP and NADPH in BS and M, to counter the availability under fluctuating light quality. I then modelled the C_4 biochemistry and the complex metabolite exchange between BS and M. Finally I tested the model and parameterized it under low light, which, for what said above are highly relevant for C_4 biochemical limitations.

1.9 A model for C_4 photosynthesis

To capture the complex C_4 physiology, several models of C_4 photosynthesis have been proposed (Berry and Farquhar, 1978; Laisk and Edwards, 2009; Laisk and Edwards, 2000; von Caemmerer, 2000). The earlier approaches were developed into the von Caemmerer (2000) C_4 model. In particular, the associated light limited equations (referred subsequently as the 'C_4 model'), are extensively used in this research and are worth introducing here. The C_4 model is based on the assumption that under limiting light, C_4 photosynthesis is solely limited by the total quantity of ATP available (see also Paragraph 1.8). The leaf-level total ATP production rate J_{ATP} is therefore used as a proxy to derive other physiological quantities, hence it has critical importance. A first, completely model based approach, uses the C_4 model to simulate J_{ATP} (in this case the simulated, or modelled J_{ATP} is referred as J_{MOD}) and then uses J_{MOD} to simulate the other quantities of the C_4 model (Ubierna *et al.*, 2013). This approach is evidently underconstrained, nevertheless it has proved useful in certain conditions (Ubierna *et al.*, 2013).

To better constraint these estimates to real leaf-level characteristics, J_{ATP} is generally related to the total electron transport rate (ETR in this work, also referred as J). ETR has traditionally been calculated from PSII yield, leaf absorptance and two other parameters (see '1.7.2 leaf level ATP production rate'). ETR is then used to calculate J_{ATP} by means of an assumed stoichiometric conversion coefficient (von Caemmerer, 2000). This approach has been extensively used, also in this lab, e.g. (Kromdijk *et al.*, 2010), however, the

parameterization requires assumptions and relies on difficult measurements, which by necessity must be undertaken on separate leaves. The values of J_{ATP} derived with this traditional leaf absorptance method are therefore not mirroring the actual portion on which the ecophysiology is characterized, and different methods, based on the optical characteristics of the leaf being measured have been developed [for critical assessment (Martins ***et al.***, 2013)].

Here, I used one of these approaches, which was firstly proposed by Yin and colleagues (Yin and Struik, 2009; Yin and Struik, 2010; Yin ***et al.***, 2011b), and uses gas exchange under non photorespiratory conditions and chlorophyll fluorescence to calibrate the relationship between photosystem II yield and J_{ATP} [for critical assessment (Martins ***et al.***, 2013)]. J_{ATP} is therefore derived from gas exchange measurements under low O_2 (and high CO_2), under the assumption that in these conditions photorespiration and leakiness are minimal and predictable, and the ATP requirement for assimilation is close to the theoretical minimum. The relationship between ETR and $J_{ATPLOWO2}$ derived under non photorespiratory conditions is used to calculate the actual J_{ATP} under ambient O_2. The method is highly suitable to parameterize the C_4 model as it derives ATP under the same model assumptions: the value for J_{ATP} represents the ATP available for photosynthesis and it is inherently unaffected by ATP consumption by alternative sinks. Furthermore J_{ATP} is measured concurrently with gas trapping and gas exchange measurements, notably on the same portion of the leaf. Note that this leaf-level J_{ATP} represents the total ATP available for photosynthesis, which includes the conjoint photophosphorylation in M and BS chloroplasts. This is sufficient to parameterize the C_4 model, which does not require knowing where J_{ATP} is produced. In Chapter 3 the partitioning of ATP production will be predicted for the first time, using an optical model.

Once a value for J_{ATP} is available, the C_4 model pragmatically splits it between ATP consumed by the C_4 cycle and ATP consumed by the rest of metabolism (also referred to as C_3 activity, including PGA reduction, RuBP regeneration and glycolate recycling). It is very important to note that the C_4 model does not locate these metabolic activities in a specific cellular compartment, since no physical separation between BS and M is accounted for.

The ATP consumed by the C_4 cycle supplies the PEP regenerating activity of pyruvate-phosphate dikinase (PPDK). The PEP regeneration rate, at steady state, equals the activity of PEPC (V_P) and the rate of malate diffusion to BS, hence V_P corresponds to the rate of CO_2

delivery to BS. The CO_2 delivered to BS is fixed by Rubisco at a rate depending on the CO_2 concentration in BS, and of the kinetic properties of Rubisco. The Rubisco carboxylation rate (V_C), and Rubisco oxygenation rate (V_O) are calculated using the equations of the C_3 model of photosynthesis. In particular, V_C and V_O are constrained with the total ATP available for C_3 activity, described above, using the equations derived for *J*-limited C_3 photosynthesis (von Caemmerer, 2013). Furthermore, some CO_2 may diffuse back to M. The rate of CO_2 retrodiffusion (leak rate, see 1.6.1) is dependent on the gradient of CO_2 concentration between BS and M, and on the permeability of BS to retrodiffusion (bundle sheath conductance to CO_2, g_{BS}). Finally, at steady state, all the CO_2 available in BS (delivered by the CCM + produced in BS by respiration + photorespiration) is either fixed by Rubisco, or it retrodiffuses.

Unfortunately, to date, there is no method available to distinguish experimentally the CO_2 concentration in the BS (C_{BS}), bundle sheath conductance (g_{BS}) and the partitioning factor between C_4 and C_3 activity (x), therefore the C_4 model is underconstrained. To overcome this issue, x is generally assumed (x = 0.4), while g_{BS} is generally obtained by curve fitting and C_{BS} results from resolving the model given all the other constraints.

1.10 Leakage and Leakiness

1.10.1 The phenomenon of CO_2 leakage

As described above, carbon fixation in C_4 photosynthesis involves a two-step carboxylation. PEP carboxylase (PEPC), the primary carboxylating enzyme, fixes HCO_3^- into a C_4 intermediate, which diffuses to BS and is subsequently decarboxylated. The released CO_2 supplies Rubisco activity (Figure 3.1). If BS cells were absolutely gas tight, the CO_2 produced from decarboxylation would be entirely fixed by Rubisco, instead, a fraction of CO_2 leaks back to mesophyll (c. 15-30%). This retrodiffusion of CO_2 (leakage) is an inherent and inevitable feature of the CCM and it is imputable to the existence of plasmodesmata, connecting BS and M cells. This reliance on plasmodesmata may appear counterproductive, but it is part of a grand design recurrent in all lineages of C_4 photosynthesis and, hence, it has to be associated to biochemical advantages. Firstly, if the C_4 intermediates were to be translocated from M to BS using membrane transporters, C_4 intermediates would follow an apoplastic pathway, and a large area of adjacent plasmalemma would be needed to

compensate for the diffusive resistance brought about by the cell wall. Since membranes are permeable to CO_2, this strategy would probably be effective only if the C_4 intermediates were decarboxylated in a very small (intra-chloroplast) compartment, where Rubisco would need to be compartmentalized. Furthermore, efficient mechanisms to prevent CO_2 from escaping that compartment (and reach the CO_2-permeable plasmalemma) would need to be in place, as, for instance, in algal lineages (Meyer and Griffiths, 2013), to prevent high leak rates (Stutz *et al.*, 2014).

In contrast, the apoplastic pathway can be blocked by the deposition of a suberin lamellae between M and BS cells (it may not be present in NAD-ME species). This limits the diffusion of CO_2 through the plasmalemma but also makes impossible transmembrane transport. With this solution, C_4 intermediates are forcedly transported symplastically through plasmodesmata. The C_4 metabolite flux has traditionally been considered to be mediated by simple diffusion (Weiner *et al.*, 1988), but some calculations suggest that it might be a more complex phenomena (Sowinski *et al.*, 2008). In an evolutionary perspective, the symplastic pathway has been chosen probably because the symplastic retrodiffusion is perhaps less severe than the retrodiffusion through plasmalemma. I propose that, in addition, the symplastic pathway can sustain higher photosynthetic rates. In fact the symplastic metabolite diffusion rate does not saturate, as opposed to the typical Michaelis-Menten type saturation of transmembrane carriers. Furthermore, symplastic transport does not require ultrastructural rearrangements within the chloroplast to localize decarboxylation in close proximity to the active site of Rubisco and impede CO_2 to escape out of the chloroplast. However, if symplastic transport is effective in limiting the CO_2 retrodiffusion through membranes, it offers wide open plasmodesmata through which CO_2 can escape BS. This phenomenon is known as CO_2 leakage, and it is expressed as leak rate (L).

The CO_2 leak rate can be estimated using the C_4 model described above and it has been experimentally determined using radioactively labelled C_4 intermediates. For instance, Hatch et al. (1995) labelled the pool of organic acids by supplying leaves with $^{14}CO_2$ and then measured the release of the radioactive isotope when the leaves were supplied with normal air.

1.10.2 Leakiness, Φ

The quantity 'leakiness' is defined as the leak rate (L) relative to PEP carboxylation rate (V_P). This quantity was coined by Farquhar in the description of carbon isotope discrimination (Farquhar, 1983) as it could be resolved from the leaf-level ^{13}C isotope discrimination during photosynthesis (Kromdijk *et al.*, 2014; von Caemmerer, 2013). Isotopic discrimination is a valid tool to study C_4 photosynthesis: since it is non-invasive and relatively straightforward (compared to radioactive labelling), it has been extensively used, also in this lab (Kromdijk, 2010; Kromdijk *et al.*, 2010; Kromdijk *et al.*, 2008). For the importance in this research, the ^{13}C technique merits a brief description here [but see also the recent reviews (Cernusak *et al.*, 2013; Kromdijk *et al.*, 2014; von Caemmerer *et al.*, 2014)].

^{12}C and ^{13}C are the two stable isotopes of carbon, occurring in a natural proportion of approximately 99:1. ^{13}C is heavier: it has lower diffusion and reaction rates but it forms slightly stronger bonds. For this reason, reactions which are far from the thermodynamic equilibrium tend to favour the lighter isotope while reactions that proceed to equilibrium tend to favour the heavier one. It follows that, during the photosynthetic CO_2 uptake, from atmosphere to PGA, each process slightly modifies the natural ^{13}C / ^{12}C ratio (Griffiths, 1998). This modification of the isotopic composition is called discrimination (Δ). Both enzyme-mediated-processes and non-catalysed processes discriminate. For example, the inherent discrimination by Rubisco is high (≈ 30 ‰) (PGA contains less ^{13}C than substrate CO_2), while the combined hydration of CO_2 and carboxylation by PEPC discriminates -5.7 ‰ at 25°C (malate contains more ^{13}C than the substrate HCO_3^-). As a result, the ^{13}C / ^{12}C ratio not only is slightly altered, compared to atmospheric CO_2, but the magnitude of alteration is a 'fingerprint' that allows the magnitude of the different processes to be calculated.

This 'fingerprint' also includes the signature of leakiness. In a closed system, Rubisco would express little discrimination, but if the BS allows back-diffusion (leakiness), then Rubisco expresses a proportionally high level of the inherent fractionation. Most C_4 plants allow 20 – 30 % of CO_2 to leak from the Bundle sheath, with the isotopic composition of carbon fixed being shifted from ≈ -2 ‰ to ≈ -12 ‰. Of course, any discrimination against ^{13}C means that CO_2 passing over the leaf will become proportionally enriched in $^{13}CO_2$. By collecting the CO_2 in air downstream of the leaf cuvette, one can capture the 'instantaneous' discrimination being expressed by the leaf. The on-line technique is the one that uses the

smallest possible integration time (Evans *et al.*, 1986), allowing, in effect, the concurrent determination of discrimination and metabolic state through gas exchange measurements. With this technique samples of air collected before entering the leaf cuvette (reference gas) and from the exhaust of the leaf cuvette (sample gas) are collected during photosynthesis, purified, and analysed with an isotopic ratio mass spectrometer. From the isotopic composition of the sample gas and the reference gas, the isotopic discrimination during photosynthesis (Δ) is derived (Evans *et al.*, 1986).

The individual contributions to Δ, including leakiness, can be resolved by means of an isotopic model. The model has to gauge the metabolic state of the leaf during the discrimination experiment so as to assign to every reaction the right contribution to discrimination. Several models have been developed (O'Leary, 1981; Peisker, 1982), however, the model used in the latest works (Cousins *et al.*, 2006, 2008; Gandin *et al.*, 2014; Henderson *et al.*, 1992; Kromdijk, 2010; Kromdijk *et al.*, 2010; Kromdijk *et al.*, 2008; Stutz *et al.*, 2014; Sun *et al.*, 2012; Tazoe *et al.*, 2008; Tazoe *et al.*, 2006; Ubierna *et al.*, 2013) was developed by Farquhar (Farquhar, 1983; Farquhar and Cernusak, 2012) and takes also into account photorespiration, ternary effects, and respiratory contributions to discrimination [see all details in (Stutz *et al.*, 2014)].

After estimates for Φ were made available e.g. (Bowman *et al.*, 1989), later research referred to this parameter. For instance, since leakiness and C_3 fixation in BS are complementary, Φ can been used as an index of the ratio between the C_4 activity and the C_3 activity. Leakiness has also been used as an index of operating efficiency, as, in fact, the refixation of the escaping CO_2 increases the ATP cost of photosynthesis. These concepts will be covered in great detail in the next Chapters. However, it is important to highlight that: i) Φ is not a physiological entity itself, but a ratio between two quantities (L and V_P) that are regulated independently. When these quantities have divergent trends, patterns of Φ are observed, e.g. the typical hyperbolic leakiness increase that has been extensively documented under low light (Cousins *et al.*, 2008; Henderson *et al.*, 1992; Kromdijk *et al.*, 2010; Kromdijk *et al.*, 2008; Pengelly *et al.*, 2010; Stutz *et al.*, 2014; Tazoe *et al.*, 2008; Tazoe *et al.*, 2006); ii) when Φ is used as a proxy for C_4 efficiency, or as a proxy for CCM / C_3 activity, the implicit assumption that PEPC is the sole process loading CO_2 in BS is made, which may have led to possible misinterpretation of experimental results; iii) empirical values

for Φ are highly derived quantities, and, to obtain them, two complex models are required (an isotopic discrimination model and a C_4 model, which have recurrently been updated and modified in the last 35 years). Attempts were made to validate the isotopic discrimination data by estimating Φ with an independent technique. Firstly, leakiness was derived solely from gas exchange data using the quantum yield of assimilation as a proxy (Farquhar, 1983; Kromdijk *et al.*, 2014). A second attempt involved the use of chlorophyll fluorescence to assess the quantum efficiency of photosystem II, to derive electron transport rate (ETR) and then to calculate the biochemical efficiency of assimilation. This methods relies on the assumption that quantum efficiency depends on leakiness with a predictable and fixed relationship. Chapter 4 will show that this relationship may be not be as clearly defined as previously thought. In addition, the method relies on several other assumptions regarding the energy requirement of C_4 photosynthesis, the end products of photosynthesis, spectral differences in quantum requirements, and the proportion of absorbed quanta that are used for processes other than photosynthesis (Furbank *et al.*, 1990; Kromdijk *et al.*, 2014), which has prevented to clarify the magnitude and dynamics of Φ with conclusive experimental evidence, and responses of Φ to various environmental pressures are still debated. Further, isotopic discrimination is still considered the best way to get an indirect estimate for leakiness [for review (Kromdijk *et al.*, 2014; Ubierna *et al.*, 2011; von Caemmerer and Furbank, 2003; von Caemmerer *et al.*, 2014)].

1.11 Description of the research projects

1.11.1 Overview

At the beginning of this research programme there was an on-going debate on Φ dynamics and magnitude in maize, therefore clarifying values and trends for maize leakiness was timely and necessary. For this reason, this research programme set out to continue with the project previously carried out in this lab (Kromdijk, 2010) and was initially aimed at refining the estimates of leakiness for maize and the understanding of the dynamic leakiness response to low light intensities. This involved optimising the experimental setup, in order to get more accurate data. The previous experimental setup was already highly sophisticated and optimized. Nevertheless, the experiment was patiently dissected and each step was relentlessly optimised. Since technicalities and data treatment are mutually intertwined, this

optimisation took the best part of the experimental work. The optimisation phase was of critical importance and underpinned all advances made in this research. The details of the optimisation phase are not thoroughly addressed in the experimental Chapters, hence they will be addressed in the next section.

In a subsequent step, different approaches to address the issue of C_4 efficiency were explored. Two hypotheses were formulated: 1) Φ is not an absolute constraint of C_4 photosynthesis but plants have systems to regulate Φ in response to environmental pressures; 2) biological systems are highly optimized, so 'efficiency loss' of C_4 photosynthesis is either underpinned by a rationale or it does not occur.

These two hypotheses matured together with the experimental optimisation, and they were tested in three distinct experiments that will be briefly outlined below, after describing the experimental optimization.

1.11.2 Experiment optimization

Firstly, the plant growth protocol was completely revised. Since plants are highly sensitive to any environmental change, measuring uniform plants is of pivotal importance. To improve uniformity, a weekly schedule was introduced. Plants were sown every Monday, grown under high light (HL, 600 $\mu E\ m^{-2}\ s^{-1}$) or low light (LL, 100 $\mu E\ m^{-2}\ s^{-1}$) for three (HL) or four (LL) weeks and discarded afterwards. Plants were watered manually every day, to avoid possible overwatering resulting from automated irrigation. Furthermore, plants were removed from the growth chamber at the same time of the day and they were measured (with a standardised routine) so as not to disturb the daily photosynthetic activation cycle.

Gas exchange and gas trapping

Trade-offs exists in gas exchange and gas trapping. For instance, precision of the mass spectrometer benefits from a higher amount of CO_2, which requires a long trapping time and limits the number of measurements that can be performed in a day (i.e. limited number of technical replicates). The trapping time can be shortened by increasing the air flow in the cuvette, but that would imply a lower difference in CO_2 concentration between the air in the cuvette and the external air, which in turn would translate into higher ξ-dependent amplification of error [e.g. Figure 3.6 (Evans *et al.*, 1986)]. The difficult optimisation of this phase involved several expedients. Firstly, the possibility of ambient air contaminating the

CO_2 in the cuvette was reduced by (i) a more compact design of the trapping line so as to have the lowest number of junctions, (ii) shortening the piping, (iii) reassembling the cuvette with black neoprene gaskets which seal better, and (iv) sealing leaves to gaskets with vacuum grease. The latter expedient was recently identified as the best way to reduce errors in gas exchange measurements (Boesgaard ***et al.***, 2013). Secondly, to minimise the effect of external contamination, the infra-red gas analyser (IRGA) was operated with cartridges of CO_2 with an isotopic composition similar to that of atmosphere, instead of using the normal ^{13}C depleted CO_2 (Gandin and Cousins, 2012; Ubierna ***et al.***, 2011). Thirdly, to save gas, a slight overpressure was maintained by bubbling gas into water, which consumes less gas (to the limit none) than the 'conventional' flow-meter. Fourthly, the sampling apparatus of the gas trapping line was reengineered to allow reference gas collection during light adaptation of the leaf, so as to collect more samples in a day. Finally, a dew point generator with an external CO_2 scrubber was used to stabilize the air supply to the IRGA throughout the day.

Leaf level ATP production rate

Leaf level estimates for J_{ATP} were derived and used together with the isotopic discrimination model for the first time. As described in '1.5 A model for C_4 photosynthesis' a reliable value for J_{ATP} is needed to parameterise the model. With the approach reported in von Caemmerer (2000), J_{ATP} is calculated from the electron transport rate J [for details on J and J_{ATP} see (Yin and Struik, 2009; Yin ***et al.***, 2004)], assuming a conversion factor of 1 (von Caemmerer, 2000). J is then calculated as J=PAR·absorptance·a·correction factor (f)·$Y(II)$, where a, the light exciting partitioning to PSII is generally assumed, while the absorptance is generally measured on leaves different from those subject to gas exchange and isotopic discrimination e.g. (Kromdijk et al 2010). In this work J_{ATP} was derived under low O_2 and high CO_2. Notably this procedure derived J_{ATP} under the same light quality and on the same leaf portion used during CO_2 trapping. This value for $J_{ATPLOWO2}$ was then recalibrated at ambient O_2 using yield of PSII, $Y(II)$ as a proxy to determine the small fraction of J_{ATP} consumed by photorespiration. Low O_2 was used together with high CO_2 because under these conditions leakiness and photorespiration are negligible, and the ATP cost for gross assimilation (ATP / GA) is known, close to the theoretical minimum of 5 (3 / 0.59 = 5.08 Eqn 2.1). Any correction was minimal, because photorespiration is largely suppressed in maize. This direct measurement relied for a great part upon gas exchange measurements that, for

their nature, integrate the entire leaf cross-sectional profile, therefore the J_{ATP} estimates are potentially not biased by different light qualities.

Data analysis and modelling

A novel fitting approach, referred to as the J / J approach, was used in Chapter 2 to fit the C_4 model and estimate mesophyll conductance. The J / J approach acknowledges the traditional gas exchange and stable isotope modelling approaches but removes an element of circularity whereby bundle sheath conductance and leakiness are both derived from carbon isotope discrimination (Chapter 2). In Chapter 3, the C_4 model of photosynthesis (see '1.5, A model for C_4 photosynthesis') was developed to address the spatial separation between BS and M. The resultant comprehensive biochemical model described the different pathways of CO_2 delivery to BS, and the ATP consuming processes (PGA reduction, carbohydrate synthesis and PEP regeneration). On the basis of this comprehensive metabolic description, the ATP demand for assimilation was predicted in the two compartments BS and M. This allowed a comparison of the newly-derived total ATP demand for gross assimilation with the conventional approach based on Φ as the sole proxy for C_4 efficiency, and with empirical results (Chapter 4).

1.11.3 Maize acclimation to low light (Chapter 2)

This Chapter describes most of the technical advances mentioned above. The hypothesis that plants *grown* under low light intensity cope with short-term exposure to low light in a different way to plants *grown* under high light intensity was tested. That is, answering the question of whether Φ is a built-in and invariable constraint of C_4 photosynthesis or it can be acclimated in response to environmental conditions. Long-term acclimation to low-light brought about a series of physiological changes that resulted in the modification of Φ trends and magnitudes. This response was interpreted by means of the C_4 model and could potentially result in optimising limited ATP resources under limiting light conditions.

1.11.4 Plasticity of C_4 biochemistry (Chapter 3)

It had been previously proposed that, since some wavelengths penetrate the leaf deeper than others, light quality may influence the partitioning of ATP production in BS and M (Evans *et al.*, 2007). Theoretical considerations have associated these light-induced imbalances to a reduced capacity to regenerate RuBP and to fix CO_2 in BS, with a consequent

loss of assimilatory efficiency (Evans ***et al.***, 2007). In contrast to that hypothesis, this Chapter proposes that plants have efficient mechanisms to cope with different light qualities without losing assimilatory efficiency. To test this hypothesis, the light induced ATP imbalances were estimated by means of a newly developed optical model. Concurrent gas exchange, isotopic discrimination and chlorophyll fluorescence data showed that photosynthetic efficiency was not influenced by light quality. Finally, the biochemical mechanisms underpinning the capacity to maintain high photosynthetic conversion efficiency in spite of the imbalanced ATP production were predicted by use of a novel comprehensive metabolic model. This model provides compelling justification for the existence of two distinct pathways of CO_2 delivery to BS and for the extensive overlap between BS and M biochemical functions.

1.11.5 Maize re-acclimation to low light (Chapter 4)

This Chapter completes the acclimation experiment of the second Chapter and integrates the bioenergetics presented in the third. Plants were grown under high and low light; HL plants were ***then*** transferred to low light. This two-step acclimation, or re-acclimation, mimics the transition from full sunlight conditions to shaded conditions that leaves undergo when shaded by newly emerging leaves in a crop canopy. Re-acclimation brought about physiological traits which were similar to those deployed by plants ***grown*** under low light conditions. The ATP cost for gross assimilation was predicted with the metabolic model derived in Chapter 3, and compared with the traditional calculation based solely on Φ and with the empirical results.

2 Maize acclimation to low light

Published in Plant, Cell and Environment as: Acclimation to Low Light by C_4 maize: Implications for Bundle Sheath Leakiness (Bellasio and Griffiths, 2014b).

A commentary on this Chapter by Rowan Sage was recently published (Sage, 2014).

2.1 Introduction

The C_4 metabolic syndrome evolved from C_3 photosynthesis under declining ambient CO_2 and increasing transpiration demand in semi-arid environments (Griffiths *et al.*, 2013; Osborne and Sack, 2012). In these environments, characterized by high irradiances (where energy supply is not limiting) and high temperatures, C_4 plants have higher photosynthetic rates than C_3 plants (Pearcy and Ehleringer, 1984). For this reason many C_4 plants are important agricultural crops and weeds: maize, for example, has been the world's leading grain production cereal (FAO, 2012). Following concerns about climate change, the high productivity of C_4 plants in warm climates has drawn additional attention to C_4 physiology, also with the goal of introducing 'beneficial' C_4 traits into C_3 crops such as rice (Covshoff and Hibberd, 2012; Kajala *et al.*, 2011; Sheehy, 2007).

The high productivity of C_4 plants derives from an active suppression of the oxygenase activity of Rubisco by means of a biochemical carbon concentrating mechanism (CCM) that concentrates CO_2 in the cellular compartment where Rubisco is exclusively expressed (bundle sheath, BS). The CCM has a notable metabolic cost (a theoretical minimum of 2 moles of ATP per mole of CO_2 assimilated) (Furbank *et al.*, 1990) and involves complex anatomical and biochemical machinery that decrease efficiency when light is limiting.

Although up to 50 % of C_4 crop canopy photosynthesis may be carried out by shaded leaves (Baker *et al.*, 1988), light limitations play an important role in limiting canopy productivity, and severe effects on net canopy photosynthetic uptake have been reported (Kromdijk *et al.*, 2008). Most leaves progressively acclimate to shade, since they emerge at the top of the canopy (as high light leaves) and become shaded by newly emerging leaves. This permanent long-term acclimation is accompanied by a transitory short-term acclimation response (e.g. daily shading). Understanding acclimation strategies, i.e. how C_4 metabolism copes with light limitations, is therefore relevant to crop production as well as providing insights for C_4 energetic efficiency.

This Chapter investigates the influence of long-term acclimation on C_4 inefficiencies under low light intensities. Previous studies have associated the inefficiency of the CCM under low light to an increase in leakiness (Φ), i.e. the rate of CO_2 retrodiffusion out of the BS relative to the rate of PEP carboxylation (V_P) [for review (Ubierna *et al.*, 2011)]. Φ is inevitable and an inherent feature of a biochemical CCM because a CO_2 concentration

gradient is established by overcycling CO_2 between cellular compartments connected by plasmodesmata. Φ is considered a wasteful process since the refixation of that escaping CO_2 results in an additional ATP cost of the CCM [Φ times higher than the theoretical minimum of 2 ATP per CO_2 (Furbank *et al.*, 1990; Tazoe *et al.*, 2008)]. Φ results in enriched $^{13}CO_2$ retrodiffusing from BS, thus enabling Φ to be estimated by studying real-time carbon isotope discrimination during photosynthesis, as Δ_{OBS} (Evans *et al.*, 1986).

Φ is one of the discrimination processes operating in C_4 photosynthesis that were resolved into weighted individual fractionations by the model originally derived by G.D. Farquhar (1983). In the model, diffusion in air, dissolution in water, PEP carboxylation, mitochondrial decarboxylation, Rubisco carboxylation and diffusion through plasmodesmata are assigned individual fractionation values. The magnitude of the component fractionation effects are weighted by the gradient in CO_2 concentrations between the different cellular compartments. The estimation of these concentrations is not entirely straightforward. C_a, the atmospheric CO_2 concentration in the cuvette, can be measured directly with the gas exchange analyser. C_i, the CO_2 concentration in the substomatal cavity, and C_M, the CO_2 concentration in mesophyll cells, are calculated using the equations for steady-state photosynthesis (Farquhar *et al.*, 1980; von Caemmerer and Farquhar, 1981). C_{BS}, the CO_2 concentration in BS, cannot be measured directly and is either assumed or estimated. When a large C_{BS} is assumed e.g. (Kromdijk *et al.*, 2008; Pengelly *et al.*, 2010; Tazoe *et al.*, 2008) an evident bias is introduced for high leakiness values (Ubierna *et al.*, 2011). When C_{BS} is estimated through a model for C_4 photosynthesis (von Caemmerer, 2000), a parameterization with assimilation (A), total ATP production rate (J_{ATP}), respiration in the light (R_{LIGHT}) and bundle sheath conductance (g_{BS}) is needed.

Measurement of A, J_{ATP} and R_{LIGHT} present some technical issues. Assimilation can be measured directly: good practices allowing measurements with suitable accuracy are well codified from studies on C_3 plants (Flexas *et al.*, 2007; Long and Bernacchi, 2003; Pons *et al.*, 2009). J_{ATP}, R_{LIGHT} and g_{BS} are more difficult to distinguish experimentally and the approach followed by the latest studies leaves room for improvement: i) J_{ATP} has been traditionally resolved from a theoretical relationship between quantum yield of photosystem II and ATP production rate. This estimate relies on parameters that are difficult to measure, some of which are still unknown (von Caemmerer, 2000). ii) R_{LIGHT} has often been assumed

equal to respiration in the dark, which is relatively simple to measure [e.g. (Ubierna *et al.*, 2013)]. Growing awareness of the mechanisms of regulation of respiration in the light (Tcherkez *et al.*, 2008) reveal the limits of the traditional assumption. iii) g_{BS} has been traditionally resolved by calculating a 'modelled' isotopic discrimination during photosynthesis, $\Delta_{MOD,}$ and fitting Δ_{MOD} to the observed discrimination during photosynthesis Δ_{OBS} (later referred to as Δ / Δ approach) [for review (Ubierna *et al.*, 2011)]. This approach introduces a certain degree of circularity, since C_{BS} and Φ are both estimated from Δ_{OBS}.

In order to develop these technical issues I introduced three major experimental advances: i) R_{LIGHT} was measured through the combined use of fluorescence and gas exchange (Yin *et al.*, 2011a); ii) the total ATP production rate, J_{ATP}, was measured at low O_2 and the value was corrected by the small ATP demand for photorespiration (Yin and Struik, 2009; Yin *et al.*, 2011b); iii) using the precise estimate of J_{ATP}, g_{BS} could be estimated by curve fitting based on J_{ATP} (J / J approach). Since g_{BS} and Φ were derived from independent datasets, the J / J approach did not suffer the circularity of the Δ / Δ approach; finally, plants were grown under two contrasting light regimes with the lowest (100 μE m^{-2} s^{-1}) well below that used in comparable studies (Kromdijk *et al.*, 2010; Pengelly *et al.*, 2010; Tazoe *et al.*, 2008).

Results showed that long-term acclimation influenced the way maize plants responded to decreasing light intensities. When plants grown in high light (HL, 600 μ E m^{-2} s^{-1}) were exposed to decreasing light intensities, they responded with an increase in Φ. Conversely and in contrast to the pattern reported in previous studies, plants grown in low light (LL) did not show any increase in Φ. By refitting the C_4 model I hypothesized the possible underlying physiological processes. HL and LL plants deployed a contrasting strategy at limiting light intensities: while HL plants maintained a high CCM activity, resulting in high CO_2 overcycling, LL plants decreased the CCM activity and coped with the resulting decrease of CO_2 flow to BS by adjusting carboxylase activity or bundle sheath conductance, effectively optimising scarce ATP supply.

2.2 Results

Maize plants were grown under two different light regimes and their photosynthetic response was studied under decreasing light intensities. Carbon isotope discrimination, PSI / PSII photochemistry and gas exchange were measured concurrently. CO_2 concentration in BS

(C_{BS}) and bundle sheath conductance (g_{BS}) were estimated by implementing a C_4 photosynthesis model. The C_4 model was constrained with two different datasets: the ATP production rate J_{ATP} (J / J approach) and the real-time isotope discrimination data Δ_{OBS} (Δ / Δ approach). In this way two different sets of values for C_{BS} and g_{BS} were estimated and were used, in turn, to resolve leakiness (Φ_{id}) from Δ_{OBS} by Eqn 2.3.

Figure 2.1. Gas exchange responses of HL and LL plants

LL plants (triangles) and HL plants (squares) under low O_2 (open symbols) or ambient air (filled symbols) were exposed to decreasing light intensity. **(A)**: net assimilation, *A*. The curves were fitted in order to calculate the compensation point with the use of dedicated software (Photosyn assistant 1.2, Dundee Scientific, Dundee, UK) (Dougherty *et al.*, 1994; Prioul and Chartier, 1977). The inset shows a magnification in the vicinity of the compensation point. **(B):** C_i / C_a. **(C):** stomatal conductance, g_s. Error bars represent standard error. HL n = 3; LL n = 4.

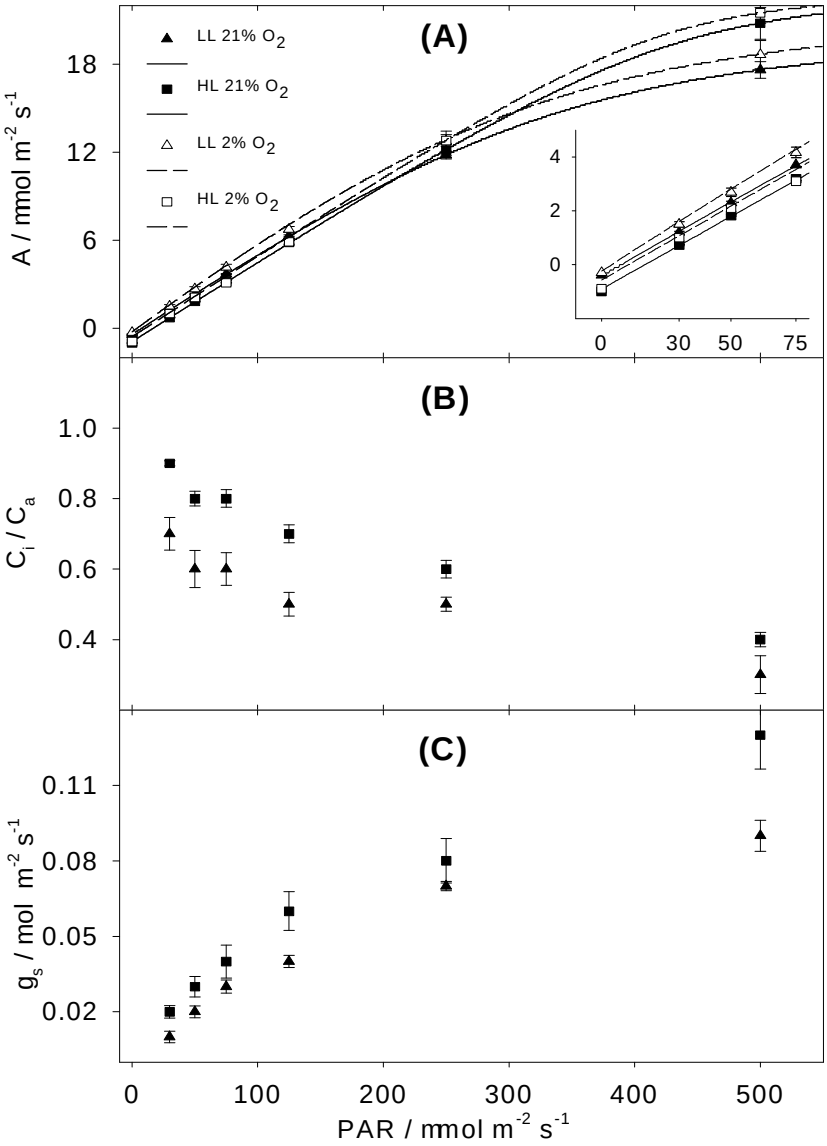

2.2.1 Physiological response to decreasing light intensities

Assimilation (*A*) differentiated LL plant and HL plant responses (Figure 2.1 A). LL plants had lower *A* at high PAR, but relatively higher *A* at lower PAR. Consistently, the light compensation point (*LCP*) and respiration in the light (R_{LIGHT}) of LL plants were lower (Table 2.2). When low O_2 was supplied, *A* of LL plants increased on average by 0.3 μmol m^{-2} s^{-1}, while *A* of HL plants increased by an average of 0.2 μmol m^{-2} s^{-1} (Figure 2.1)

Figure 2.1 B shows that C_i / C_a was higher than 0.6 at PAR < 125 μE m^{-2} s^{-1} (LL plants) or PAR < 500 μE m^{-2} s^{-1} (HL plants). This was a remarkable result considering maize typical stomatal responses e.g. (Ubierna ***et al.***, 2013) and reflected efforts made during the measurements to induce stomatal opening (see methods for details). A high C_i / C_a was important to maximise the contribution of biochemical processes to total isotopic discrimination, and it was a prerequisite for resolution of the isotopic discrimination model. Compared to HL plants, LL plants showed slightly reduced C_i / C_a, as a consequence of lower stomatal conductance (Figure 2.1 C).

The photochemical yield of PSII *Y(II)* decreased linearly at increasing PAR in both HL plants (Figure 2.2 A) and LL plants (Figure 2.2 B). Consistently, the quantum yield for CO_2 assimilation decreased, and a linear relationship between quantum yield of CO_2 assimilation and *Y(II)* was observed in all samples (not shown). In LL plants, *Y(II)* was unaffected by O_2 concentration whereas HL plants displayed a tendency to have lower *Y(II)* under low O_2 (Figure 2.2 A). The photochemical yield of PSI *Y(I)* decreased at decreasing PAR (Figure 2.7). To the best of my knowledge this is the first study where maize *Y(I)* is measured concurrently to a complex physiological characterization.

The total ATP production rate (J_{ATP}) is shown by symbols in Figure 2.3 A. J_{ATP} was derived from gross assimilation under low O_2 (Eqn 2.1) and then corrected for photorespiration at ambient O_2 using the ratio of photochemical yield (Eqn 2.2). At high PAR, J_{ATP} of LL plants was lower than J_{ATP} of HL plants because of the lower ATP demand for lower *A* (Figure 2.1). At low PAR, J_{ATP} of LL plants matched J_{ATP} of HL plants, suggesting that the higher *A* of LL plants at limiting PAR (inset in Figure 2.1) was achieved through a higher conversion efficiency and lower respiration rate (Table 2.2).

Isotopic discrimination during photosynthesis (Δ_{OBS}) is shown by symbols in Figure 2.3 B. In LL plants Δ_{OBS} was relatively low (around 4 ‰) and unaffected by light intensity. In HL

plants Δ_{OBS} increased from 2.6 ‰ at 500 μE m^{-2} s^{-1} to 22.1 ‰ at 30 μE m^{-2} s^{-1}. These responses were confirmed by measurements on an independent batch of plants (not shown).

Figure 2.2. Yield of photosystem II, *Y(II)* at decreasing light intensity

Response of *Y(II)* of HL plants **(A)** and LL plants **(B)** measured in low O_2 (open symbols) or ambient air (filled symbols) to decreasing light intensities. Error bars represent standard error. n = 4.

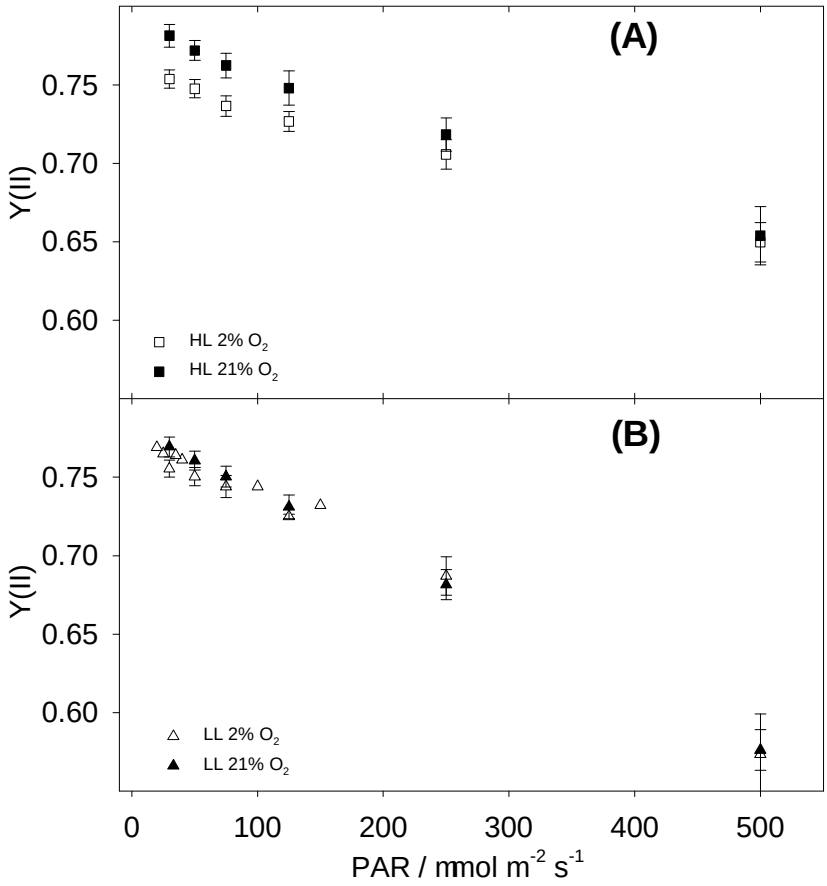

2.2.2 Modelled C_4 photosynthesis: model fitting and estimation of g_{BS} and C_{BS}

An estimate of BS conductance to CO_2, g_{BS}, was obtained for each individual plant. Table 2.3 shows that g_{BS} was lower when obtained through the J / J approach. Table 2.3 also shows that LL plants had lower g_{BS} than HL plants. These g_{BS} values were used in Eqn 2.8, the supply function of BS, to calculate C_{BS}. C_{BS} differentiated between fitting approaches. With the J / J approach, C_{BS} of HL and LL plants were similar, decreasing from (2400 to 1000) μmol / mol at decreasing PAR. With the Δ / Δ approach, C_{BS} was substantially lower than calculated using the J / J approach and differed between the two growth regimes. In LL plants C_{BS} ranged from (1700 to 700) μmol / mol, while in HL plants C_{BS} ranged from (970 to 570) μmol / mol.

Figure 2.3. Datasets and model fitting

1) Total ATP production rate, J_{ATP}, and isotopic discrimination during photosynthesis Δ_{OBS}. Symbols in panel **(A)** show J_{ATP} for LL plants (triangles) and HL plants (squares). Symbols in panel **(B)** show Δ_{OBS} for LL plants (triangles) and for HL plants (squares).
2) Model fitting with J / J and Δ / Δ approaches. In order to estimate g_{BS}, the C_4 photosynthesis model (lines) was fitted to the two different datasets alternatively. In the J / J approach the C_4 model (solid lines) was expressed as J_{MOD} and fitted to J_{ATP} measured on LL plants [Panel **(A),** thin solid line] and to J_{ATP} measured on HL plants [Panel **(A),** thick solid line]. In the Δ / Δ approach the C_4 model (dotted lines) was expressed as Δ_{MOD} and fitted to Δ_{OBS} measured on LL plants [Panel **(B),** thin dotted line] and on Δ_{OBS} measured on HL plants [Panel **(B),** thick dotted line].
3) Note the trade-off between fitting approaches. As the C_4 model is the same, by fitting J_{MOD} to J_{ATP}, Δ_{MOD} is distanced from Δ_{OBS} [see solid lines in panel **(B)**]. Similarly, by fitting Δ_{MOD} to Δ_{OBS}, J_{MOD} is distanced from J_{ATP} [see dotted lines in panel **(A)**]. Error bars represent standard error. HL n = 3; LL n = 4.

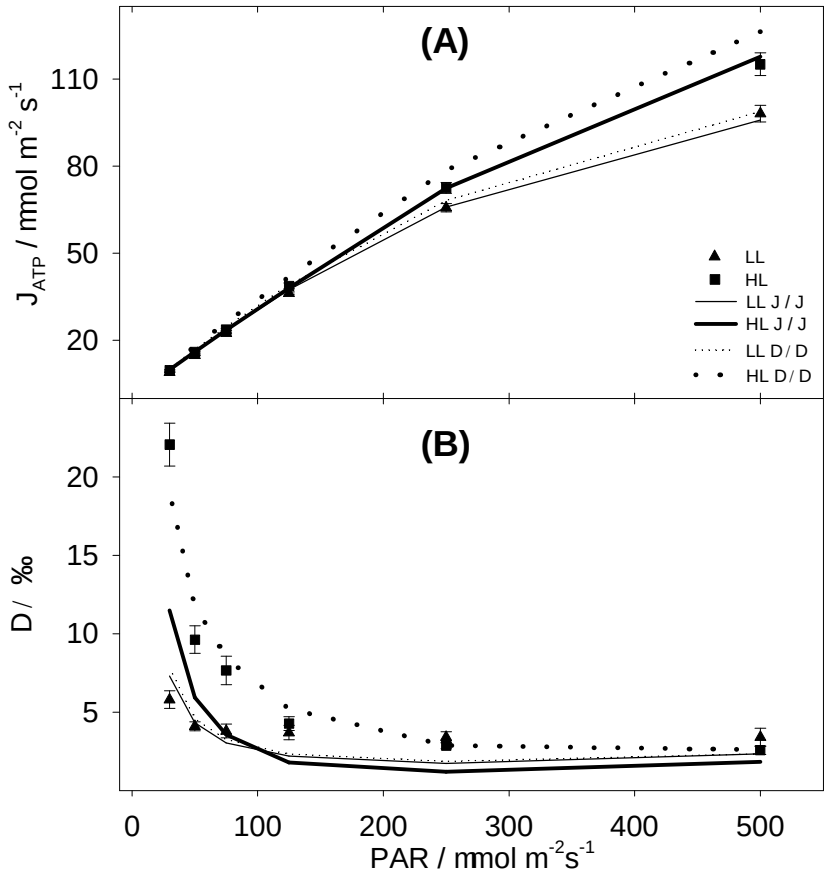

2.2.3 Response of F_{id} to light intensity

Symbols in Figure 2.4 B and C show that in LL plants leakiness, F_{id}, derived from real-time carbon isotope discrimination data, Δ_{OBS}, was constant at decreasing PAR, while in HL plants F_{id} increased hyperbolically at decreasing PAR. To derive F_{id} from Δ_{OBS}, Eqn 2.3 was parameterized with the output of the C_4 model, fitted with the J / J approach or Δ / Δ approach (compare symbols in Figure 2.4 B and C). With the J / J approach (symbols in Figure 2.4 B), LL plants Φ_{id} (triangles) was close to 0.24 and HL plants Φ_{id} (squares) ranged from 0.17 to 0.67. With the Δ / Δ approach (Figure 2.4 C, symbols) LL plants Φ_{id} was close to 0.22 (triangles), and HL plants Φ_{id} (squares) ranged from 0.16 to 0.49.

Figure 2.4. Output of the C_4 model and the isotopic discrimination model

(A): response of C_{BS}, calculated either with J / J approach (solid lines), or with the Δ / Δ approach (dotted lines), of LL plants (thin lines) and HL plants (thick lines) to decreasing light intensities. **(B)**: J / J approach. Symbols represent leakiness based on isotopic discrimination data Φ_{id} (Eqn 2.3) for LL plants (triangles) and for HL plants (squares); lines represent modelled leakiness Φ_{MOD} (Eqn 2.11) for LL plants (thin solid line) and for HL plants (thick solid line). **(C)**: Δ / Δ approach. Symbols represent leakiness based on isotopic discrimination data Φ_{id} (Eqn 2.3) for LL plants (triangles) and for HL plants (squares); lines represent modelled leakiness Φ_{MOD} (Eqn 2.11) for LL plants (thin dotted lines) and for HL plants (thick dotted line). Error bars represent S.E. HL n = 3; LL n = 4.

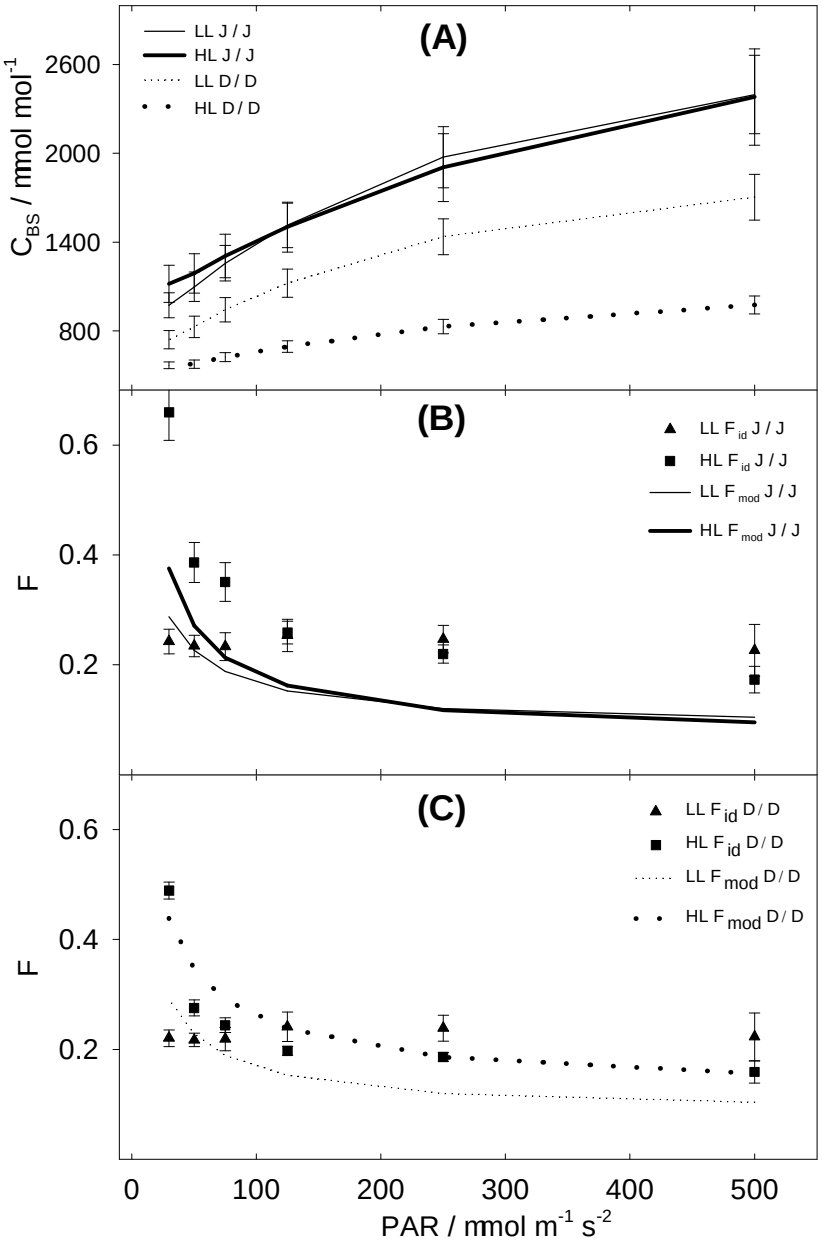

2.2.4 Modelled leakiness Φ_{MOD}

Figure 2.4 B shows that with the J / J approach, Φ_{MOD} underestimated Φ_{id} both in LL and HL plants. With the Δ / Δ approach (Figure 2.4 C dotted lines) Φ_{MOD} and Φ_{id} were not independent estimates of Φ (see discussion).

Interestingly, with both approaches Φ_{MOD} did not describe the constant Φ_{id} trend observed in LL plants. In fact, fitting varied Φ_{MOD} magnitude, but did not change the shape of the function, with Φ_{MOD} hyperbolically increasing at decreasing PAR (compare lines in Figure 2.4 B and C). As a consequence, the linear Φ_{id} trend observed was not predicted by the conventional fitting but required a more complex procedure.

2.2.5 Model refitting

Figure 2.5 A shows the values of x (the ATP partitioning between PEPC activity and C_3 activity) that were required to refit Φ_{MOD} to Φ_{id}. Interestingly, x showed a contrasting tendency in the two different treatments: in LL plants there was a tendency of fitted x to decrease at decreasing light intensities while in HL plants there was no clear trend. Figure 2.5 B shows the g_{BS} values that refitted Φ_{MOD} to Φ_{id}. g_{BS} differentiated between LL and HL plants: in LL plants there was a clear decrease of refitted g_{BS} at decreasing light intensities (Figure 2.5 B) while in HL plants refitted g_{BS} did not show a pattern.

Figure 2.5. Model refitting

In panel **(A)** Φ_{MOD} was fitted to Φ_{id} varying x between light intensities. x is the factor partitioning J_{ATP} between C_4 activity (PEPC carboxylation) and the C_3 activity (RPP cycle + glycolate recycling). The line displayed is an inverse quadratic regression fitted to LL data. In panel **(B)** Φ_{MOD} was fitted to Φ_{id} varying bundle sheath conductance g_{BS} between light intensities**.** The line displayed is a quadratic regression fitted to LL data. All the other parameters were unvaried from the previous fitting step. Error bars represent standard error. HL n = 3; LL n = 4.

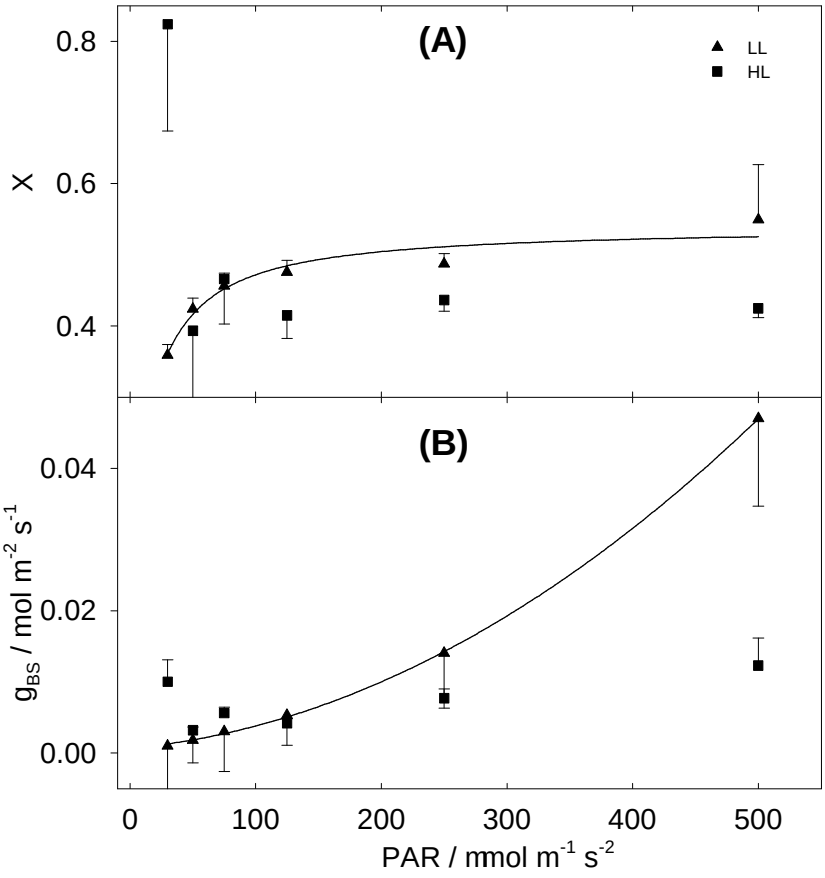

2.3 Discussion

2.3.1 Technical optimization: R_{LIGHT}, J_{ATP} and J / J fitting approach

By measuring J_{ATP} directly, I parameterized the isotopic discrimination model with a suitable novel approach, independent of Δ_{OBS}. Plants were subject to gas exchange and photochemical investigations at low O_2 and to gas exchange, isotopic discrimination and photochemical investigation at ambient O_2. This complex setup allowed estimation of R_{LIGHT} and derivation of J_{ATP} for the portion of the leaf clamped in the cuvette at the very moment that gas exchange and isotopic discrimination were being measured. The availability of precise independently estimated values for J_{ATP}, offered a valid dataset for fitting the C_4 model. This 'J / J approach' was used together with isotope discrimination data for the first time in the present work. In fact in studies where J_{ATP} was modelled, and therefore not independently obtained, the J / J fitting was not possible e.g. (Ubierna *et al.*, 2013)]. Nor was it possible when J_{ATP} was calculated using parameters derived from leaves differing from those subject to gas exchange, because, in this case, J_{ATP} did not strictly represent the portion of the leaf subject to isotopic discrimination and gas exchange investigations e.g. (Kromdijk *et al.*, 2010).

The J / J approach suited the C_4 model parameterization. Firstly, J_{ATP} was derived from gas exchange measurements under the same assumptions of the C_4 model. Under these assumptions J_{ATP} represented the fraction of ATP available for photosynthesis and was not influenced by the ATP allocation to alternative sinks. Secondly, the J / J approach did not suffer the circularity of the Δ / Δ approach, where C_{BS} and g_{BS} are not independent, being both derived from Δ_{OBS} (Kromdijk *et al.*, 2010; Ubierna *et al.*, 2013). It was recently argued that the J / J approach and the Δ / Δ approach suffer the same degree of circularity since with both approaches g_{BS} and C_{BS} are calculated from the same dataset (Kromdijk *et al.*, 2014). I believe that such an argument is misleading since g_{BS} and C_{BS} are not independent ($A = g_{BS}(C_{BS} - C_M)$). Here I am suggesting that while with the J /J approach g_{BS} and C_{BS} are calculated on gas exchange data and Φ_{id} is derived from isotopic discrimination, with the Δ / Δ approach g_{BS}, C_{BS} and Φ_{id} are all calculated from isotopic discrimination. For these reason it is worth stressing that the J / J approach is less circular than the Δ / Δ approach. Thirdly, with the J / J approach, the estimate of C_{BS} and g_{BS}, relied uniquely on gas exchange and

fluorescence data, without requiring isotopic discrimination data. This had major benefits: i) since there was no amplification of error dependent on ξ (Appendix 2 and Table 2.4), J_{ATP} could be measured at any light intensity, even below the compensation point; ii) the equipment was relatively cheap and easy to maintain; iii) data had low noise / signal ratio. For these reason the J / J approach should be considered as a substantial refinement in the derivation of Φ_{id} with non-destructive techniques.

2.3.2 J / J compared to Δ / Δ

To show these differences and the similarities between the two approaches, model parameters other than g_{BS} were kept constant throughout, using consensus values derived from the literature (Table 1). The different approaches yielded different g_{BS} and C_{BS} values, but this resulted in different Φ_{id} only in HL plants. Bundle sheath conductance (g_{BS}) derived with the J / J approach was one third of the value of g_{BS} derived with the Δ / Δ approach. The overall range ($8.2 \cdot 10^{-4}$ to $46 \cdot 10^{-4}$) mol m^{-2} s^{-1} was within the range previously reported: $15 \cdot 10^{-4}$ mol m^{-2} s^{-1} (Ubierna *et al.*, 2013); ($8 \cdot 10^{-4}$ to $103 \cdot 10^{-4}$) mol m^{-2} s^{-1} (Yin *et al.*, 2011b); ($3.7 \cdot 10^{-4}$ to $23.5 \cdot 10^{-4}$) mol m^{-2} s^{-1} (Kromdijk *et al.*, 2010). The corresponding C_{BS} values estimated with the J / J approach were on average 70 % higher than those estimated with the Δ / Δ approach. The range I reported (500 to 2500) μmol mol^{-1}, was consistent with values reported for maize [for review (von Caemmerer and Furbank, 2003)]. In spite of these C_{BS} differences, in LL plants the two approaches yielded identical Φ_{id}, indicating that Φ_{id} is fairly insensitive to variations of C_{BS} when Δ_{OBS} is low. Conversely, in HL plants the two approaches yielded different Φ_{id}, because of the big difference in C_{BS} and the higher values of Δ_{OBS}.

Modelled leakiness, Φ_{MOD}, is one of the outputs of the C_4 model and carries different information, depending on the C_4 model parameterization. With the J / J approach (Figure 2.4 B solid lines), Φ_{MOD} was calculated with gas exchange and photochemical data only, therefore Φ_{MOD} (Figure 2.4 B lines, Eqn 2.11) and Φ_{id} (Figure 2.4 B symbols, Eqn 2.3) represented two independent estimates of Φ. The discrepancy between Φ_{MOD} and Φ_{id} is dependent on the different assumptions made in the calculations. One could decrease this discrepancy by progressively increasing g_{BS} until the distance between Φ_{MOD} and Φ_{id} is minimized. Now, Φ_{MOD} and Φ_{id} are not independent estimates of Φ because Φ_{MOD} was varied to fit Φ_{id}. This situation corresponds to the Δ / Δ fitting (fitting Δ over Δ corresponds to fitting

Φ_{MOD} over Φ_{id} as the same model is used to interconvert Φ and Δ). Note that the better fit between Φ_{MOD} and Φ_{id} not only is reached at expense of arising circularity, but also it distances J_{MOD} from J_{ATP}. When the distance between Φ_{MOD} and Φ_{id} is lowest (Figure 2.4 C), the distance between J_{MOD} and J_{ATP} is highest (Figure 2.3 A dotted lines). When the distance between Φ_{MOD} and Φ_{id} is highest (Figure 2.4 B), the distance between J_{MOD} and J_{ATP} is lowest (Figure 2.3 A solid lines).

2.3.3 Leakiness responses at decreasing PAR

While the Φ_{id} response for HL plants was expected, LL plants displayed a particular response that could not be simulated under conventional constraining of the C_4 model. In HL plants, grown under PAR = 600 µE m^{-2} s^{-1}, Φ_{id} ranged from 0.17 to 0.66, in agreement with previous findings, and showed the conventional hyperbolic increase at decreasing PAR (Kromdijk *et al.*, 2010; Ubierna *et al.*, 2011; Ubierna *et al.*, 2013; von Caemmerer and Furbank, 2003). However, in LL plants, grown under 100 µE m^{-2} s^{-1}, Φ_{id} was constant under decreasing PAR, a response that has not been shown before. In comparable studies, maize HL grown plants [500 µE m^{-2} s^{-1} (Ubierna *et al.*, 2013)] or maize plants grown under intermediate irradiance [250 µE m^{-2} s^{-1} (Kromdijk *et al.*, 2010)] showed a Φ increase at low PAR. This increase was observed also in other C_4 species (Pengelly *et al.*, 2010; Tazoe *et al.*, 2008). In my experiment the gas exchange measurement routine may have contributed to showing the traits acquired during growth. The experiment included a strict 20 min short-term-acclimation after each change in PAR. During this acclimation, LL plant metabolism tuned and reach a status of low Φ_{id}.

Interestingly, the Φ_{id} trend observed in LL plants could not be simulated by the C_4 model with the first fitting procedure, as the model described a hyperbolic increase of Φ_{MOD} at decreasing PAR, similar to the Φ_{id} response observed in HL plants. The hyperbolic increase is due to the effect of constant x (the ATP partitioning between PEPC activity and C_3 activity) and R_{LIGHT}. In the C_4 model, two contributions to CO_2 flux to BS are considered: i) the contribution of malate decarboxylation (equals PEPC activity at steady state); ii) the CO_2 respired in BS. When PAR decreases, while PEPC and Rubisco activities proportionally decrease, the BS respiration stays constant. In these conditions, BS-respired CO_2 is not fixed by the reduced Rubisco activity and is free to diffuse out of BS. As BS respiration progressively outweighs V_P, the ratio of retrodiffusing CO_2 over PEP carboxylation rate (Φ =

L / V_P) becomes progressively higher, hence the characteristic hyperbolic Φ increase at limiting PAR. For these reasons the flat Φ_{id} response at decreasing PAR cannot be explained under the conventional model constraints: to explain the response I explored two scenarios involving unusual regulation of metabolism.

2.3.4 Acclimation scenarios

By refitting the C_4 model, I associated the flat Φ_{id} pattern observed in LL plants with variable physiological traits. BS conductance to CO_2 (g_{BS}) and the C_4 / C_3 ATP partitioning factor (x) were chosen as their values were not derived from direct measurements and could be varied without changing the model assumptions or overriding data. Refitting differed from the fitting described above. Fitting assigned a value of g_{BS} to each individual plant, constant at all light intensities, and a value of x, constant for all plants in all conditions. In refitting, either x or g_{BS} were varied between light intensities, while all other parameters were maintained as constants from the previous step. Refitting resulted in a tight match between Φ_{MOD} and Φ_{id} and, according to the parameter varied, described two alternative scenarios.

A first scenario explaining the flat Φ_{id} pattern observed in LL plants involved variable partitioning between C_4 and C_3 activity (x) as a function of light intensity. Under LL intensities x was downregulated (Fig 2.5 A). This meant that the fraction of ATP consumed by PEPC over the total ATP consumed by assimilation became progressively lower. In other words, when PAR decreased, PEPC was downregulated more than the C_3 activity and there was a shift from a PEPC-driven CCM to a respiration-driven CCM, effectively cutting the ATP cost of the CCM when light was limiting. This particular type of respiration-driven CCM resembles forms of CCM at the early stage of evolution of C_4 photosynthesis (also known as C_2 photosynthesis), when the biochemical exchange of acids between BS and M had not been optimized yet (Griffiths ***et al.***, 2013). As a consequence of the decreased CO_2 flux to BS, C_{BS} would decrease. To maintain a physiological assimilation rate (Fig 2.1 A) an increased activity of Rubisco would have to compensate for the lower C_{BS}. I could not quantify the differential Rubisco activity with the equations used here, because of the way the model is designed: Rubisco is assumed fully activated, saturated by RuBP and uniquely limited by J_{ATP}. The influence of differential relative Rubisco / PEPC activity on Φ was shown in a modelling study, where the enzyme activation state was taken into account (Peisker and Henderson, 1992). A 10 % reduction in Rubisco activity relative to PEPC

activity resulted in Φ increasing by 14 %. A similar result was obtained experimentally in sugarcane where a 50 % higher relative Rubisco / PEPC activity measured in vitro corresponded to a 16 % lower Φ estimated from isotopic discrimination of total leaf dry matter (Saliendra *et al.*, 1996).

The second scenario formulated to explain the flat Φ_{id} pattern observed in LL plants, involved varying g_{BS} between light intensities. Under decreasing PAR, LL plants showed a differential capacity to retain CO_2 in BS. When, under limiting light, PEPC was downregulated, and CO_2 flux to BS was reduced, the CO_2 available in BS was trapped more effectively. In other words BS had the capacity to maintain high C_{BS} even under decreased PEPC activity. This relatively higher CO_2 concentration would maintain a physiological Rubisco carboxylation rate without any relative change in activity. Although counterintuitive, the idea of tuneable g_{BS} is supported by some theoretical considerations. Sowinsky and colleagues (2008) showed that the dimensions of plasmodesmata in maize are insufficient to account for a passive flow of solutes from BS to M at physiological rate, and they postulated the existence of active transport (mass flow or vesicle transport). If active transport is involved in metabolite trafficking, the cell could easily regulate the transport rate between M and BS, thus g_{BS}.

2.3.5 Wider implications

The long-term and short-term acclimation to LL has implications at field level. In crop canopies leaves emerge fully exposed (equivalent to HL plants) and then undergo a low-light acclimation when progressively shaded by newly emerging leaves. I showed that maize leaves grown under HL did not short-term acclimate Φ [in agreement with (Ubierna *et al.*, 2013)], nor did plants grown under intermediate light (Kromdijk *et al.*, 2010). However, plants grown under diffuse LL did display the capacity to short-term acclimate Φ (flat Φ response). I hypothesised two scenarios, both involving the capacity of optimising limiting ATP resources under low PAR. If plants were deploying similar strategies in the field, the impact of leakiness-dependent carbon losses at canopy scale may be much smaller than previously thought (Kromdijk *et al.*, 2008).

Future work will be oriented towards studying whether the ‘low leakiness state’ is also expressed under different light qualities and will investigate whether the ‘low leakiness at

low light state' can be induced in HL plants upon exposure to LL for a suitable acclimation period, thus mimicking the temporal transition that leaves undergo in the canopy.

2.4 Conclusion

The phenomenon of leakiness, Φ, the amount of CO_2 diffusing out of the bundle sheath, expressed as relative to PEP carboxylation rate, was studied in maize by isotopic discrimination, gas exchange and photochemistry measurements. Respiration in the light and ATP production rate were measured directly. Data were interpreted using the established approach of fitting Δ to Δ and using a novel approach of fitting J to J that removes the circularity of the Δ / Δ approach.

Plants grown in LL showed constant Φ at decreasing light intensities, a response not reported in previous findings. This particular response was not predicted by the C_4 model under common constraints but, by releasing the constraint of equal C_4 / C_3 energy partitioning (x) or equal bundle sheath conductance between light intensities, it was possible to formulate hypotheses to describe the two different acclimation strategies. HL plants operated efficiently at HL but maintained a high PEPC activity at low light, resulting in high CO_2 overcycling. At limiting light intensities LL plants downregulated PEPC more than proportionally to the C_3 activity and there was a shift from a PEPC-driven CCM to a respiration-driven CCM, effectively cutting the ATP cost of the CCM when light was limiting. Physiological assimilation rates were maintained either by increasing Rubisco activity or by tuning g_{BS}, effectively trapping the CO_2 resulting from decarboxylation of malate, pyruvate, and glycine (see Paragraph 1.2). In both cases the plant could optimise scarce ATP resources. The actual impact of leakiness on canopy net photosynthetic uptake may need to be revised in light of this surprising acclimation plasticity.

2.5 Materials and Methods

2.5.1 Plants

Maize plants were grown at the Plant Growth Facility located at the University of Cambridge Botanic Garden in controlled environment growth rooms (Conviron Ltd, Winnipeg, Canada) set at 16 h day length, temperature of 25 °C / 23 °C (day / night) and 40 % relative humidity.

The growth protocol was designed to standardize age and watering conditions throughout the experiment. Every Monday, seeds of *Zea mays* L. (F1 Hybrid PR31N27, Pioneer Hi-bred, Cremona, Italy) were sown in 1.5 L pots filled with Levington pro M3 pot & bedding compost (Scotts Miracle-Gro, Godalming, UK) and positioned in HL (PAR = 600 μE m^{-2} s^{-1}) or in LL (PAR = 100 μE m^{-2} s^{-1}). LL intensity was obtained through shading to mimic the understory of a canopy. Plants were manually watered daily with particular care to avoid overwatering. At the fully expanded 4th leaf stage (3 weeks, HL; 4 weeks, LL) plants were measured once and then discarded.

2.5.2 Respiration in the light R_{LIGHT}

Respiration in the light was estimated independently at 2 % O_2 and at 21 % O_2 with the chlorophyll fluorescence method proposed by Yin and colleagues (Yin and Struik, 2009; Yin *et al.*, 2011a). Briefly, *A* (see below) was plotted against PAR·*Y(II)* / 3 (where *Y(II)* is PSII yield, Eqn 2.12, Appendix 1, the coefficient 3 was maintained to ease comparison with previous work); the y-intercept of the linear regression gives an estimation of $-R_{LIGHT}$ (Figure 2.6).

Figure 2.6. Example of the chlorophyll fluorescence method for the determination of respiration in the light R_{LIGHT}

Net assimilation in high O_2 (filled squares) and in low O_2 (open squares) were plotted against PAR·*Y(II)* / 3 (a quantity proportional to electron transport rate, where the coefficient 3 is maintained for consistency with previous reports). The *y*-intercept of the fitted line was taken as estimate of $-R_{LIGHT}$. The slope of the regression line (*s′*, Table 2.2) is a conversion efficiency parameter that lumps together quantities that are difficult to measure and parameters that are often assumed: leaf absorptance; correction for light spectral quality; coefficient of excitation partitioning between PSII and PSI; stoichiometric conversion coefficient of electron transport rate into J_{ATP} (protons extruded in the lumen per electron flowing through PSII / protons used by ATP synthase per each ATP synthesized). n = 1.

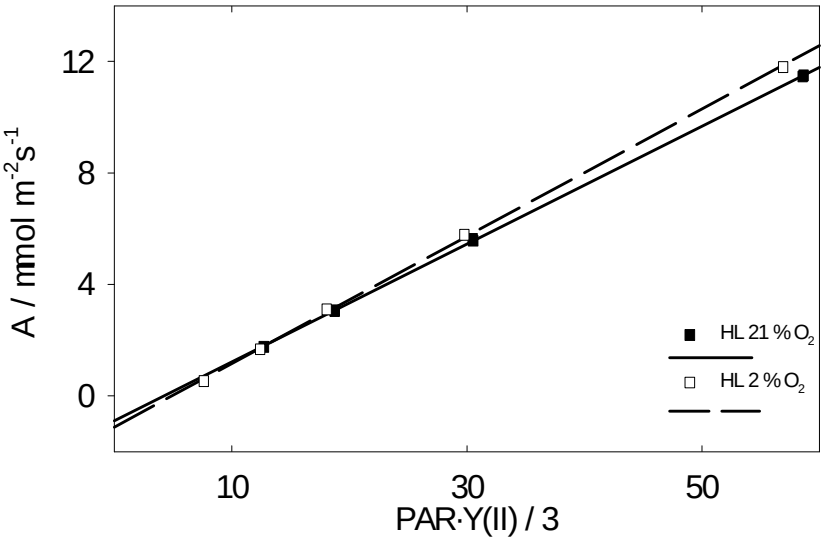

2.5.3 Gas exchange measurements with concurrent PSI / PSII Yield and carbon isotopic discrimination

The experimental setup for measuring J_{ATP} and Δ concurrently on the same sample consisted of an infra-red gas analyzer (IRGA), a Dual PAM and a trapping line. The IRGA, a LI6400XT (Li-Cor, Lincoln Nebraska, USA), was fitted with a 6400-06 PAM2000 adapter, holding a fiber probe in the upper leaf cuvette distant enough to avoid shading. Light was provided by a Li-Cor 6400-18 RGB light source, positioned to uniformly illuminate the leaf. Measurements with low gas flow, indispensable to measure discrimination at low light intensities, required careful optimization to minimize leaks. Neoprene gaskets were used on both sides of the cuvette and a tiny ridge of vacuum grease was laid on gaskets so as to seal the leaf upon closure. A 2 % O_2 / N_2 (pre-mixed, BOC, UK) or ambient air was CO_2-scrubbed with soda lime and humidified to a dew point of 19 °C upstream of the inlet. Natural abundance CO_2 (δ = -9.46 ‰) used to reduce artefacts (Gandin and Cousins, 2012; Ubierna *et al.*, 2011) was added from a cylinder (Isi, Wien, A), with use of the CO_2 injection unit of the IRGA.

To determine the most suitable 'high CO_2' concentration (used to measure J_{ATP}, see below) a set of pilot light response curves at decreasing C_a were performed. 600 µmol mol^{-1} was chosen because i) further increases in CO_2 concentration did not result in higher A; ii) stomatal closure was not strongly induced; iii) it was sufficiently similar to lab CO_2 concentration (550 µmol mol^{-1}) to minimize the problem of CO_2 diffusion out of the cuvette (Flexas *et al.*, 2007). Gas flow was set at 150 µmol s^{-1} (PAR = 500 and 250 µE m^{-2} s^{-1}), 100 µmol s^{-1} (PAR = 125 µE m^{-2} s^{-1}), 75 µmol s^{-1} (PAR = 75 µE m^{-2} s^{-1}) and 50 µmol s^{-1} (PAR ≤ 50 µE m^{-2} s^{-1}). Block temperature was controlled at 26 °C. Stomatal ratio was set to 0.7 (Driscoll *et al.*, 2006). Water pressure deficit was carefully kept below 1 KPa to foster stomatal opening. PSI and PSII yield were measured in reflectance mode with a Dual Pam-F (Heinz Walz GmbH, Effeltrich, D). Pulse intensity was set to 20 mE m^{-2} s^{-1}, enough to saturate F and P signals (saturation occurred between 8 and 10 mE m^{-2} s^{-1}, data not shown). To measure Δ_{OBS}, the IRGA was connected to a cryogenic H_2O and CO_2 trapping-purification line (Griffiths *et al.*, 1990), that concentrated the CO_2 in the low IRGA flow rates. The trapping line consisted of a glass coil in which CO_2 and water were frozen under liquid N_2. 40-50 µmol s^{-1} of gas, taken either from the leaf cuvette or from the reference gas tube, were

trapped for 15 min. A minimum surplus was vented to ensure overpressure in the piping. To match IRGAs the sample flow was periodical redirected towards the IRGA reference channel. After trapping, CO_2 was purified by differential sublimation in a sealed vial for mass spectrometry.

Measurements were performed with a rigid acclimation routine. Before measurements plants were dark-adapted and watered to pot capacity. The distal part of the youngest fully expanded leaf was clamped in the leaf cuvette in the dark. Maximum yield of PSII (F_v / F_m) and P_m, signal were registered (details of PSI measurements are reported in Figure 2.7). An initial light response curve (500, 250, 125, 75, 50 and 30) μE m^{-2} s^{-1} was registered at 2 % O_2 and C_a = 600 μmol / mol. Leaves were acclimated for > 30 min at the beginning and > 15 min between each change in PAR level. At steady state, a saturating pulse was applied and assimilation was recorded every 30 s for 5 min. A second light response curve was registered at 21 % O_2 and reference CO_2 set at 400 μmol / mol, during which exhaust gas was trapped to determine Δ_{OBS}. A rigorous routine, consisting of 20 min acclimation, 15 min trapping, 7 min acclimation and 15 min trapping was followed for each PAR level. Assimilation was recorded every 30 s throughout trapping, while pulses were applied twice to minimise photobleaching.

This routine yielded a total of 12 CO_2 samples collected during trapping and 6 reference gas collected during acclimation for each of 4 LL plants and 3 HL plants. CO_2 was analysed directly with a VG SIRA dual inlet isotope ratio mass spectrometer (modified and maintained by Pro-Vac Services Ltd, Crewe, UK). Values were corrected for presence of N_2O and ^{17}O. Δ_{OBS} was calculated according to Evans et al. (1986) and reflects an average for 15 minutes continuous photosynthetic discrimination (equations are reported in supporting Text 2).

Figure 2.7. Photosystem I yield determined with the saturating pulse method

P_m, the *P* signal corresponding to the total oxidation of PSI, was determined right after the determination of *Fv* / *Fm*. To increase *P* signal a 5 mm wide strip of aluminium foil (reflecting IR radiation) was fitted 4 mm below the leaf (E. Pfündel, personal communication). PSI was activated for 5 min with a low intensity red light (red LED, maximum emission at 635 nm, 40 µE m^{-2} s^{-1}), then the P_m determination procedure was triggered: it consists of 10 s of strong far red light (735 nm) and a saturating pulse (intensity 20 mE m^{-2} s^{-1} as rated by the instrument, duration 100 ms). The impulse was sufficient to induce F signal saturation (which occurred between 8 and 10 mE m^{-2} s^{-1}, data not shown) and full oxidation of PSI, whereby the *P* signal was at maximum P_m. The Yield of photosystem I *Y(I)* was determined according to (Klughammer and Schreiber, 1994, 2008) as

$$Y(I) = \frac{P_m' - P}{P_m - P_0} \qquad (17)$$

where: P_m' is the saturating pulse induced P signal during steady state photosynthesis, *P* is the steady state *P* signal and P_m is the maximum *P* signal and P_0 is the minimum *P* signal.

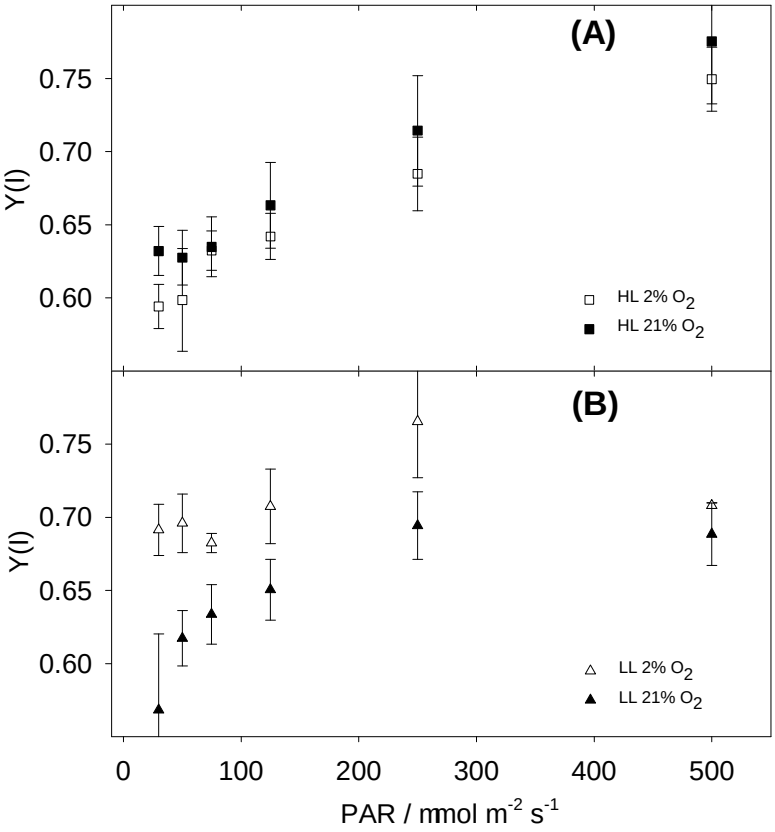

2.5.4 Total ATP production rate J_{ATP}

J_{ATP} was derived from gas exchanges at low O_2 concentration and corrected under ambient O_2. I adopted a gas exchange / fluorescence approach as it did not rely on assumptions or uncertain parameterization. This method was used in previous studies (Yin and Struik, 2009; Yin *et al.*, 2011b) where a linear relationship between J_{ATP} and electron transport rate, ETR (Krall and Edwards, 1990; Oberhuber *et al.*, 1993) was assumed. I observed a slight deviation of J_{ATP} / ETR from linearity at irradiance 500 µE m^{-2} s^{-1}, consistent with previous data (D'Ambrosio *et al.*, 2003). Instead of linearizing the relationship, I scaled J_{ATP} to ETR individually at each irradiance (the calculation is identical to the original method when the relationship is linear).

$J_{ATP\ Low\ O2}$ was calculated from gross assimilation (*GA*) measured under low O_2. Under low O_2, Φ and photorespiration are minimal (Kromdijk *et al.*, 2010) and the ATP requirement of *GA* (3 / 0.59) is similar to the theoretical minimum (Yin and Struik, 2009; Yin *et al.*, 2011b).

$$J_{ATP\ Low\ O_2} = \frac{3\ GA_{Low\ O_2}}{0.59} \quad (2.1)$$

J_{ATP} (at ambient O_2) was calculated from $J_{ATP\ Low\ O2}$ by correcting for photorespiration using ETR as a scaling factor.

$$J_{ATP} = \frac{J_{ATP\ Low\ O_2}\ Y(II)}{Y(II)_{Low\ O_2}} \quad (2.2)$$

Eqn 2.2 was calculated at each light intensity, the results are the symbols shown in Figure 2.3 A. Note that, of the components of ETR, only *Y(II)* shows in Eqn 2.2 as PAR and compound conversion efficiency (*s'*) simplify. For the derivation of Eqn 2.2 see Appendix 1. In C_4 plants photorespiration is low, therefore the difference between $J_{ATP\ LOW\ O2}$ and J_{ATP} was minimal (c. 1 %). Photochemical yield appears both at the numerator and at the denominator of Eqn 2.2, therefore this robust approach is independent of systematic errors that affect both *Y(II)* and $Y(II)_{LowO2}$.

This procedure to derive J_{ATP} was particularly suitable to parameterize and fit the C_4 model. Since J_{ATP} was measured concurrently to gas exchange and isotopic discrimination, it represented the actual J_{ATP} of the portion of the leaf that was subject to isotopic discrimination measurements. Furthermore, J_{ATP} was derived under the same assumptions of the C_4 model (Eqn 2.4 to 2.10, see below). Under these assumptions J_{ATP} represented the fraction of ATP available for photosynthesis and it was not influenced by the ATP allocation to alternative sinks.

2.5.5 Estimated leakiness from isotopic discrimination Φ_{id}

Leakiness was resolved from carbon isotope discrimination (Farquhar, 1983; Farquhar and Cernusak, 2012; Ubierna *et al.*, 2013):

$$\Phi_{id} = \frac{C_{BS} - C_M}{C_M} \frac{b_4 C_M (1+t) + a(C_a - C_i) - C_a \Delta_{OBS} (1-t)}{(1+t)[C_a \Delta_{OBS} (1-t) - a(C_a - C_i) - b_3 C_{BS} + s(C_{BS} - C_M)]} \quad (2.3)$$

Where the subscript 'id' reminds that Φ was obtained from isotopic discrimination, C_a, C_i, C_{BS}, C_M are the CO_2 concentrations in the different compartments; a is the fractionation during CO_2 diffusion in air; s is the fractionation during CO_2 leakage; b_3 is the fractionation of Rubisco CO_2 fixation, corrected for respiration and photorespiration; b_4 is the combined fractionation of $CO_2 \leftrightarrow HCO_3^-$ conversion and PEPC fixation, corrected for mitochondrial respiration in the mesophyll; t represents the ternary effects; other quantities are listed in Table 2.1.

C_a is measured directly by the IRGA, whilst the estimations of C_i, C_M and C_{BS} require modelling.

2.5.6 Modelled C_4 photosynthesis

The C_4 model described below estimated the CO_2 concentrations in the different compartments (C_i, C_M and C_{BS}) that are required to parameterize Eqn 2.3. C_i was estimated through the equations for steady state photosynthesis (Farquhar *et al.*, 1980; von Caemmerer and Farquhar, 1981), directly by the IRGA software. C_M was calculated from the supply function of M as (von Caemmerer, 2000):

$$C_M = C_i - \frac{A}{g_M} \quad (2.4)$$

Where g_M is the mesophyll conductance to CO_2.

C_{BS} was derived from the supply function of BS:

$$C_{BS} = \frac{L}{g_{BS}} + C_M \quad (2.5)$$

Where g_{BS} is BS conductance to CO_2 and L, the leakage rate was calculated from M mass balance:

$$L = V_P - R_M - A \quad (2.6)$$

Where R_M, M respiration rate in the light was assumed half the R_{LIGHT}. V_P, the PEP carboxylation rate is limited by PEP regeneration and ATP supply. It was calculated by partitioning J_{ATP} between C_4 activity (V_P) and C_3 activity (reductive pentose phosphate pathway + photorespiratory cycle) by means of a partitioning factor (x, Table 2.1):

$$V_P = \frac{x J_{ATP}}{2} \quad (2.7)$$

Eqn 2.5, 2.6 and 2.7 can be combined to give:

$$C_{BS} = \frac{\frac{xJ_{ATP}}{2} - \frac{R_{LIGHT}}{2} - A}{g_{BS}} + C_M \quad (2.8)$$

Eqn 2.8 describes the dependency of C_{BS} on the measured quantities A, R_{LIGHT} and J_{ATP}, as a function of g_{BS}. g_{BS} cannot be estimated directly or be derived from previous studies (it

varies between individuals), so it was estimated by curve fitting. To do so, the C_4 model was rearranged to express a measured quantity.

In a first approach (referred to as J / J method) the model was rearranged to express a modelled ATP production rate J_{MOD} (Ubierna ***et al.***, 2013):

$$J_{MOD} = \frac{-y + \sqrt{y^2 - 4wz}}{2w} \quad (2.9)$$

Where $w = \frac{x - x^2}{6A}$; $y = \frac{1-x}{3}\left[\frac{g_{BS}}{A} + \left(C_M - \frac{R_M}{g_{BS}} - \gamma^* O_M\right) - 1 - \frac{\alpha\gamma^*}{0.047}\right] - \frac{x}{2}\left(1 + \frac{R_{LIGHT}}{A}\right)$; $z = \left(1 + \frac{R_{LIGHT}}{A}\right)\left(R_M - g_{BS}\, C_M - \frac{7\, g_{BS}\, \gamma^* O_M}{3}\right) + (R_{LIGHT} + A)\left(1 - \frac{7\alpha\gamma^*}{3 \cdot 0.047}\right)$; α is the fraction of PSII activity in BS cells; γ* is a parameter related to Rubisco O_2 / CO_2 specificity; O_M is the O_2 concentration in M; other variables were previously defined (see also Table 2.1).

J_{MOD} was iteratively calculated at varying g_{BS} until the J_{MOD} matched J_{ATP}. The g_{BS} value that yielded the best fit was assumed as g_{BS} of that individual plant. This operation can be visualized in Figure 2.3 A: the solid lines represent Eqn 2.9 calculated for HL (thick solid line) and LL (thin solid line), with g_{BS} varied until the modelled values (solid lines in Figure 2.3 A) matched J_{ATP} (symbols in Figure 2.3 A). Notably, with the J / J approach g_{BS} was obtained independently of Δ_{OBS} (see discussion).

A different approach (referred to as Δ / Δ method) involved rearranging the C_4 model to express a modelled isotopic discrimination (Kromdijk ***et al.***, 2010):

$$\Delta_{MOD} = a\frac{(C_a - C_i)}{C_a} + (e_s + a_d)\frac{(C_i - C_M)}{C_a} + \frac{b_4 V_P + b_3 L\frac{C_{BS}}{C_{BS} - C_M} - sL}{V_P + L\frac{C_M}{C_{BS} - C_M}}\frac{C_M}{C_a} \quad (2.10)$$

Where (a, a_d, b_3, b_4, e_s, s) are the individual contribution to discrimination and other variables were previously defined (Table 2.1).

Δ_{MOD} was iteratively calculated at different g_{BS}, and the value of g_{BS} that fitted Δ_{MOD} to Δ_{OBS} was assumed as g_{BS} for that individual. This operation can be visualized in Figure 2.3 B. The dotted lines represent Eqn 2.10 calculated for HL (thick dotted lines) and LL (thin dotted

lines), with g_{BS} varied until Δ_{MOD} (dotted lines in Figure 2.3 B) matched Δ_{OBS} (symbols in Figure 2.3 B).

The values obtained for C_{BS} and g_{BS}, with the two fitting approaches described, were used to derive Φ_{id} from isotopic discrimination data Δ_{OBS} as described above.

Modelled leakiness was calculated to compare results of different modelling approaches:

$$\Phi_{MOD} = \frac{L}{V_P} \tag{2.11}$$

2.6 Chapter 2 Tables

Table 2.1. Abbreviations, definitions and units for variables and acronyms described in Chapter 2

Symbol	Definition	Values / Units / References
δ	Isotopic composition relative to Pee dee belemnite	‰
a	^{13}C fractionation due to diffusion of CO_2 in air. Because of vigorous ventilation I neglected the fractionation of the boundary layer.	4.4 ‰ (Craig, 1953; Kromdijk *et al.*, 2010)
A	Net assimilation	µmol m^{-2} s^{-1}
a_d	^{13}C fractionation due to diffusion of CO_2 in water	0.7 ‰ (O'Leary, 1984)
ATP	Adenosine triphosphate	
b_3	^{13}C fractionation during carboxylation by Rubisco including respiration and photorespiration fractionation $b_3 = b'_3 - \frac{e \cdot R_{LIGHT} + f \cdot \frac{1}{2} V_o}{V_c}$.	‰ (Farquhar, 1983)
b_3'	^{13}C fractionation during carboxylation by Rubisco	30 ‰ (Roeske and Oleary, 1984)
b_4	Net fractionation by CO_2 dissolution, hydration and PEPC carboxylation including respiratory fractionation $b_4 = b'_4 - \frac{e' R_M}{V_P}$.	‰ (Farquhar, 1983; Henderson *et al.*, 1992)
b_4'	Net fractionation by CO_2 dissolution, hydration and PEPC carboxylation.	-5.7 ‰ at 25 °C but variable with temperature (Farquhar, 1983; Henderson *et al.*, 1992; Kromdijk *et al.*, 2010).
BS	Bundle sheath	
C_a	CO_2 concentration in the cuvette as measured by IRGA	µmol mol^{-1}
C_{BS}	CO_2 concentration in the bundle sheath	µmol mol^{-1}
C_i	CO_2 concentration in the intercellular spaces as calculated by the IRGA.	µmol mol^{-1} (Li-cor manual Eqn 1-18)
C_M	CO_2 concentration in the mesophyll Eqn 2.8	µmol mol^{-1}
e	^{13}C fractionation during decarboxylation	0 ‰ to -10 ‰ (Barbour *et al.*, 2007; Ghashghaie *et al.*, 2001; Gillon and Griffiths, 1997; Hymus *et al.*, 2005; Igamberdiev *et al.*, 2004; Sun *et al.*, 2012), -6 ‰ in this studystudy (Kromdijk *et al.*, 2010).
e'	^{13}C fractionation during decarboxylation, including the correction for measurement artefacts: $e' = e + \delta\ ^{13}C_{measurements} - \delta\ ^{13}C_{growth\ chamber}$ In this study $\delta^{13}C_{measurements}$ = -9.46 ‰; $\delta^{13}C_{growth\ chamber}$ = -8 ‰	‰ (Stutz *et al.*, 2014; Wingate *et al.*, 2007)
e_s	^{13}C fractionation during internal CO_2 dissolution	1.1 ‰ (Mook *et al.*, 1974; Vogel, 1980; Vogel *et al.*, 1970).
f	^{13}C fractionation during photorespiration.	11.6 ‰ (Lanigan *et al.*, 2008).
F_s	Steady state fluorescence signal	Volts, arbitrary

F_m	Maximum fluorescence signal of dark adapted leaves	Volts, arbitrary
F_m'	Saturating pulse induced F signal during steady state photosynthesis	Volts, arbitrary
GA	Gross assimilation $GA = A + R_{LIGHT}$	µmol m^{-2} s^{-1}
g_{BS}	Bundle sheath conductance to CO_2, calculated by curve fitting	mol m^2 s^{-1}
g_M	Mesophyll conductance to CO_2	1 mol m^2 s^{-1} bar^{-1} (Kromdijk *et al.*, 2010)
g_s	Stomata conductance to CO_2	mol m^2 s^{-1}
HL	High light	
IRGA	Infra red gas analyzer	
J_{MOD}	Modelled ATP production rate Eqn 2.9	µE m^{-2} s^{-1}
J_{ATP}	ATP production rate	µmol m^{-2} s^{-1}
$J_{ATP\ Low\ O2}$	ATP production rate at low O_2 and high CO_2 Eqn 2.1	µmol m^{-2} s^{-1}
L	Rate of CO_2 Leakage from BS to M Eqn 2.6	µmol m^{-2} s^{-1}
LCP	Light compensation point	
LL	Low light	
M	Mesophyll	
O_M	O_2 mol fraction in the mesophyll cells (in air at equilibrium)	210000 µmol mol^{-1}
O_{BS}	O_2 mol fraction in the bundle sheath cells (in air at equilibrium) $O_{BS} = O_M + \frac{\alpha A}{0.047\, g_{BS}}$ (von Caemmerer, 2000)	µmol mol^{-1}
PAR	Photosynthetically active radiation	µE m^{-2} s^{-1}
PEP	Phosphoenolpyruvate	
PEPC	Phosphoenolpyruvate carboxylase	
R_{LIGHT}	Total non photorespiratory CO_2 production in the light	µmol m^{-2} s^{-1}
R_M	Mesophyll non photorespiratory CO_2 production in the light $R_M = 0.5\ R_{LIGHT}$	µmol m^{-2} s^{-1} (Kromdijk *et al.*, 2010; Ubierna *et al.*, 2011; von Caemmerer, 2000)
Rubisco	Ribulose bisphosphate carboxylase oxygenase	
s	Fractionation during leakage of CO_2 out of the bundle sheath cells	1.8 ‰ (Henderson *et al.*, 1992).
s'	Lumped conversion efficiency. Includes leaf absorptance, the partitioning of light to photosystem II and the conversion of energy into ATP	Dimensionless (Yin and Struik, 2009; Yin *et al.*, 2011b)
t	Ternary effects $t = \frac{(1+a)\,E}{2000\, g_{ac}}$ where E / mmol m^{-2} s^{-1} is the transpiration rate (calculated by the IRGA software, parameter Trmmol), g_{ac} / mol m^{-2} s^{-1} is the conductance to diffusion of CO_2 in air (calculated by the IRGA software, parameter CndCO2), a is the isotopic fractionation during diffusion in air.	‰ (Farquhar and Cernusak, 2012)
V_C	Rubisco carboxylation rate $V_C = \frac{(A+R_{LIGHT})}{1-\frac{\gamma^* O_{BS}}{C_{BS}}}$	µmol m^{-2} s^{-1} (Ubierna *et al.*, 2011)

V_O	Rubisco oxygenation rate $V_O = \frac{V_C - A - R_{LIGHT}}{0.5}$	µmol m^{-2} s^{-1} (Ubierna *et al.*, 2011)
V_P	PEP carboxylation rate Eqn 2.7	µmol m^{-2} s^{-1}
x	Partitioning factor of J_{ATP} between C_4 activity V_P (PEP regeneration and PEP carboxylation, Eqn 2.7) and C_3 activity V_C+V_O (reductive pentose phosphate pathway and photerespiratory cycle)	0.4 (Kromdijk *et al.*, 2010; Ubierna *et al.*, 2011; Ubierna *et al.*, 2013; von Caemmerer, 2000)
α	Fraction of PSII active in BS cells	0.15 (Edwards and Baker, 1993; Kromdijk *et al.*, 2010; von Caemmerer, 2000).
γ^*	Half of the reciprocal of the Rubisco specificity	0.000193 (von Caemmerer, 2000).
Δ	Carbon Isotope discrimination against ^{13}C	‰
Δ_{OBS}	Observed carbon Isotope discrimination against ^{13}C, Eqn 2.16 Appendix 1	‰
Φ	Leakiness $\Phi = L/V_p$	dimensionless
Φ_{id}	Leakiness estimated with the isotope method including respiratory and photorespiratory fractionation and calculating C_{BS} Eqn 2.3	dimensionless (Ubierna *et al.*, 2011)
Φ_{MOD}	Leakiness estimated with the C_4 light limited photosynthesis equations Eqn 2.11	dimensionless
Y(II)	Yield of photosystem II $Y(II) = \frac{F'_m - F_s}{F'_m}$	dimensionless (Genty *et al.*, 1989)

Table 2.2. Response of HL plants and LL plants to different O_2 concentrations

Assimilation at 50 µE m^{-2} s^{-1} (A_{50}) is shown to exemplify limiting light conditions. The light compensation point *LCP* was determined fitting a quadratic equation with the use of dedicated software (Photosyn assistant 1.2, Dundee Scientific, Dundee, UK) (Dougherty *et al.*, 1994; Prioul and Chartier, 1977). Respiration in the light R_{LIGHT} was determined by linear regression of *A* against PAR·*Y(II)* / 3 (see Appendix 1 to Chapter 2). *s′* was the slope of the linear regression of *A* against PAR·*Y(II)* / 3 and represented the lumped conversion efficiency of PAR into ATP.

Means ± SE are shown. Within rows means were not significantly different in a t-test for P < 0.05. n = 7

		21 % O_2		2 % O_2	
	Unit	**LL**	**HL**	**LL**	**HL**
A_{50}	µmol m^{-2} s^{-1}	2.29 ± 0.0096	1.83 ± 0.022	2.69 ± 0.11	2.10 ± 0.18
LCP	µE m^{-2} s^{-1}	8.35 ± 0.12	17.0 ± 0.18	3.83 ± 1.4	12.3 ± 2.8
R_{LIGHT}	µmol m^{-2} s^{-1}	0.520 ± 0.017	1.00 ± 0.069	0.291 ± 0.036	0.924 ± 0.099
s′	1	0.224 ± 0.0019	0.225 ± 0.0062	0.231 ± 0.0044	0.248 ± 0.0094

Table 2.3 Bundle sheath conductance estimated by curve fitting

J / J fitted a modelled ATP production ratio (J_{MOD}), on a measured J_{ATP} (determined with the chlorophyll fluorescence – low O_2 method). Δ / Δ fitted a modelled isotopic discrimination Δ_{MOD}, to the measured isotopic discrimination Δ_{OBS}. Different letters were deemed significant for $P < 0.05$ in a Tukey multiple comparison test (Genstat). Average values ± S.E. LL n = 4; HL n = 3.

		g_{BS}	
Fitting approach	**Unit**	**LL**	**HL**
J / J	mol m^{-2} s^{-1}	$8.20 \cdot 10^{-4} \pm 1.4 \cdot 10^{-4}$ a	$10.3 \cdot 10^{-4} \pm 1.8 \cdot 10^{-4}$ a
Δ / Δ	mol m^{-2} s^{-1}	$12.7 \cdot 10^{-4} \pm 1.3 \cdot 10^{-4}$ a	$46.4 \cdot 10^{-4} \pm 8.8 \cdot 10^{-4}$ b

3 Plasticity of C_4 biochemistry

Published in Plant Physiology as: 'The operation of two decarboxylases (NADPME and PEPCK) and partitioning of C_4 metabolic processes between mesophyll and bundle sheath cells allows light capture to be balanced by the maize C_4 pathway'. (Bellasio and Griffiths, 2014c).

3.1 Introduction

Interest in the C_4 pathway has been increased by the potential for enhancing crop productivity and maintaining yield stability in the face of global warming and population pressure (Covshoff and Hibberd, 2012; Friso *et al.*, 2010; Zhu *et al.*, 2010). Maize (*Zea mays*, L.), a C_4 plant of the NADP-ME subtype, is a leading grain production cereal (FAO, 2012). C_4 photosynthesis is a shared activity between mesophyll (M, abbreviations listed in Table 1) and bundle sheath (BS) cells, coupled to allow the operation of a biochemical carbon concentrating mechanism (CCM). The CCM effectively minimizes photorespiration by increasing the CO_2 concentration in BS (C_{BS}), where Rubisco is exclusively expressed. Since BS and M are connected by plasmodesmata, some CO_2 retrodiffuses. The refixation of that escaping CO_2 by the CCM increases the activity of the CCM and the total ATP demand ($ATP_{BS} + ATP_M$) for gross CO_2 assimilation (GA), ($ATP_{BS} + ATP_M$) / GA), from a theoretical minimum of 5 ATP (Furbank *et al.*, 1990). Leakiness (Φ), the amount of CO_2 retrodiffusing relative to PEP carboxylation rate, is therefore a proxy for the coordination between the CCM and assimilatory activity (Bellasio and Griffiths, 2014b; Henderson *et al.*, 1992; Kromdijk *et al.*, 2010; Tazoe *et al.*, 2008; Tazoe *et al.*, 2006; Ubierna *et al.*, 2011).

The NADP-ME subgroup has been shown to be complicated by the presence of two BS decarboxylation enzyme systems (NADP-ME and PEP carboxykinase, PEPCK), presumably both acting as CO_2 delivery pathways (respectively *via* malate, MAL or aspartate, ASP) (Eprintsev *et al.*, 2011; Furbank, 2011; Furumoto *et al.*, 1999, 2000; Pick *et al.*, 2011; Wingler *et al.*, 1999). There is also an extensive overlap between BS and M functions since both cell types can synthesize carbohydrates (Kanai and Edwards, 1999; Spilatro and Preiss, 1987) and reduce phosphoglyceric acid, PGA (Majeran and van Wijk, 2009) (see the overall scheme in Fig. 3.1). Additionally, energetic partitioning can also vary between cell types, since the total ATP produced (J_{ATP}) per CO_2 fixed in GA (J_{ATP} / GA) may be produced in BS (mainly through cyclic electron flow around PSI) or in M (mainly through linear electron flow) depending on the light *locally* available in BS or M (Kramer and Evans, 2011; Yin and Struik, 2012). Furthermore, although all NADPH is produced in M, the only compartment operating linear electron transport and oxidising water [(Majeran *et al.*, 2005; Majeran *et al.*, 2010), see also refs in Paragraph 3.3.3], a fraction of NADPH is exported to BS through MAL diffusion, to meet the reducing power demand therein ($NADPH_{BS}$). To capture the

complex C_4 physiology, several models of C_4 photosynthesis have been developed (Berry and Farquhar, 1978; Laisk and Edwards, 2009; Laisk and Edwards, 2000; von Caemmerer, 2000). The earlier approaches were developed into the von Caemmerer (2000) C_4 model. In particular the associated light limited equations (referred subsequently as the 'C_4 model'), are used to estimate the parameters needed to resolve the isotopic discrimination model, widely employed to study leakiness under low light conditions [for review see (Kromdijk *et al.*, 2014; Ubierna *et al.*, 2011; von Caemmerer, 2013)]. The C_4 model partitions J_{ATP} into two fractions: i) the ATP consumed by PEP carboxylase (PEPC) and ii) the ATP consumed by the C_3 activity (glycolate recycling, PGA reduction, and RuBP regeneration). These activities are located in M, BS or in both compartments (see the overall scheme in Figure 3.1). However, the C_4 model simplifies the spatial compartmentalization between BS and M, and in this Chapter I now develop the energetic implications of the differential contribution of M and BS to C_4 photosynthesis under different light regimes.

Because of these anatomical, metabolic and energetic complexities, C_4 metabolism is highly sensitive to limiting light intensity [Chapter 2, (Bellasio and Griffiths, 2014b)], and potentially light quality (Evans *et al.*, 2007; Sun *et al.*, 2014; Sun *et al.*, 2012; Wang *et al.*, 2014a). Light quality has a greater influence on C_4 photosynthesis than on C_3. Leaf pigments preferentially absorb the blue and red region of the spectra and some wavelengths penetrate deeper into leaves. It was shown in C_3 leaves that exposure to different wavelengths results in characteristic light penetrations profiles, which translated into different gradients in photosystem II yield, rates of ATP production and assimilation (A) within the leaf (Terashima *et al.*, 2009). In C_4 leaves, because of the concentric anatomy, light reaches M cells before the deeper BS (Evans *et al.*, 2007), and could alter the balance between light harvesting and energetic partitioning between BS and M (Sun *et al.*, 2014; Sun *et al.*, 2012).

In this Chapter, I model the likely profiles of light penetration for specific wavelengths associated with Red, Green and Blue (R, G, B) light within a maize M and BS leaf cross section, and calculate the impact on potential ATP production for each cell type. I calculate the proportion of absorbed light (AB) for each wavelength, expressed as $AB\ BS\ /\ M$, the fraction of photons absorbed in BS relative to the photons absorbed in M, from which I derive J_{ATPBS} / J_{ATPM}, the fraction of ATP produced in BS relative to the ATP produced in M. Secondly, I developed a steady-state metabolic model (Fig. 3.1, Table 3.2), which augments

the conventional C_4 model (von Caemmerer 2000), to capture the spatial separation between BS and M and partitions the ATP demand between BS and M cells in terms of PGA reduction (PR), carbohydrate synthesis (SS) and PEP regeneration, so as to meet the ATP availability in each cell type (Evans ***et al.***, 2007). Thirdly, photosynthetic characteristics (leaf level ATP production rate, CO_2 assimilation, stomatal conductance and Φ derived from on-line carbon isotope discrimination) were measured under R, G, B, and RGB in combination, using a decreasing photon flux density (from 500 to 50 μE m^{-2} s^{-1}) to investigate the importance of metabolic plasticity under limiting light intensities.

For instance, ***AB BS / M*** and J_{ATPBS} / J_{ATPM}, were both lower under the blue wavelengths (460 nm), which are rapidly extinguished within the M leaf profile, than under white light, confirming that light quality perturbs C_4 energetics. In spite of this shift, when maize plants were exposed to different light qualities there was no change in Φ indicating that, ***at steady state***, the co-ordination between CCM activity and Rubisco assimilation was retained (Sun ***et al.***, 2012; Ubierna ***et al.***, 2011). The modelled metabolic plasticity projected a window for ATP demand partitioning, ATP_{BS} / ATP_M, which matched the values for J_{ATPBS} / J_{ATPM} supply estimated under B, G and R wavelengths. I show that the plasticity of C_4 metabolism, and in particular the possibility of shifting between malate and aspartate as primary carboxylase product, were of pivotal importance in allowing plasticity of ATP and NADPH demand. In conclusion, this Chapter explains the extensive overlap between BS and M functions and the requirement for at least two decarboxylase systems in NADP-ME subtype plants such as maize, providing an explanation for empirical observations on diversity of decarboxylase activities and PEP regeneration pathways (Chapman and Hatch, 1981; Eprintsev ***et al.***, 2011; Furbank, 2011; Pick ***et al.***, 2011; Rathnam, 1978; Wingler ***et al.***, 1999).

Figure 3.1. Metabolic model of C₄ assimilation: BS/M reaction rates and fluxes

The overall scheme reports the reactions of the CCM (Furbank, 2011), Rubisco carboxylation, the reactions of the RPP pathway, the synthesis of starch, respiration and glycolate recycling reactions. The tables, with the corresponding enzyme name, show the actual reaction rates, expressed as relative to *GA* (5.13 μmol /m^{-2} s^{-1}), per unit of substrate transformed. Rates were estimated by parameterizing the model equations (Table 3.2) with data measured under PAR = 125 μE m^{-2} s^{-1} (A = 3.96 μmol m^{-2} s^{-1}; R_{LIGHT} = 1.17 μmol m^{-2} s^{-1}; J_{ATP} = 28.6 μmol m^{-2} s^{-1}), the output of the C₄ model (V_C=5.35 μmol m^{-2} s^{-1}; V_P=5.89 μmol m^{-2} s^{-1}; V_O=0.44 μmol m^{-2} s^{-1}) and the output of the isotopic discrimination model (Φ = 0.23), under three characteristic ratios of ATP partitioning. These were numbered 1, 2 and 3. Condition 1 corresponds to the lowest ATP available in BS (ATP partitioning similar to that under blue light, Fig. 4 B), condition 2 correspond to an intermediate ATP availability in BS (ATP partitioning equal to that under red light, Fig. 3.4 B), condition 3 corresponds to the highest ATP available in BS (ATP partitioning equal to that under green light, Fig. 3.4 B). The inset shows net metabolite fluxes between M and BS in multiples of *GA*. The ATP demand in BS (ATP_{BS}) and M (ATP_M), the total NADPH demand ($NADPH_{TOT}$) and the NADPH demand in BS ($NADPH_{BS}$) were also calculated in the same three relevant conditions.

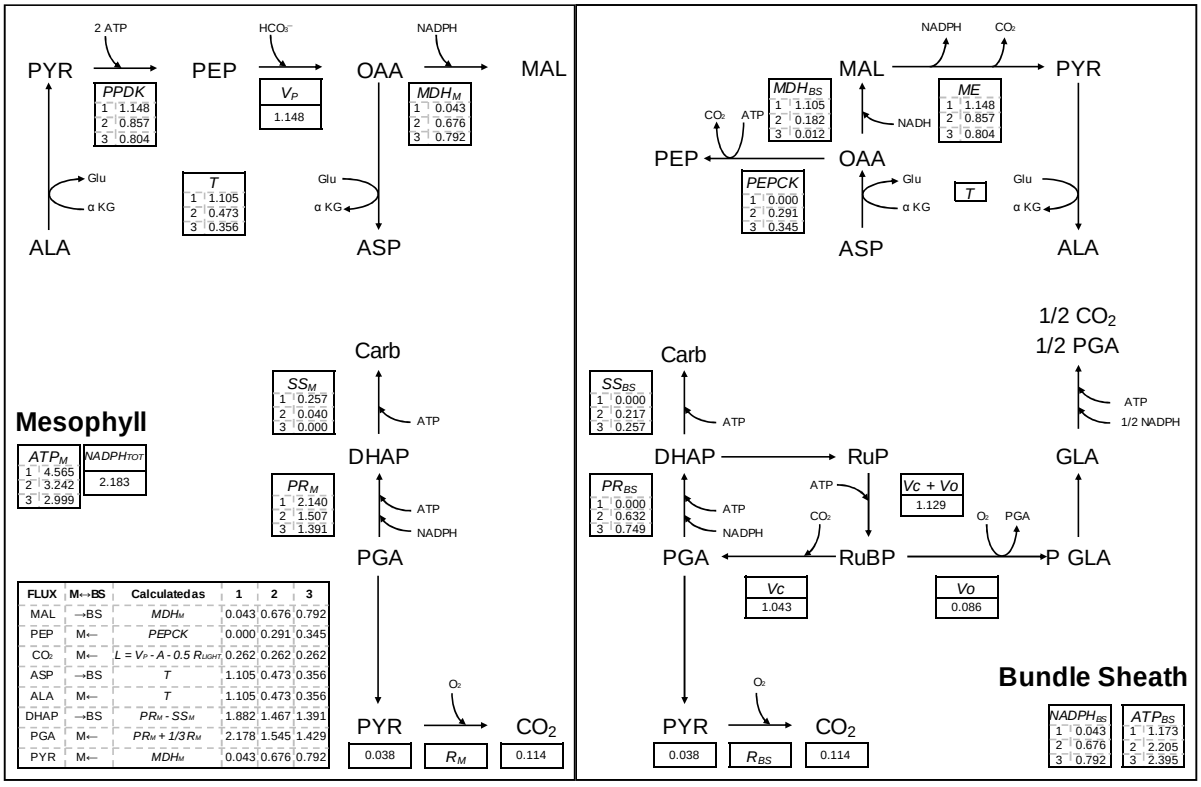

3.2 Results

3.2.1 Metabolic modelling of partitioning between BS and M

The complexity of C_4 biochemistry (Furbank, 2011) was first integrated in a comprehensive steady-state model (Fig. 3.1), with key processes described by rate equations (Fig. 3.1, Box; Table 3.2) and associated ATP demand (Eqn 3.11-3.13 in Table 3.2). This model captures the spatial separation between BS and M, the different pathways of the CCM (through ASP and MAL), the different carboxylating enzymes and the process of carbohydrate synthesis, as a means to develop the traditional C_4 model (von Caemmerer 2000). The metabolic model (Fig. 3.1) was generated on the assumption that ATP does not freely diffuse between BS and M and any light-induced J_{ATPBS} / J_{ATPM} fluctuations have to be countered by changing the partitioning of ATP demand (for a list of abbreviations see Table 3.1). Fig. 3.1 depicts the reactions which are localized in BS, in M or in both compartments. RuP phosphorylation is uniquely localized in BS to supply RuBP directly in proximity to Rubisco, and facilitate the substrate saturation of the enzyme. Glycolate recycling is also a BS exclusive reaction (Fig. 3.1) (Yoshimura *et al.*, 2004). This feature contributes to the CCM (the so called C_2 cycle) and, in an evolutionary perspective, it was acquired at an early stage (Sage *et al.*, 2012; Schulze *et al.*, 2013). PEP regeneration through PEP carboxykinase (PEPCK) is located uniquely in BS (Wingler *et al.*, 1999), while PEP regeneration through pyruvate phosphate dikinase (PPDK), is located primarily in M (Fig. 3.1) (Bailey *et al.*, 2007; Friso *et al.*, 2010; Majeran *et al.*, 2010), and any PPDK activity in BS is generally neglected (von Caemmerer, 2000) (see also Discussion). PGA reduction (PR), respiration, and carbohydrate synthesis (SS) are processes located both in BS and M (Friso *et al.*, 2010; Kanai and Edwards, 1999; Majeran and van Wijk, 2009; Spilatro and Preiss, 1987).

These processes are described in detail below, after an initial comparison of modelled light profiles and measured photosynthetic characteristics under R, G and B wavelengths, to give a quantitative description of the biochemical mechanisms underpinning acclimation, fluxes and reaction rates, the dynamics of Φ and the effects on the total and relative ATP demand for assimilation.

3.2.2 Effect of light quality on ATP production in BS and M

To study the influence of light quality on ATP production partitioning, J_{ATPBS} / J_{ATPM}, I first modelled C_4 anatomy (Figure 3.2 left). Light penetration was modelled in two characteristic profiles using the absorption-scattering theory (Figure 3.2 right). Profiles were calibrated with leaf transmittance and reflectance at different wavelengths. Blue light was strongly absorbed (steep profile), green light was weakly absorbed (gradual profile) while red light had an intermediate profile of light penetration. These three profiles were integrated to estimate the contribution of absorbed light within abaxial + abaxial mesophyll, interveinal mesophyll and bundle sheath (Figure 3.2), and calculated the partitioning of absorbed light (AB) in BS and M (***AB BS / M***) under five relevant conditions (Table 3.3). ***AB BS / M*** was used in turn to estimate the partitioning of ATP production, J_{ATPBS} / J_{ATPM} (Table 3.3) under the assumption that photochemical yield did not vary through the leaf profile (see 'Estimated ATP production partitioning' in Material and Methods). At 400 nm, ***AB BS / M*** was lowest, representing J_{ATPBS} / J_{ATPM} of 0.29; at 540 nm, ***AB BS / M*** was highest together with J_{ATPBS} / J_{ATPM} (0.96). Under blue light, J_{ATPBS} / J_{ATPM} was close to the lowest value (0.31), increasing under red (0.68), natural white light (0.76) and green light (0.80). These values were derived independently of light intensity so they can be considered to reflect the actual ATP availability in BS and M under a wide range of light intensities. Since it is assumed that ATP does not diffuse between BS and M, and has a relatively small pool, at steady state, J_{ATPBS} / J_{ATPM} can be directly compared to the ATP demand partitioning, ATP_{BS} / ATP_M. For this comparison, the values for J_{ATPBS} / J_{ATPM} under blue, red, white and green light were used subsequently to plot Fig. 3.4 B. The model predicts that light quality will unbalance the partitioning of ATP production, and a comprehensive ecophysiological investigation was therefore used to compare gross assimilation and ATP supply and partitioning between B and M cells.

Figure 3.2. Light penetration in a maize leaf

Left panel shows the modelled maize anatomy: a square BS is surrounded by three portions of mesophyll: interveinal mesophyll (MI), adaxial mesophyll (MAD) and abaxial mesophyll (MAB). Epidermis was approximated as a flat reflecting surface. Light penetration was studied through profiles P1 and P2. Right panel shows P1-light profiles (bold lines) and P2-light profiles (thin lines) calculated with the Kubelka-Munk (absorption + scattering) theory and calibrated with spectroscopic data (Table 3.3). Radiation is expressed as the sum of downward + upward photon flux, as a fraction of incident photon flux (dimensionless), and plotted against the depth in the absorbing path of the leaf.

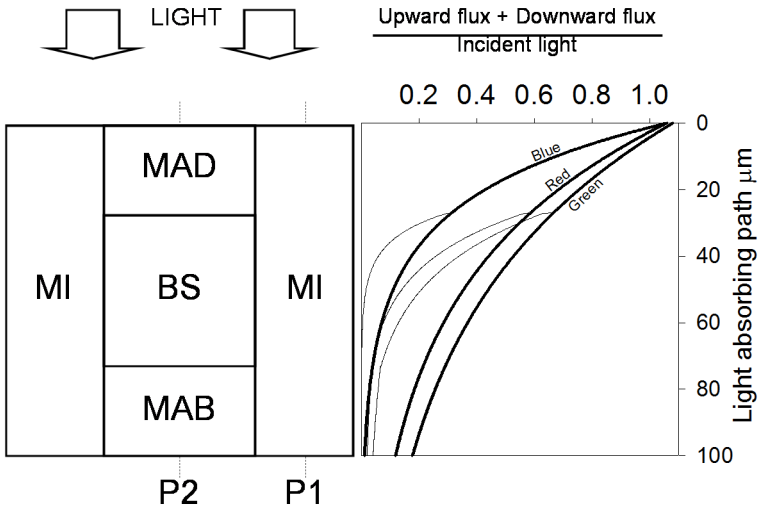

3.2.3 Effect of light quality on assimilatory traits

Figure 3.3 shows the responses of maize to different light qualities (Red, R; Green, G; Blue, B; or RGB combined) measured under decreasing irradiance. Net assimilation (*A*), measured through gas exchange (Figure 3.3 A), and J_{ATP} (Figure 3.3 B) measured with the low O_2 - ETR method using a saturating light pulse, were significantly higher under R light and decreased under RGB, G and B. Light quality had no significant effect on stomatal conductance (g_s, Figure 3.5 A), but *Ci* / *Ca* was lower under R light (Figure 3.5 B) as a consequence of the higher *A*. The CO_2 concentration in BS (C_{BS}), estimated by fitting a C_4 photosynthesis model to J_{ATP}, was higher under R and G light (Figure 3.5 C), because of the higher *A*. The light compensation point (*LCP*), bundle sheath conductance (g_{BS}) and respiration in the light (R_{LIGHT}) were not significantly influenced by light quality (Table 3.4).

With the precise estimate of R_{LIGHT} and J_{ATP}, I calculated J_{ATP} / *GA*, which represents the experimentally-determined ATP cost for gross assimilation. J_{ATP} / *GA* was not influenced by light intensity but varied between light qualities from 5.37 to 5.73, under B, R, RGB and G light. J_{ATP} / *GA* was then used in Figure 3.4 B, plotted against the ATP production partitioning J_{ATPBS} / J_{ATPM}, found above. The relatively minor increase in J_{ATP} / *GA* (c 0.3 ATP / CO_2) observed experimentally contrasts with the metabolic disruption theoretically predicted under these conditions (Evans *et al.*, 2007). My data were supported by real-time isotopic discrimination, Δ (Figure 3.3 C) and leakiness, Φ (Figure 3.3 D), which were not influenced by light quality, showing that the plant coped with a 2.5x shift in J_{ATPBS} / J_{ATPM} without any imbalance in the CCM / assimilation coordination. Leakiness, J_{ATP} / *GA* and the window of J_{ATPBS} / J_{ATPM} formed the basis of a metabolic model used to describe these biochemical responses.

Figure 3.3. Maize responses to decreasing light intensity under different light qualities

Net assimilation (*A*). The curves were fitted in order to calculate the light compensation point (Table 3.4). The inset shows a magnification. **(B)** Total ATP production rate (J_{ATP}), measured with the low O_2 - ETR method. **(C)** On-line isotopic discrimination during photosynthesis (Δ). **(D)** Leakiness (Φ) resolved from Δ. Error bars represent standard error. n=4.

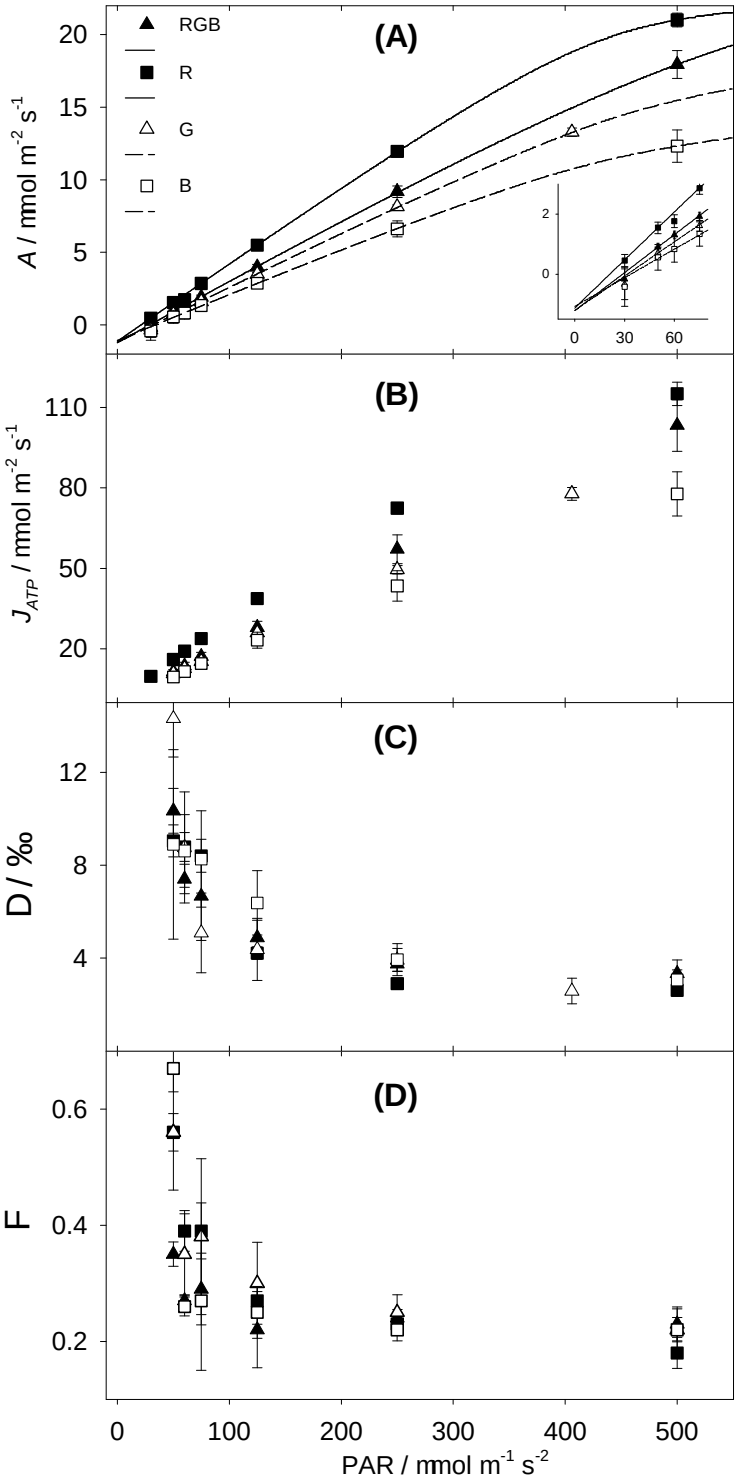

Figure 3.4. Partitioning of metabolic activities and associated ATP and NADPH demand

Partitioning of metabolic activities in BS cells and associated shifts in ATP and NADPH demand. Panel (A), the output of the metabolic model, shows as a function of increasing theoretical ATP demand partitioning (ATP_{BS} / ATP_M), i) the increasing contribution of BS (solid lines) to the total PGA reduction (PR, relative to the total), carbohydrate synthesis (SS, relative to the total) and PEPCK (relative to the highest rate); ii) the predicted NADPH demand in BS, relative to the total ($NADPH_{BS}$ / $NADPH_{TOT}$, dotted line), and iii) the predicted transamination rate, relative to V_P (T / V_P, dashed line). In panel (B) the output of the metabolic model is compared with the empirical data. Model output is shown by a dashed line: the predicted ATP demand for gross assimilation (ATP_{BS} + ATP_M) / GA is plotted as a function of predicted ATP demand partitioning ATP_{BS} / ATP_M. Empirical data are shown as diamonds: the measured J_{ATP} / GA, under blue, red, RGB and green light (Table 3.1), is plotted against the estimated ATP production partitioning J_{ATPBS} / J_{ATPM} at 460 nm, 635 nm, white light and 522 nm (estimated through the optical model, Table 3). The lowest ATP_{BS} / ATP_M was named condition 1 (left arrow), the partitioning corresponding to red light was named condition 2 (central arrow) while the highest ATP_{BS} / ATP_M was named condition 3 (right arrow).

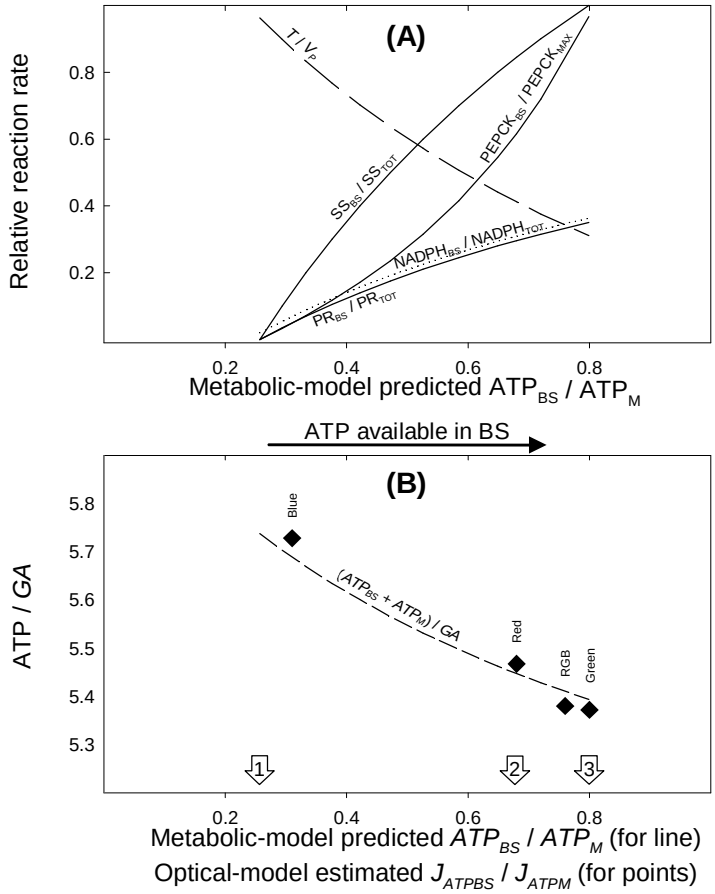

Figure 3.5. Stomatal responses and modelled CO_2 concentration in bundle sheath cells

(A) Stomatal conductance and **(B)** *Ci* / *Ca* responses measured by gas exchange under decreasing light intensity, and under different light qualities; **(C)**: response of C_{BS} to decreasing light intensity, under different light qualities, estimated by the C_4 model. Error bars represent standard error. n=4.

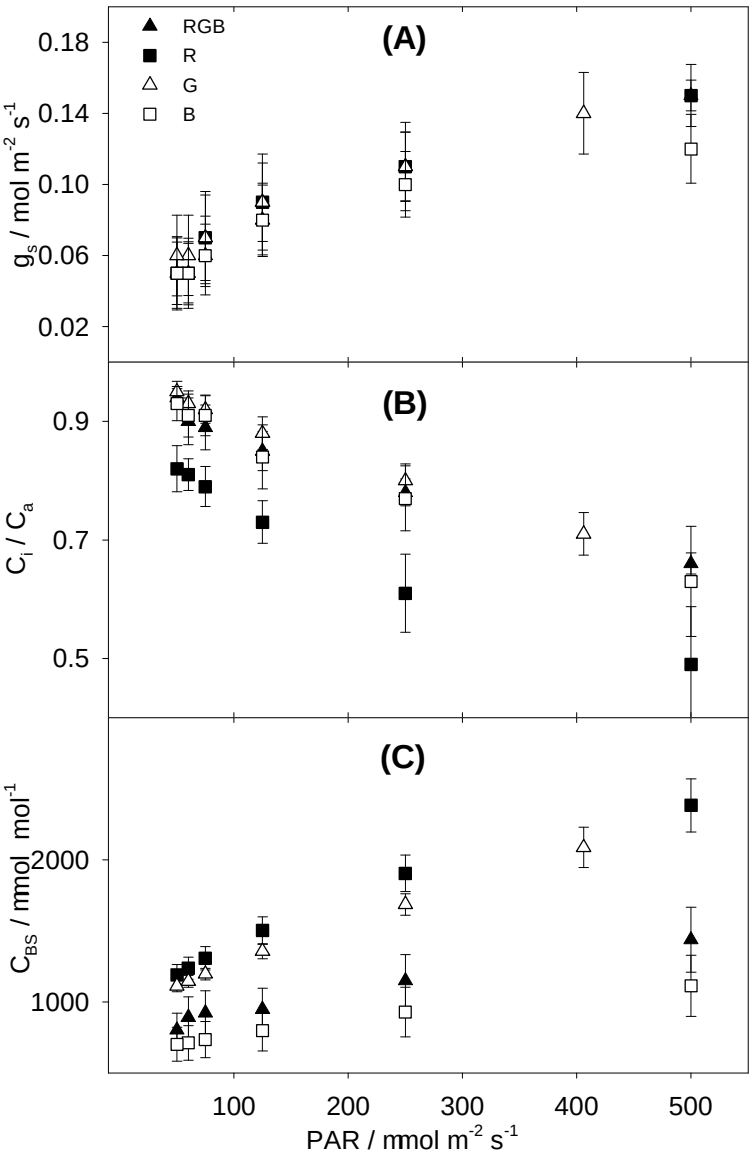

3.2.4 Influence of BS activity on assimilatory metabolism and ATP demand (total and relative)

The comprehensive metabolic model (Figure 3.1) was developed to describe the biochemical reactions directly and indirectly involved in C_4 assimilation by rate equations (Table 3.2). Three assimilatory ATP-consuming processes [carbohydrate synthesis (SS), phosphoglyceric acid reduction (PR) and PEP carboxykinase (PEPCK)] were increasingly manipulated to increase in BS (Figure 3.4 A). These processes overlap between BS and M and could be increasingly allocated to BS without influencing the overall assimilation rate. By means of this progressive allocation, I predicted: i) the minimum and maximum ATP demand partitioning, ATP_{BS} / ATP_M (Eqn 3.12 / Eqn 3.13, Table 3.2); ii) the reaction rates and metabolite fluxes at a given ATP_{BS} / ATP_M, including the rate of PEPCK and PPDK, the relative CO_2 flux through ASP and MAL and the partitioning of PGA reduction between BS and M; iii) the dynamics of total ATP demand for gross assimilation (ATP_{BS} + ATP_M) / GA at variable ATP_{BS} / ATP_M.

When the BS projected activation rate of PR, PEPCK and SS was zero (referred as condition 1 in Figure 3.1 and Figure 3.4 B), the predicted ATP_{BS} / ATP_M was lowest (0.27). This value was comparable to J_{ATPBS} / J_{ATPM} resolved from the optical model under blue light (400 nm and 460 nm, Table 3.3), showing that metabolism could reduce ATP demand to match even the lowest ATP supply in BS. In this condition the ATP demand in BS was brought about by RuP phosphorylation and glycolate recycling, two processes that are forcedly localized in BS. The predicted (ATP_{BS} + ATP_M) / GA was 5.74 (Figure 3.4 B, dashed line), in agreement with J_{ATP} / GA measured under blue light (5.73, Figure 3.4 B, blue square). Since photosynthetic PGA production is always localized in BS (primarily from Rubisco carboxylase, or oxygenase activity and glycolate recycling), when there is no ATP available for PGA reduction, (in condition 1) the PGA diffuses to M and is reduced therein. After reduction, DHAP could supply carbohydrate synthesis in M and diffuse back to BS to regenerate RuBP. The predicted NADPH demand in BS ($NADPH_{BS}$) was therefore the lowest (Eqn 3.14, Table 3.2; Figure 3.4 A, dotted line), corresponding to the NADPH demand for glycolate recycling in BS. The activity of malate dehydrogenase in M (MDH_M), process responsible for exporting NADPH, was reduced by diverting the substrate oxaloacetate (OAA) to transamination to aspartate (ASP). Hence, in condition 1, MDH_M had the lowest

activity (Figure 3.1, Eqn 3.16 in Table 3.2) while ***T*** had the highest rate (Figure 3.1, Figure 3.4 A, dashed line, Eqn 3.17 in Table 3.2). Once ASP diffused to BS, it underwent a futile reduction-oxidative decarboxylation [see also (Eprintsev ***et al.***, 2011; Furbank, 2011), and references therein] that resulted in net CO_2 flux without a conjoint NADPH translocation (Figure 3.1).

When PR and SS were progressively manipulated to increase in BS, the predicted ATP demand ATP_{BS} / ATP_M (Figure 3.1, Figure 3.4) progressively increased. The activation of PEPCK in BS not only contributed to the predicted increasing ATP demand in BS, but also lowered the predicted ATP cost of assimilation (ATP_{BS} + ATP_M) / GA because PEPCK regenerates PEP with half the ATP demand of PPDK [although the PEP produced in BS may be recycled to the C_4 cycle through multiple pathways (Smith and Woolhouse, 1983), for simplicity here I assumed that the PEP produced by PEPCK is recycled through the most energy-efficient pathway according to (Rathnam and Edwards, 1977): PEP directly diffuses to M and supplies the activity of PEPC,.]. Condition 2 represents a state where ATP_{BS} / ATP_M equals J_{ATPBS} / J_{ATPM} resolved from the optical model under red light (0.68, Table 3.3). The predicted (ATP_{BS} + ATP_M) / GA (5.45, Figure 3.4 B, dashed line) agreed with J_{ATP} /GA measured under red light (5.47, Figure 3.4 B, red square).

When the projected allocation of PR, PEPCK and SS to BS was highest (referred as condition 3, Figure 3.1, Figure 3.4 A), the predicted ATP_{BS} / ATP_M was 0.8. This partitioning equals J_{ATPBS} / J_{ATPM} estimated by the optical model under green light, and it is similar to J_{ATPBS} / J_{ATPM} estimated under natural white light (0.76, Table 3.3). Because PEPCK was activated at a highest rate, only 70 % of PEP was regenerated through PPDK and (ATP_{BS} + ATP_M) / GA was lowest (5.39, Figure 3.4 B, dashed line), predicting well J_{ATP} /GA values measured under RGB (5.38, Figure 3.4 B, RGB square) and green light (5.37, Figure 3.4 B, green square). In condition 3, PGA reduction in BS was highest, determining the highest $NADPH_{BS}$ (Figure 3.1; Figure 3.4 A dotted line; Eqn 3.14, Table 3.2) and the highest MDH_M activity (Figure 3.1, Eqn 3.16 in Table 3.2). Because most of the OAA produced by PEP carboxylase was reduced by MDH_M, T was lowest, just enough to supply PEPCK activity in BS.

3.2.5 Estimate of actual reaction and diffusion rates

Since all C_4 reactions were described by rate equations (Table 3.2) I could estimate actual reaction rates. Although the predictions shown so far (including the optical part) are largely independent of light intensity, in this step rates had to be calculated at a specific light intensity. In order to compare these values in a wider range of light intensities, rates were expressed as relative to *GA*. This had the advantage to avoid any computational distortion caused by respiration in the vicinity of the compensation point. The irradiance of 125 $\mu E\ m^{-2}\ s^{-1}$, characteristic of illumination in the shade, was chosen because ongoing studies on low light and light quality are relevant to the physiology of shading (see also discussion). Furthermore, since low light provides a mean to directly manipulate C_4 metabolism, a great deal of comparable work has been undertaken both in this lab (Bellasio and Griffiths, 2014b; Kromdijk *et al.*, 2010; Kromdijk *et al.*, 2008) and by other investigators (Ubierna *et al.*, 2011; Ubierna *et al.*, 2013) under low irradiances. Reaction rates, shown in the boxes within Figure 3.1 were obtained by parameterizing the model with the data obtained during the experiment and with the output of the C_4 model [all equations are reported in Table 3.6 but see also Chapter 2, (Bellasio and Griffiths, 2014b), and references therein], in the three relevant conditions mentioned above.

3.3 Discussion

The implications of the metabolic model for partitioning ATP demand are firstly considered in terms of previous studies of C_4 decarboxylases in NADP-ME systems. The resultant ATP partitioning and metabolic plasticity provided by these processes is then considered in terms of overall C_4 energetic limitations (Evans *et al.*, 2007). Finally, I go on to consider the implications for multiple decarboxylase function in terms of C_4 pathway evolution, as well as light use and energy partitioning within a C_4 crop canopy.

3.3.1 Modelling ATP demand: decarboxylase diversity in C_4 systems

Recent developments in C_4 research have highlighted the complexity of C_4 metabolism, in terms of extensive overlapping of BS and M functions (Friso *et al.*, 2010; Majeran *et al.*, 2010; Wang *et al.*, 2014a), the presence of two distinct decarboxylating pathways (Meister *et al.*, 1996; Pick *et al.*, 2011; Wingler *et al.*, 1999), and plasticity in malate metabolism [(Eprintsev *et al.*, 2011) and references therein]. Although an involvement in balancing the

energetic capacity in responses to environmental conditions has been proposed (Furbank, 2011), empirical evidence and an associated metabolic model were needed to validate this suggestion. In this Chapter, I tested the capability of metabolism to respond to different ATP allocation between BS and M by means of a newly developed comprehensive metabolic model. The model was parameterized with experimental data, however it is worth noting that such a data-based parameterization is not necessary and the metabolic model can also be used independently of measured data, to facilitate formulating alternative scenarios of energy and metabolites allocation. To overcome uncertainties in the causal relationship between ATP availability and enzyme kinetics, I deduced the highest and lowest possible BS reaction rates from physiological considerations and studied how the theoretical ATP demand partitioning ATP_{BS} / ATP_M would vary in response to incremental activation. I found that ATP_{BS} / ATP_M could vary between 0.27 to 0.80 if carbohydrate synthesis, PGA reduction (PR) and PEP regeneration were freely allocated between BS and M. In particular, the rate of PEP regeneration in BS was modulated by manipulating the engagement of PEPCK. The availability of PEPCK in BS and the possibility to engage PEPCK at a variable rate had a twofold importance. Firstly, it expanded the window of ATP_{BS} / ATP_M to match the predicted window of J_{ATPBS} / J_{ATPM}. Secondly, it allowed to closely predict the decreasing ATP cost of *GA* at increasing J_{ATPBS} / J_{ATPM}, observed experimentally. In other words, metabolism could take advantage of the increased ATP availability in BS under penetrating light quality by activating PEPCK, which regenerates PEP with half the ATP cost of PPDK in M (see also 3.2.4 above). In addition, I suggest that higher ATP consumption in BS than the predicted maximum, could result from the transient activation of PPDK in BS (Aoyagi and Nakamoto, 1985; Friso *et al.*, 2010) or in a long-term response, from the de-novo synthesis of PR enzymes. This shows the importance of the presence of PPDK in BS and the possibility of metabolism to regulate the maximum BS rate of PGA reduction in response to contrasting environmental conditions. These processes could take advantage of the increased ATP availability in BS under 540 nm green light (Table 3.3) or under high irradiances when ATP production in M is reduced (because of PSII yield quenching; Figure 3.6).

The extensive overlap between BS and M functions was important for preserving the overall assimilation rate, and for any process activated in BS, a complementary decrease in M could rebalance overall metabolism so as the total rate of assimilation and ATP demand to

remain constant in spite of contrasting BS / M engagement. In addition, I showed the importance of transamination (T) in balancing the reducing power needs in BS. When the ATP availability in BS was low (e.g. condition 1), PGA reduction in BS was down-regulated, and therefore there was a reduced NADPH demand in BS (Figure 3.4 A, dotted line). Under these conditions, CO_2 was predicted to be delivered to BS through ASP, a pathway that bypasses malate reduction in M and, hence, NADPH export to BS. This shift between ASP and MAL-mediated CCM indicates the importance of maintaining both pathways in NADP-ME subtype C_4 plants. The predicted T rate varied in response to environmental conditions from a minimum of 0.35 V_P to the entirety of the CO_2 delivered to BS, in line with the observation that ASP can support physiological rates of photosynthesis (Chapman and Hatch, 1981; Meister *et al.*, 1996; Pick *et al.*, 2011; Rathnam, 1978). Under white light, the model predicted a 33 % T / V_P, which is in line with radiolabelling and biochemical observations (Chapman and Hatch, 1981; Downton, 1970; Hatch, 1971). These predictions are not influenced by whether transamination is mediated by the 'conventional' glutamate aminotransferases (Figure 3.1), or by the more recently discovered aspartate aminotransferases (Pick *et al.*, 2011), because, in the model, transamination is simply assumed to be a fast, passively regulated process at equilibrium, in line with (Wang *et al.*, 2014a; Wang *et al.*, 2014b). In addition, having two independent pathways of CO_2 delivery (through MAL and ASP) decreases the MAL concentration gradient required to sustain a physiological assimilation rate (Pick *et al.*, 2011).

Although a mechanistic explanation goes beyond the scope of this study, it is worth noting that the fine tuning between contrasting scenarios may be relatively straightforward at the metabolic level. In fact, both the CCM and the RPP pathway share diffusible metabolites between BS and M cells and are mediated by fast reactions, which, in physiological conditions, are close to the thermodynamic equilibrium (e.g. transamination reactions or sugar phosphate conversions). The regulation of the fluxes may therefore be regulated in just a few key steps, for instance at the level of PGA reduction, or malate decarboxylation. These have long been known to be regulated by the stromal pH, by feedback from metabolite pools and by feed forward from light reactions (Detarsio *et al.*, 2003; Drincovich and Andreo, 1994; Eprintsev *et al.*, 2011; Johnson and Hatch, 1970; Murmu *et al.*, 2003; Trost *et al.*, 2006). There is also abundant evidence of post-translactional modification of enzymes such

as PEPC, PPDK and PEPCK, e.g. (Chastain, 2011; Jeanneau *et al.*, 2002; Wang *et al.*, 2011). The adjustment of the other reaction and diffusion rates may then follow passively, mediated by the feedback provided by changing relative metabolite concentrations in one or the other compartment.

Figure 3.6. Responses to decreasing light intensity under different light qualities

(A) Yield of photosystem I, determined with the low O_2-Electron Transport Rate method (Bellasio and Griffiths, 2014b); **(B)** Yield of photosystem II, *Y(II)*, determined by chlorophyll fluorescence; **(C)** *Y(I)* / *Y(II)*. Error bars represent standard error. n=4.

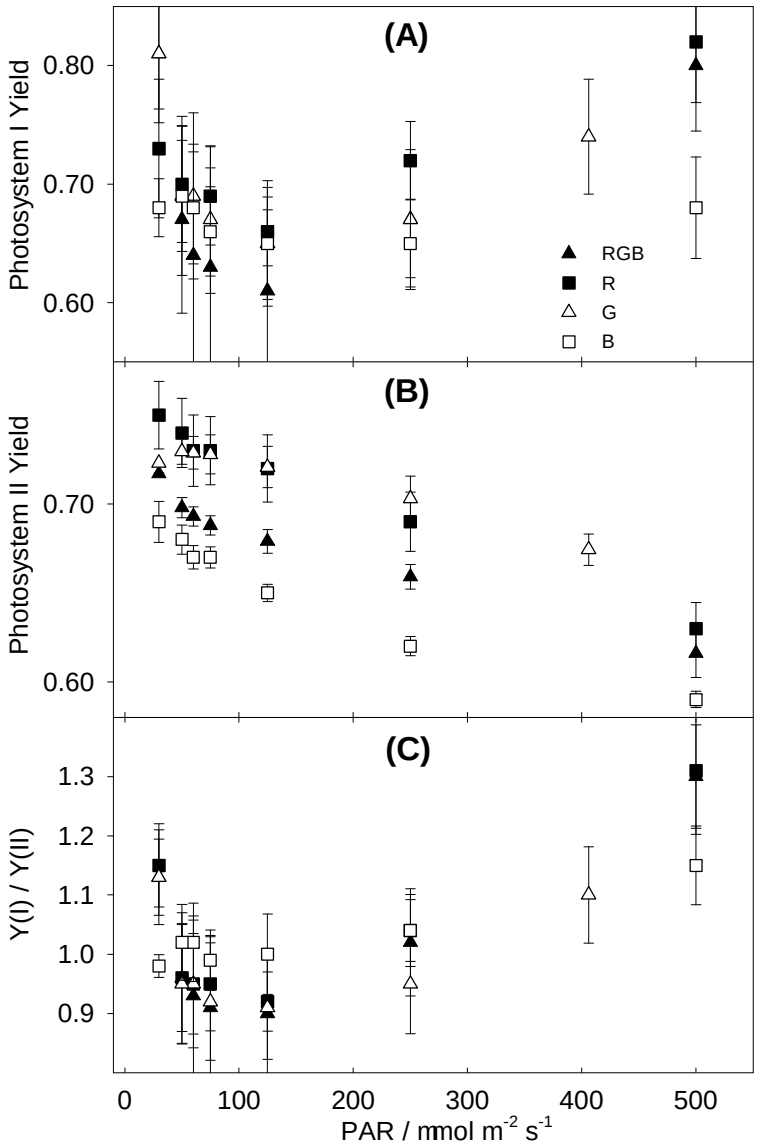

3.3.2 Modelling ATP supply as a function of light quality

Previously, fluorescence microimaging had shown that, because of the characteristic C_4 concentric leaf anatomy, strongly absorbed blue wavelengths would result in preferential absorption in M cells as compared to wavelengths of light which could penetrate deeper into the leaf profile (Evans *et al.*, 2007). However, difficulties in the interpretation of fluorescence imaging, which are dependent on the different fluorescence yield of PSI-rich-BS and PSII-rich-M, have prevented investigators from predicting the relative light harvesting in BS and M (Evans *et al.*, 2007). To overcome these difficulties, I estimated the profiles of light penetration in a maize leaf by means of an absorption-scattering model, which represents a first attempt to calculate the extent of light absorption imbalance caused by light quality. Because both BS and M produce ATP in light reactions, light harvesting imbalances would alter ATP partitioning. These ATP production imbalances were estimated using the relative stoichiometry of the electron transport operating in BS and M. The effect was very different from the response to changing light intensity, in fact, light quality only marginally influenced the total ATP available at leaf level but resulted in a 3-fold difference in the fraction of ATP produced in the BS, from 0.29 to 0.96 (Table 3.3).

This ***spatial*** partitioning of ATP production J_{ATPBS} / J_{ATPM} is different from the ***functional*** partitioning of ATP consumption of the C_4 model (Bellasio and Griffiths, 2014b; Ubierna *et al.*, 2011; von Caemmerer, 2000) and from the theoretical partitioning of ATP demand ATP_{BS} / ATP_M of the metabolic model presented here. In the C_4 model, the total ATP production, J_{ATP}, is simply assumed to be produced by an undivided electron transport chain (Yin and Struik, 2012), then partitioned to PEP regeneration activity or C_3 activity by a parameter known as x (Table 3.6). This operation does not involve spatial separations between BS and M. In this study I followed this conventional approach, which has been widely validated, then captured the partitioning between BS and M with the equations of the metabolic model (Table 3.2). On the basis of this division of work I calculated the theoretical partitioning of ATP demand ATP_{BS} / ATP_M. Values for ATP_{BS} / ATP_M were therefore derived independently from J_{ATPBS} / J_{ATPM} (J_{ATPBS} / J_{ATPM} was not used in model parameterization). These independently derived J_{ATPBS} / J_{ATPM} and ATP_{BS} / ATP_M were compared in Figure 3.4.

3.3.3 Implications for electron transport processes

These ATP partitioning rearrangements need to be underpinned by a high degree of flexibility at the electron transport chain level. In fact, although linear electron flow (LEF) activity in BS is often neglected [because of negligible expression of the O_2 evolving complex (Friso *et al.*, 2010; Majeran and van Wijk, 2009) and non-appreciable O_2 evolving activity (Meierhoff and Westhoff, 1993)] evidence that appreciable linear flow can be supported by stromal reductants as glutathione and ascorbate has been presented (Ivanov *et al.*, 2007; Ivanov *et al.*, 2005; Ivanov *et al.*, 2001; Walker and Izawa, 1979). These reductants are likely to be produced from NADPH, supplied by malate imported from M (Kanai and Edwards, 1999; Laisk and Edwards, 2000). These processes couple reductant pools at thylakoid and stromal level, and are likely to function as plasticity mechanisms, playing a pivotal role in acclimation to changing light conditions.

Most of the LEF activity is localized in M chloroplasts, which evolve O_2 and supply all reducing power requirements. For this reason, many reactions requiring NADPH (such as nitrogen reduction) are localised in M, to benefit from NADPH availability (Majeran *et al.*, 2005). Even if M chloroplasts are specialized in NADPH production, the ratio of ATP versus NADPH demand is highly sensitive to BS / M assimilation partitioning (Figure 3.1). Meeting this variable requirement may involve differential engagement of LEF versus cyclic electron flow (CEF). The particular features of the CEF operating in maize (Hertle *et al.*, 2013; Ivanov *et al.*, 2007; Laisk *et al.*, 2010; Munekage *et al.*, 2010), may reflect, beyond the heterogeneity between BS and M specialization, this characteristic need for plasticity in CEF / LEF engagement.

Regardless of this electron transport plasticity, the ATP production deficits induced by changing light quality cannot be rebalanced within the individual BS chloroplast. In fact, increasing the ATP production at the electron transport chain level would require light (Kramer and Evans, 2011; Takabayashi *et al.*, 2005), whose availability is not under metabolic control. At the same time, the electron transport mediated dark production of ATP (Bukhov and Carpentier, 2004; Egorova and Bukhov, 2004; Kuntz, 2004; Morstadt *et al.*, 2002), has low conversion efficiency (Kramer and Evans, 2011), hence an engagement of ATP chemiosynthesis would be incompatible with the observed pattern of J_{ATP} / GA. ATP itself is not a suitable shuttle to rebalance ATP deficits because the ATP molecule is

relatively big, it has a relatively small pool and homeostasis is critical, therefore every chloroplast has an independent ATP pool. Maintaining balanced ATP consumption in spite of local ATP deficits requires rearranging the localization of ATP demand, the fluxes, and the partitioning of metabolic work between the mutually interdependent BS and M cells.

3.3.4 Metabolic plasticity is effective in maintaining overall assimilation efficiency

Previously, on the basis of theoretical considerations, it had been predicted that an unbalanced ATP supply would result in a disruption of the delicate equilibrium between BS and M functions with consequent loss in assimilatory efficiency (Evans *et al.*, 2007; Henderson *et al.*, 1992; Tazoe *et al.*, 2008). This prediction arose because metabolic rigidity would be expected under some of the common simplifications used for C_4 biochemistry, whereby transamination is neglected, PGA is reduced at a fixed rate in BS and NADPH delivery to BS is equimolar to CO_2 delivery (Laisk and Edwards, 2009). In the updated description of C_4 metabolism provided in this Chapter, reaction rates are variable and tuneable. When the ATP availability in BS was low (e.g. condition 1), PGA reduction in BS was downregulated, leaving all available ATP for RuBP regeneration, resulting in unaltered Rubisco efficiency. Because the ASP-mediated CCM delivers solely CO_2, while the MAL mediated CCM delivers both NADPH and CO_2, the variable engagement of the two pathways allows the activity of the CCM to be regulated independently of NADPH demand in BS, hence the optimal C_{BS} could be maintained under all light qualities.

These predictions are supported by further model outputs, where I found no significant effect of light quality on Φ and on C_{BS}, confirming the response found in a similar experiment where plants were acclimated under high light (Sun *et al.*, 2012). This observation, together with the relatively minor change in J_{ATP} / GA (Figure 3.4 B) show that C_4 metabolic balance was adjusting to the shifts in ATP supply without the potential major disruptions mentioned above.

3.3.5 Implications for light use at leaf and canopy level

Photosynthesis in shaded conditions has critical importance in C_4 canopies as it may represent up to 50 % of CO_2 uptake (Baker *et al.*, 1988; Kromdijk *et al.*, 2008; Long, 1993). Shade light has a reduced intensity [typically 1 / 20 of full sunlight (Shirley, 1929)], and differs in spectral quality from red-rich sunlight: diffuse sky radiation is enriched in blue,

whereas canopy filtered light is enriched in green (Smith, 1982). Under low light conditions it has been shown that Φ may increase both at leaf e.g. (Bellasio and Griffiths, 2014b; Kromdijk *et al.*, 2010) and at canopy level (Kromdijk *et al.*, 2008). Theoretical considerations have associated this Φ increase with decreased C_4 efficiency and a potential loss of photosynthetic carbon uptake (Furbank *et al.*, 1990; Kromdijk *et al.*, 2008; Tazoe *et al.*, 2008; von Caemmerer, 2000). Although other studies have compared the effect of light quality on Φ under low irradiance or under different light qualities (Bellasio and Griffiths, 2014b; Kromdijk *et al.*, 2010; Sun *et al.*, 2012; Ubierna *et al.*, 2013), the novelty of the approach presented here has been to couple the measured and predicted ATP supply during assimilation under these conditions. In this experiment, which was specifically optimized to acquire data under low light (Bellasio and Griffiths, 2014b), I showed that the total ATP cost of gross assimilation was not significantly influenced by light intensity, and underwent a little variation under different light wavelengths (Figure 3.4 B). This showed that metabolism *at steady state under low light intensities*, maintained efficiency in spite of changes in light quality or intensity. This implies that the hyperbolic increase of Φ observed under decreasing light intensities (Figure 3.3 D), which underpins the predicted photosynthetic efficiency loss, actually did not cost additional ATP, but resulted instead from mitochondrial decarboxylation in BS (Bellasio and Griffiths, 2014b). This observation is consistent with V_P / V_C and the optimal '*x*' being largely independent of light intensity (Kromdijk *et al.*, 2010; von Caemmerer, 2000), indicating a constant degree of engagement of the CCM even under an apparent leakiness increase. Care should therefore be taken when the ATP cost (and quantum yield) of C_4 photosynthesis is derived from Φ, measured either at leaf or canopy scale, particularly in the vicinity of the compensation point (Furbank *et al.*, 1990; Tazoe *et al.*, 2008; von Caemmerer, 2000). In these conditions I propose that the ATP cost should be calculated by summing the ATP cost of all the active biochemical processes (e.g. Eqn 3.11, Table 3.2), instead of using leakiness as a proxy for C_4 biochemical efficiency (see developments in Chapter 4). The actual impact of Φ on canopy-level carbon uptake may depend upon the extent of steady-state photosynthesis under low light or altered light quality conditions (e.g. green enriched), and shorter-term, more transient conditions, when Φ may be more variable.

3.4 Conclusion

In this Chapter I set out to investigate whether the maize C_4 system could respond to changing environmental conditions by adjusting the C_4 (amino)acid (MAL or ASP) delivered from M to BS, as well as the proportions of other metabolic reactions shared between both cell types, such as carbohydrate synthesis, PGA reduction and PEP regeneration (Friso *et al.*, 2010; Furbank, 2011; Majeran *et al.*, 2010; Spilatro and Preiss, 1987; Walker *et al.*, 1986; Wingler *et al.*, 1999). Using contrasting light qualities and their projected extinction within the leaf profile, I could then estimate the rate of ATP synthesis in M and BS compartments, as compared to the overall leaf-level operating efficiency measured by gas exchange and real-time carbon isotope discrimination. I depicted a scenario whereby metabolism, although subject to the general constraints imposed by C_4 physiology, was able to take the maximum advantage of environmental conditions by changing the relative engagement of BS and M functions, which were ultimately under environmental control. The outputs, based on metabolic modelling and empirical measurements, provide definitive evidence for the role of complementarity between BS and M functions, allowing ATP demand to be regulated in response to contrasting environmental conditions. The two decarboxylase systems in BS of maize, with a variable rate of transamination, allow the regulation of NADPH supply to match demand in BS independently of the delivery of CO_2.

The findings of this study highlight the importance of C_4 metabolic models in helping to explain acclimation and adaptation to changing light intensity for all C_4 subgroups. The emerging complexity of the NADP-ME / PEPCK interactions certainly demands some refinement to the widespread simplifications used to describe C_4 systems and to the assumptions regarding the relatively fixed energetic partitioning in maize. Furthermore, I have clearly linked metabolic plasticity to the capacity to maintain high photosynthetic efficiency under changing environmental conditions. Finally, the extent that such steady state conditions of low light and altered light quality affect carbon uptake within an intact crop canopy remain to be determined, as compared to more transient responses which may well increase leakiness and reduce carbon assimilation under low light conditions.

3.5 Materials and Methods

3.5.1 Metabolic model

The processes contributing to assimilatory metabolism in maize (Furbank, 2011) were integrated in a comprehensive steady-state model (Figure 3.1). Some functional simplifications were made. Cells were decompartmentalized. NADPH and NADH were considered equivalent or convertible. The final product of photosynthesis was collectively referred to as 'carbohydrates' (starch synthesis has the same ATP cost per hexose than phloem-loaded sucrose, considering the stoichiometry of 1 ATP / H^+ of the membrane H^+ - ATPase and 1 H^+ / sucrose of the sucrose synporter). The ATP + NADH produced during respiration (assumed supplied by PGA) were neglected in calculations because they are likely to be consumed by basal metabolism. Transamination (T) was assumed to be passively regulated by substrate availability (all OAA not reduced by MDH was transaminated), as T reactions are rapid conversions at equilibrium in line with (Wang *et al.*, 2014a; Wang *et al.*, 2014b).

The specialization of BS and M was captured by assigning processes to BS, M, or to the conjoint work of both compartments (allocatable processes). PEPCK (Furumoto *et al.*, 1999, 2000; Walker *et al.*, 1986; Wingler *et al.*, 1999) and glycolate recycling (Yoshimura *et al.*, 2004) were allocated to BS; linear electron flow (Friso *et al.*, 2010; Kramer and Evans, 2011; Majeran and van Wijk, 2009; Meierhoff and Westhoff, 1993; Romanowska *et al.*, 2006) and PPDK (see discussion) were allocated to M; R_{LIGHT} was split equally between M and BS (Kromdijk *et al.*, 2010; Ubierna *et al.*, 2011; von Caemmerer, 2000); PGA reduction (PR) and carbohydrate synthesis (SS) were variably allocated. T rate was equal in BS and M as the pool of ASP and ALA is shared. The model was described by steady state rate equations (Table 3.2).

Minimum and maximum BS allocation

The rate of variably allocated processes ranged between a minimum and maximum rate, deduced from physiological considerations (but see 3.3 discussion for the environmental influence on maximum rates). Both BS and M synthesize carbohydrates e.g. (Kanai and Edwards, 1999; Rascio *et al.*, 1980), so SS was allocated to BS between 0 and SS_{TOT}. PR is not essential to BS so PR_{MIN} was set at 0. PR is mainly a M process (Kanai and Edwards,

1999; Majeran *et al.*, 2005; Majeran and van Wijk, 2009; Rascio *et al.*, 1980), so PR_{MAX} was limited at $0.35 \cdot PR_{TOT}$. PEPCK is not essential to BS so $PEPCK_{MIN}$ was set at 0. $PEPCK_{MAX}$ was set at $0.3 \cdot V_P$, identified by fitting the total ATP demand of assimilation to J_{ATP} / GA (Figure 3.4 B).

Parameterization

Equations describing overall assimilation (Eqn 3.4 to 3.10, in Table 3.2), were parameterized with the measured data A, R_{LIGHT}, the output of the von Caemmerer C_4 model (V_O, V_P and V_C, Table 3.6) (Bellasio and Griffiths, 2014b) and Φ calculated from Δ under PAR = 125 μE m^{-2} s^{-1} (see below). Then, reaction rates (Eqn 3.4 to 3.21 in Table 3.2) were calculated under the minimum (condition 1) and the maximum (condition 3) BS allocation (Figure 3.1 and Figure 3.4 B). Finally, intermediate states (e.g. condition 2) were calculated by allocating reactions to BS in linear increments (see continuous lines in Figure 3.4 A).

The ATP demand in BS (ATP_{BS}) was calculated by adding the ATP demand of BS processes (Table 3.2, Eqn 3.12; Table 3.5). Analogously, ATP_M was calculated by summing the ATP demand of M processes (Table 3.2, Eqn 3.13; Table 3.5), and the partitioning of ATP demand (ATP_{BS} / ATP_M) was calculated by dividing Eqn 3.12 by Eqn 3.13. Similarly the NADPH demand in BS ($NADPH_{BS}$) was calculated by summing the NADPH demand of BS processes (Table 3.2, Eqn 3.14; Table 3.5). Rate equations for other processes are listed in Table 3.2.

3.5.2 Estimated light harvesting in BS and M, AB BS / M

Light harvesting in BS and M was estimated through these steps: i) a leaf cross section was simplified to a square anatomy so as to be described by only two profiles of light penetration, P1 and P2; ii) the two profiles were described mathematically using an absorption-scattering model; iii) to capture the differences in light penetration, the profiles P1 and P2 were calibrated with data obtained for different wavelengths of incident light; iv) the profiles were then integrated on the M and BS area to calculate the total light absorbed in BS and M under different wavelengths of incident light. In detail, a maize leaf cross section was simulated by rectangular units, enclosing a square BS (left panel of Figure 3.2). Inter-veinal distance (IVD, 106 μm); M thickness (100 μm), BS / M area (0.26) and the resulting BS side (46 μm) were averaged from (BongardPierce *et al.*, 1996; Hattersley, 1984; Kromdijk *et al.*,

2010; Moreno-Sotomayor *et al.*, 2002; Usuda, 1985). Because of the square anatomy, the leaf light environment could be described by two light profiles: P1 and P2. These were calculated applying the Kubelka-Munk absorption – scattering theory with the method of Allen and Richardson (Allen and Richardson, 1968; Gates, 1980; Terashima *et al.*, 2009), modified to describe the simulated C_4 anatomy. Briefly, each profile was considered to be made of a number n of light absorbing and scattering elements, the total number of elements in the profile was N. The element n=0 was the illuminated, or adaxial point of the profile, which included the upper epidermis, approximated to a single reflecting element. The element N was the abaxial point of the profile, which included the lower epidermis, approximated to a single reflecting element. Radiant flux directed downward was I, and that upward was J. Incident flux was I_0, and was taken to be the unity. For each profile, the flux reflected by the first element was equivalent to the point reflectance and the flux transmitted by the last element was equivalent to the point transmittance: $J(0)$ = Point refl. and $I(N)$= Point transmission.

Incremental absorption and scattering were calculated as (Gates, 1980):

$$dI = -(k + s)Idn + sJdn \tag{3.1}$$

$$dJ = (k + s)Jdn - sIdn \tag{3.2}$$

Where k is an absorption coefficient and s is a scattering coefficient. In P1, k was constant throughout the profile. In P2 k was three times higher in the elements corresponding to BS, because chlorophyll concentration is three times higher than in the surrounding M [BS / M chl content, 0.74 (Kanai and Edwards, 1973), multiplied by M / BS area, 4; Figure 3.2, left]. I and J were solved for all elements of P1 and P2 according to the integration of Eqn 3.1 and 3.2 proposed by (Gates, 1980). Once I and J were solved, they were combined (as a weighed average) to simulate leaf-level optical properties: modelled leaf reflectance resulted from averaging $J(0)$ contributions to the total leaf reflectance from P1 and P2 (56 % P1 and 44 % P2). Similarly, modelled leaf transmittance was calculated as a weighted average of $I(N)$

from P1 and P2. These quantities were calibrated with measured leaf reflectance and transmittance at different wavelengths [Table 3.3, (Woolley, 1971)] by varying ***k*** and ***s***. This procedure allowed deriving the two light penetration profiles P1 and P2 for different light qualities (Figure 3.2 right). Absorbed light (AB) in BS resulted from integrating P2 over BS area. AB in M resulted from integrating P2 over adaxial and abaxial mesophyll (MAD + MAB) area plus the integral of P1 over the two interveinal mesophyll (MI) areas.

3.5.3 Estimated ATP production partitioning, J_{ATPBS} / J_{ATPM}

M chloroplasts are engaged in NADPH *and* ATP production, therefore, for a given number of light quanta they produce c. half the ATP produced in BS chloroplast, which produce mainly ATP. J_{ATPBS} / J_{ATPM} was calculated as:

$$\frac{J_{ATPBS}}{J_{ATPM}} = 2 \cdot AB \frac{BS}{M} \tag{3.3}$$

The coefficient 2 (in Eqn. 3.3) is based on widely accepted assumption that light is equally shared between photosystems and on the simplification that the photochemical yield is independent of the position within the leaf profile. In detail I assumed: i) exclusive linear electron transport in M with equal PSI / PSII absorption partitioning (Kramer and Evans, 2011; Meierhoff and Westhoff, 1993); ii) exclusive cyclic electron transport in BS with no PSII absorption (Majeran and van Wijk, 2009; Romanowska *et al.*, 2006); iii) equal yield of PSI and PSII (Miyake *et al.*, 2005) (Fig. 3.6 C); iv) equal H^+ / ATP stoichiometry of the ATP synthase in BS and M: the enzyme complex is the same (Friso *et al.*, 2010; Majeran and van Wijk, 2009); v) twice the H^+ per photochemical event pumped in BS versus M: in M 1.5 H^+ are extruded per photochemical event (Kramer and Evans, 2011), while in BS I assumed 3 H^+ extruded per photochemical event [average between 4 H^+ of the NDH-mediated (Kramer and Evans, 2011; Peng *et al.*, 2011) and 2 H^+ of the PGR5 / PGRL1-mediated electron flow (Hertle *et al.*, 2013; Kramer and Evans, 2011) both operating in maize BS (Ivanov *et al.*, 2007)].

3.5.4 Plants

Zea mays L. (F1 Hybrid PR31N27, Pioneer Hi-bred, Cremona, Italy) plants were grown in 1.5 L pots filled with Levington pro M3 (Scotts, UK) in growth rooms (Conviron Ltd, Winnipeg, Canada) set at 16 h day length, temperature of 25 °C / 23 °C (day/night), 40 % relative humidity and PAR = 600 μE m^{-2} s^{-1} and manually watered daily with particular care to avoid overwatering. After three weeks plants were measured once and then discarded.

3.5.5 Gas exchange measurements with concurrent PSI / PSII Yield and on-line carbon isotopic discrimination (Δ)

The experimental setup was previously described in Chapter 2 (Bellasio and Griffiths, 2014b). Briefly, an infra-red gas analyser (IRGA, a LI6400XT, Li-cor, USA), was fitted with a 6400-06 PAM2000 adapter, and with a Li-cor 6400-18 RGB light source. The IRGA was fed with CO_2 ($\delta^{13}C$ = -8.3 ‰, Isi, A) and either a mixture of 2 % O_2 / N_2 or ambient air. PS I yield and PS II yield, *Y(II)*, were measured with a Dual Pam-F (Heinz Walz GmbH, Effeltrich, D). The IRGA was connected to a cryogenic H_2O and CO_2 trapping-purification line. To determine the relationship between *Y(II)* and J_{ATP}, a light response curve was measured at 2 % O_2 and C_a = 600 μmol / mol. Under the same light quality, 21 % O_2 and reference CO_2 set at 400 μmol / mol, a second light response curve was measured, during which *Y(II)* was determined and exhaust gas was trapped to determine Δ. In one day a total of 12 CO_2 samples and 6 CO_2 references from each individual plant were analysed directly with a VG SIRA dual inlet isotope ratio mass spectrometer (modified and maintained by Pro-Vac Services Ltd, Crewe, UK). Δ was calculated as reported in Figure 3.7, using Eqn 3.22. R_{LIGHT} was calculated as the *y*-intercept of the linear regression of *A* against PAR·*Y(II)* / 3. J_{ATP} was calculated from ETR individually at each irradiance using the relationship between *Y(II)* and J_{ATP}, determined at low O_2 (Table 3.6). Light responses were treated with dedicated software (Photosyn assistant 1.2, Dundee Scientific, Dundee, UK), to calculate the light compensation point and by repeated measures anova (Genstat), point estimates were subject to anova and Tukey multiple comparison (Genstat).

Figure 3.7. ξ values for the calculation of *Δ*

Δ was calculated as (Evans *et al.*, 1986):

$$\Delta_{OBS} = \frac{\xi(\delta_o - \delta_e)}{1 + \delta_o - \xi(\delta_o - \delta_e)} \quad (3.22)$$

Where: $\xi = \frac{C_e}{C_e - C_o}$; δ_e is the isotopic composition of the reference gas. δ_o is the isotopic composition of the gas leaving the cuvette. C_e and C_o represent the CO_2 mole fraction respectively entering and leaving the cuvette. These were corrected for differences in water content according to (von Caemmerer and Farquhar, 1981).

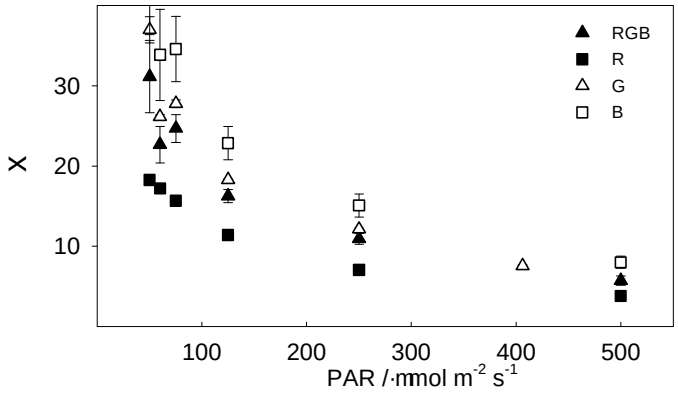

3.5.6 Leakiness, Φ, from isotopic discrimination Δ

Leakiness was resolved from isotopic discrimination by use of the full Farquhar model (Farquhar, 1983; Farquhar and Cernusak, 2012), parameterized with a C_4 photosynthesis model (von Caemmerer, 2000), using equations and a fitting approach that were previously described [Table 3.6 (Bellasio and Griffiths, 2014b)]. Briefly, leakiness, Φ was resolved from Δ by calculating the weighted individual fractionations of the discriminating processes operating in C_4 photosynthesis. The CO_2 concentration in the cellular compartments was calculated by means of a C_4 model, parameterized with the light response data (A, Ci, Ca, J_{ATP}) and respiration in the light (R_{LIGHT}). The C_4 model was rearranged to express a modelled J_{MOD} and fit to the total ATP production rate J_{ATP} (Table 3.6), to yield a value for BS conductance for each individual plant, independently from Δ.

3.6 Chapter 3 Tables

Table 3.1. Abbreviations, definitions and units for variables described in Chapter 3

A	Net assimilation	µmol m^{-2} s^{-1}
AB	Absorbed light	
AB BS / M	Partitioning of absorbed light	dimensionless
ALA	Alanine	
ASP	Aspartate	
ATP	Adenosine 5' triphosphate	
ATP_{BS}	ATP demand in BS	µmol m^{-2} s^{-1}
ATP_M	ATP demand in M	µmol m^{-2} s^{-1}
B	Blue	
BS	Bundle sheath	
C_{BS}	CO_2 concentration in BS	µmol mol^{-1}
CCM	Carbon concentrating mechanism	
CEF	Cyclic electron flow	
DHAP	Dihydroxyacetone phosphate	
ETR	Electron transport rate	µmol m^{-2} s^{-1}
G	Green	
GA	Gross assimilation ($A + R_{LIGHT}$)	µmol m^{-2} s^{-1}
g_{BS}	Bundle sheath conductance to CO_2, calculated by fitting J_{MOD} to J_{ATP}	mol m^2 s^{-1}
GLA	Glycolic acid	
IRGA	Infra-red gas analyzer	
IVD	Inter veinal distance	µm
J_{ATP}	Total ATP production rate	µmol m^{-2} s^{-1}
J_{ATPBS}	ATP production rate in BS	µmol m^{-2} s^{-1}
J_{ATPM}	ATP production rate in M	µmol m^{-2} s^{-1}
J_{MOD}	Modelled ATP production rate	µmol m^{-2} s^{-1}
LEF	Linear electron flow	
M	Mesophyll	
MAL	Malate	
MDH	Malate dehydrogenase	
MDH_{BS}	Malate dehydrogenase reaction rate in BS	µmol m^{-2} s^{-1}
MDH_M	Malate dehydrogenase reaction rate in M	µmol m^{-2} s^{-1}
ME	Malic enzyme	
ME	Malic enzyme reaction rate	µmol m^{-2} s^{-1}
NADPH	Nicotinamide adenine dinucleotide phosphate	
$NADPH_{BS}$	NADPH demand in BS	µmol m^{-2} s^{-1}
$NADPH_{TOT}$	Total NADPH demand	µmol m^{-2} s^{-1}
OAA	Oxaloacetic acid	
PAR	Photosynthetically active radiation	µE m^{-2} s^{-1}
PEP	Phosphoenolpyruvate	

PEPCK	Phosphoenolpyruvate carboxykinase	
PEPCK	PEPCK reaction rate	μmol m^{-2} s^{-1}
PGA	3-phosphoglyceric acid	
PGLA	2-phosphoglycolic acid	
PPDK	Pyruvate phosphate dikinase	
PPDK	PPDK reaction rate	μmol m^{-2} s^{-1}
PR	PGA reduction	
PR_{BS}	PGA reduction rate in BS	μmol m^{-2} s^{-1}
PR_M	PGA reduction rate in M	μmol m^{-2} s^{-1}
PSI	Photosystem I	
PSII	Photosystem II	
PYR	Pyruvic acid	
R	Red	
R_{BS}	Respiration in the light in BS	μmol m^{-2} s^{-1}
R_{LIGHT}	Respiration in the light	μmol m^{-2} s^{-1}
R_M	Respiration in the light in M	μmol m^{-2} s^{-1}
RPP	Reductive pentose phosphate	
Rubisco	Ribulose bisphosphate carboxylase oxygenase	
RuBP	Ribulose-1,5-bisphosphate	
RuP	Ribulose-5-phosphate	
SS	Carbohydrate synthesis	
SS_{BS}	Carbohydrate synthesis rate in BS	μmol m^{-2} s^{-1}
SS_M	Carbohydrate synthesis rate in M	μmol m^{-2} s^{-1}
SS_{TOT}	Total carbohydrate synthesis rate	μmol m^{-2} s^{-1}
T	Transamination	
T	Transamination rate	μmol m^{-2} s^{-1}
V_C	Rubisco carboxylation rate	μmol m^{-2} s^{-1}
V_O	Rubisco oxygenation rate	μmol m^{-2} s^{-1}
V_P	PEP carboxylation rate	μmol m^{-2} s^{-1}
Y(II)	Yield of photosystem II	
Δ	^{13}C Isotopic discrimination	‰
$\delta^{13}C$	^{13}C isotopic composition relative to Pee dee belemnite	‰
Φ	Leakiness	dimensionless

Table 3.2. Steady state equations for the metabolic model of C_4 assimilation

Processes described by Eqn 3.4 to 3.10 can be calculated directly from the measured data *A*, R_{LIGHT} and the output of the von Caemmerer C_4 model (V_O, V_P and V_C), while Eqn from 3.11 to 3.21 require prior allocation of carbohydrate synthesis (SS), PGA reduction (PR) and PEPCK. For simplicity, enzyme names in italics represent the enzyme reaction rate. For stoichiometric consistency, reaction rates are expressed as rates of substrate transformation.

Process	Symbol	Reaction rate	Eqn	Localization	Notes
Gross assimilation	GA	$A + R_{LIGHT}$	(3.4)		Gross assimilation represents the biochemical CO_2 uptake obtained by summing net assimilation and respiration in the light. *GA* and R_{LIGHT} rates are expressed per CO_2
RuP phosphorylation	RuP_{phosp}	$V_c + V_O$	(3.5)	BS	At steady state the rate of RuBP produced through phosphorylation equals the rate of RuBP consumed through Rubisco carboxylating activity (V_C), together with oxygenating activity (V_O).
PGA reduction tot	PR_{TOT}	$2V_C + \frac{3}{2}V_O - \frac{1}{3}R_{LIGHT}$	(3.6)	BS and M	2 V_C is the PGA produced by the carboxylating activity of Rubisco; V_O is the PGA produced by the oxygenating activity of Rubisco; 0.5 V_O is the PGA regenerated by the photorespiratory cycle; 1/3 is the stoichiometric conversion between respiration (expressed per CO_2), which in this model is supplied by PGA, and PR (expressed per triose).
NADPH demand tot	$NADPH_{TOT}$	$PR_{TOT} + \frac{1}{2}V_O$	(3.7)	BS and M	PGA reduction consumes 1 NADPH per triose. In the photorespiratory glycolate regeneration (per glycolate) 0.5 NADH is produced by glycine decarboxylase, 0.5 NADH is consumed by hydroxypyruvate reductase and one ferredoxin (equivalent to 0.5 NADPH) is consumed by glutamine synthetase. In total 0.5 NADPH is consumed per glycolate (at a rate equivalent to V_O, Table 3.5) (Yoshimura *et al.*, 2004).
DHAP entering RPP	$DHAP_{RPP}$	$\frac{5}{3}\mathrm{RuP}_{phosp}$	(3.8)	BS	Since carbohydrates are considered the final products of photosynthesis and are synthsized using DHAP as a precursor, the RPP supplies solely RuP regeneration. 5/3 converts the stoichiometry of *RuP* (C_5) to the stoichiometry of *DHAP* (C_3).
Carbohydrate synthesis tot	SS_{TOT}	$PR_{TOT} - DHAP_{RPP}$	(3.9)	BS and M	The total carbohydrate synthesis corresponds to the total PGA reduced minus the triose required for RuBP regeneration ($DHAP_{RPP}$). At steady state this quantity corresponds to the net CO_2 uptake, corrected for the stoichiometry ($\frac{1}{3}A$), where 1/3 converts the stoichiometry of *A* (expressed per CO_2) to the stoichiometry of *SS* (expressed per triose).
PEP regeneration tot	-	V_P	(3.10)	BS and M	PEP regeneration rate equals PEP consumption rate V_P at steady state. PEP can be regenerated either by PPDK (mainly in M, but active also in BS) or by PEPCK in BS. In this study PPDK activity was assumed to be zero in BS. In this chapter Vp was calculated with the C_4 model.
ATP demand tot	$ATP_{BS} + ATP_M$	$PR_{TOT} + V_C + 2V_O + \frac{1}{2}SS_{TOT} + PEPCK + 2PPDK$	(3.11)	BS and M	The total ATP demand is brought about by PGA reduction (1 ATP per PGA corresponding to *PR*), RuBP regeneration (1 ATP per RuP corresponding to V_C+V_O), glycolate recycling (In total the photorespiratory cycle consumes 1 ATP per glycolate, hence the consumption ratio equals V_O, of this ATP, 0.5 ATP is required for recapturing 0.5 mol of ammonia and 0.5 ATP is required to convert 0.5

					mol of glycerate in 0.5 mol of PGA), carbohydrate synthesis (0.5 ATP per triose, corresponding to *SS*) and PEP regeneration (1 ATP per PEPCK catalytic event or 2 ATP per PPDK catalytic event).
ATP demand in BS	ATP_{BS}	$PR_{BS} + V_C + 2\,V_O + \frac{1}{2}\,SS_{BS} + PEPCK$	(3.12)	BS	The ATP demand in BS is brought about by PGA reduction, RuBP regeneration, glycolate recycling (see note to 3.11 and Table 3.5), carbohydrate synthesis and PEPCK.
ATP demand in M	ATP_M	$2\,PPDK + \frac{1}{2}\,SS_M + PR_M$	(3.13)	M	The ATP demand in M is brought about by PGA reduction, carbohydrate synthesis and PPDK.
NADPH demand in BS	$NADPH_{BS}$	$PR_{BS} + \frac{1}{2}V_O$	(3.14)	BS	The NADPH demand in BS is brought about by PGA reduction and glycolate recycling.
NADPH supply to BS	-	MDH_M	(3.15)	BS	The NADPH supply to BS corresponds to the NADPH used to reduce OAA to MAL in M, and not to the rate of MAL decarboxylation in BS, which depends on *T*, *PEPCK* and MDH_{BS} (Eqn 3.19).
MDH activity in M	MDH_M	$PR_{BS} + \frac{1}{2}V_O$	(3.16)	M	MDH activity supplies the NADPH demand in BS. Eqn 3.16 was derived from Eqn 3.14 and 3.15.
Transamination	T	$V_P - MDH_M$	(3.17)	BS and M	*T* has the function of balancing NADPH supply and demand.
Malate dehydrogenase	MDH_{BS}	*T-PEPCK*	(3.18)	BS	MDH is assumed to operate a fast conversion at equilibrium therefore it is passively regulated by the substrate availability: the OAA that is not used by PEPCK is reduced to MAL by MDH. This enzyme may use NADH, since no NADPH dependent reduction of OAA has been observed in maize (Kanai and Edwards, 1999) and it is likely mitochondrial (Chapman and Hatch, 1981; Rathnam, 1978), but since the process may be more complicated [(Eprintsev *et al.*, 2011) and references therein] here, for simplicity, I assumed that cells are decompartimentalized and that NADH and NADPH are equivalent or interconvertable. PEPCK rate is regulated by ATP availability in BS.
Malic enzyme	*ME*	MDH_M+MDH_{BS}	(3.19)	BS	ME oxidises MAL deriving from M and from MDH activity in BS. NADH regeneration may be carried out by chloroplastic ME (Chapman and Hatch, 1981), however, the process may be more complicated [(Eprintsev *et al.*, 2011) and references therein].
Pyruvate phosphate dikinase	*PPDK*	V_P-*PEPCK*	(3.20)	M	The PEP regenerated by PEPCK in BS diffuses to M and reduces the requirement of PEP regenerated by PPDK in M.
PGA reduction M	PR_M	PR_{TOT} - PR_{BS}	(3.21)	M	PGA reduction is a process shared by BS and M.

Table 3.3. Energy partitioning between BS and M at different wavelengths

Measured leaf reflectance and transmittance (Woolley, 1971) was used to parameterize the optical model (Figure 3.2) to calculate the likely profiles of light penetration at different wavelengths. Absorbed light partitioning (AB BS / M) was calculated integrating such light absorption profiles (Figure 3.2, right panel) over the corresponding BS and M areas (Figure 3.2 left) and used to calculate ATP production partitioning J_{ATPBS} / J_{ATPM}.

Wavelength	Description	Refl. %	Transm. %	$AB\frac{BS}{M}$	$\frac{J_{ATPBS}}{J_{ATPM}}$
400 nm	Lowest $AB\frac{BS}{M}$	4	0.1	0.15	0.29
460 nm	Blue LED used	5	1	0.16	0.31
635 nm	Red LED used	6	7	0.34	0.68
400 – 700 nm	Natural white light	8	9	0.38	0.76
522 nm	Green LED used	8	11	0.40	0.80
540 nm	Highest $AB\frac{BS}{M}$	13	23	0.48	0.96

Table 3.4. Physiological responses of maize plants to different light qualities

The light compensation point (*LCP*) was determined by fitting light curves with dedicated software; Respiration in the light (R_{LIGHT}) was determined by linear regression of *A* against PAR·*Y(II)* / 3; bundle sheath conductance (g_{BS}) was determined by fitting a modelled J_{ATP} to the measured J_{ATP} (Figure 3.3). Differences were not significant for $P < 0.05$. Average values ± SE. n = 4

	Unit	Average	RGB	R	G	B
LCP	µE m^{-2} s^{-1}	29.04	28.05 (± 1.8)	21.24 (± 3.1)	33.10 (± 4.1)	33.75 (± 5.7)
R_{LIGHT}	µmol O_2 m^{-2} s^{-1}	1.169	1.202 (± 0.090)	1.231 (± 0.11)	1.148 (± 0.11)	1.095 (± 0.12)
g_{BS}	mol m^{-2} s^{-1}	0.00104	0.00127 (± $3.1 \cdot 10^{-4}$)	0.00117 (± $3.1 \cdot 10^{-4}$)	0.00075 (± $3.1 \cdot 10^{-4}$)	0.00247 (± $3.1 \cdot 10^{-4}$)

Table 3.5. ATP and NADPH demand for key C_4 processes

Process	Localization	Per	ATP	NADPH	Notes
PGA reduction to DHAP	M+BS	PGA	1	1	ATP required by Phosphoglycerate kinase and NADPH required by glyceraldehyde dehydrogenase
RuP phosphorylation	BS	pentose	1		Required by phosphoribulokinase
Glycolate regeneration	BS	Glycolate	1	0.5	0.5 ATP is required for recapturing 0.5 mol of ammonia by glutamine synthetase and 0.5 ATP is required to convert 0.5 mol of glycerate in 0.5 mol of PGA by glicerate kinase, which adds to 1 ATP per glycolate; 0.5 NADH is produced by glycine decarboxylase, 0.5 NADH is consumed by hydroxypyruvate reductase and one ferredoxin (equivalent to 0.5 NADPH) is consumed by glutamine synthetase, which adds to 0.5 NADPH per glycolate.
Carbohydrate synthesis	M+BS	triose	0.5		Starch synthesis has the same ATP cost per hexose than phloem-loaded sucrose, considering the stoichiometry of 1 ATP / H^+ of the membrane H^+ - ATPase and 1 H^+ / sucrose of the sucrose synporter
PEPCK		OAA	1		ATP required for PEPCK reaction
PPDK	M	PYR	2		ATP required by PPDK to regenerate PEP

Table 3.6. Definitions, equations, and values for variables used in the models

Symbol	Definition	Values / Units / References
a	^{13}C fractionation due to diffusion of CO_2 in air. Because of vigorous ventilation I neglected the fractionation of the boundary layer (Kromdijk *et al.*, 2010).	4.4 ‰ (Craig, 1953)
a_d	^{13}C fractionation due to diffusion of CO_2 in water	0.7 ‰ (O'Leary, 1984)
b_3	^{13}C fractionation during carboxylation by Rubisco including respiration and photorespiration fractionation $b_3 = b'_3 - \frac{e\prime \cdot R_{LIGHT} + f\frac{1}{2}V_o}{V_c}$ (Farquhar, 1983).	‰
b_3'	^{13}C fractionation during carboxylation by Rubisco	30 ‰ (Roeske and Oleary, 1984)
b_4	Net fractionation by CO_2 dissolution, hydration and PEPC carboxylation including respiratory fractionation $b_4 = b'_4 - \frac{e\prime R_M}{V_P}$ (Farquhar, 1983; Henderson *et al.*, 1992).	‰
b_4'	Net fractionation by CO_2 dissolution, hydration and PEPC carboxylation.	-5.7 ‰ at 25 °C but variable with temperature (Farquhar, 1983; Henderson *et al.*, 1992; Kromdijk *et al.*, 2010).
C_{BS}	CO_2 concentration in the bundle sheath $C_{BS} = \frac{\frac{xJ_{ATP}}{2} - \frac{R_{LIGHT}}{2} - A}{g_{BS}} + C_M$	µmol mol^{-1}
C_M	CO_2 concentration in the mesophyll $C_M = C_i - \frac{A}{g_M}$	µmol mol^{-1}
C_i	CO_2 concentration in the intercellular spaces as calculated by the IRGA (Li-cor manual Eqn 1-18).	µmol mol^{-1}
e	^{13}C fractionation during decarboxylation	0 ‰ to -10 ‰ (Barbour *et al.*, 2007; Ghashghaie *et al.*, 2001; Gillon and Griffiths, 1997; Hymus *et al.*, 2005; Igamberdiev *et al.*, 2004; Sun *et al.*, 2012), -6 ‰ in this study (Kromdijk *et al.*, 2010).
e'	^{13}C fractionation during decarboxylation, including the correction for measurement artefacts: $e' = e + \delta\,^{13}C_{measurements} - \delta\,^{13}C_{growth\ chamber}$ In this study $\delta^{13}C_{measurements}$ = -6.38 ‰; $\delta^{13}C_{growth\ chamber}$ = -8 ‰ (Wingate *et al.*, 2007)	‰

e_s	^{13}C fractionation during internal CO_2 dissolution	1.1 ‰ (Mook *et al.*, 1974; Vogel, 1980; Vogel *et al.*, 1970).
f	^{13}C fractionation during photorespiration.	11.6 ‰ (Lanigan *et al.*, 2008).
g_{BS}	Bundle sheath conductance to CO_2, calculated by curve fitting	mol m^2 s^{-1}
g_M	Mesophyll conductance to CO_2	1 mol m^2 s^{-1} bar^{-1} (Kromdijk *et al.*, 2010)
g_s	Stomata conductance to CO_2	mol m^2 s^{-1}
J_{ATP}	ATP production rate $J_{ATP} = \frac{3\,GA_{Low\,O_2}\,Y(II)}{0.59\,Y(II)_{Low\,O_2}}$	µmol m^{-2} s^{-1} curve (Bellasio and Griffiths, 2014b)
J_{MOD}	Modelled ATP production rate $J_{MOD} = \frac{-y+\sqrt{y^2-4wz}}{2w}$; $w = \frac{x-x^2}{6A}$; $y = \frac{1-x}{3}\left[\frac{g_{BS}}{A} + \left(C_M - \frac{R_M}{g_{BS}} - \gamma^* O_M\right) - 1 - \frac{\alpha\gamma^*}{0.047}\right] - \frac{x}{2}\left(1 + \frac{R_{LIGHT}}{A}\right)$; $z = \left(1 + \frac{R_{LIGHT}}{A}\right)\left(R_M - g_{BS}\,C_M - \frac{7\,g_{BS}\,\gamma^* O_M}{3}\right) + (R_{LIGHT} + A)\left(1 - \frac{7\alpha\gamma^*}{3 \cdot 0.047}\right)$	µmol m^{-2} s^{-1}µm (Bellasio and Griffiths, 2014b; Ubierna *et al.*, 2013; von Caemmerer, 2000)
O_M	O_2 mol fraction in the mesophyll cells (in air at equilibrium)	210000 µmol mol^{-1}
O_{BS}	O_2 mol fraction in the bundle sheath cells (in air at equilibrium) $O_{BS} = O_M + \frac{\alpha A}{0.047\,g_{BS}}$ (von Caemmerer, 2000)	µmol mol^{-1}
R_M	Mesophyll non photorespiratory CO_2 production in the light R_M = 0.5 R_{LIGHT} (Kromdijk *et al.*, 2010; Ubierna *et al.*, 2011; von Caemmerer, 2000)	µmol m^{-2} s^{-1}
s	Fractionation during leakage of CO_2 out of the bundle sheath cells	1.8 ‰ (Henderson *et al.*, 1992).
t	Ternary effects $t = \frac{(1+a)\,E}{2000\,g_{ac}}$ where E / mmol m^{-2} s^{-1} is the transpiration rate (calculated by the IRGA software, parameter Trmmol), g_{ac} / mol m^{-2} s^{-1} is the conductance to diffusion of CO_2 in air (calculated by the IRGA software, parameter CndCO2), a is the isotopic fractionation during diffusion in air.	‰ (Farquhar and Cernusak, 2012)
V_C	Rubisco carboxylation rate $V_C = \frac{(A+R_{LIGHT})}{1-\frac{\gamma^* O_{BS}}{C_{BS}}}$ (Ubierna *et al.*, 2011)	µmol m^{-2} s^{-1}

V_O	Rubisco oxygenation rate $V_O = \frac{V_C - A - R_{LIGHT}}{0.5}$ (Ubierna *et al.*, 2011)	µmol m^{-2} s^{-1}
V_P	PEP Carboxylation rate $V_P = \frac{x J_{ATP}}{2}$	
Φ	Leakiness estimated with the isotope method including respiratory and photorespiratory fractionation, ternary effects and estimating CBS with the C_4 model $\Phi = \frac{C_{BS} - C_M}{C_M} \frac{b_4 C_M (1+t) + a(C_a - C_i) - C_a \Delta_{OBS}(1-t)}{(1+t)[C_a \Delta_{OBS}(1-t) - a(C_a - C_i) - b_3 C_{BS} + s(C_{BS} - C_M)]}$	dimensionless (Farquhar and Cernusak, 2012)
x	Partitioning factor of J_{ATP} between C_4 activity V_P and C_3 activity V_C+V_O (reductive pentose phosphate pathway and photerespiratory cycle)	0.4 (Kromdijk *et al.*, 2010; Ubierna *et al.*, 2011; Ubierna *et al.*, 2013; von Caemmerer, 2000)
α	Fraction of PSII active in BS cells	0.15 (Edwards and Baker, 1993; Kromdijk *et al.*, 2010; von Caemmerer, 2000).
γ^*	Half of the reciprocal of the Rubisco specificity	0.000193 (von Caemmerer, 2000).
Y(II)	Yield of photosystem II $Y(II) = \frac{F'_m - F_s}{F'_m}$ (Genty *et al.*, 1989)	dimensionless

4 Maize re-acclimation to low light

Published in Journal of Experimental Botany as: 'Acclimation of C_4 metabolism to low light in mature maize leaves could limit energetic losses during progressive shading in a crop canopy' (Bellasio and Griffiths, 2014a).

4.1 Introduction

The C_4 pathway of photosynthesis has been attracting increasing interest in recent years for the high crop productivity potential in the face of global warming and population pressure (Covshoff and Hibberd, 2012; Friso *et al.*, 2010; Zhu *et al.*, 2010). C_4 photosynthesis evolved from C_3 photosynthesis under the environmental pressure of declining ambient CO_2 and increasing transpiration demand in semi-arid environments (Griffiths *et al.*, 2013; Osborne and Sack, 2012). Under optimal conditions, characterized by high temperatures and high light intensities, C_4 plants have higher photosynthetic rates than C_3 plants (Ehleringer and Pearcy, 1983; Pearcy and Ehleringer, 1984) and very high productivity. Many C_4 plants have been domesticated and represent irreplaceable sources of food, biomass and bioenergy. For instance, maize (***Zea mays***, L.), a C_4 plant of the NADP-ME subtype, is the leading grain production cereal (FAO, 2012).

The high productivity of C_4 plants results from the anatomical and biochemical differentiation of the leaf parenchyma into mesophyll (M) and bundle sheath (BS) cells. These are coupled to allow the operation of a biochemical carbon concentrating mechanism (CCM) that increases the CO_2 concentration in BS, the cellular compartment where Rubisco is exclusively expressed, resulting in an active suppression of the oxygenase activity of Rubisco. Since BS and M are connected by plasmodesmata, some CO_2 retrodiffuses (CO_2 leakage, 1.10). The extent of CO_2 retrodiffusion is still debated, but it is accepted that the permeability to CO_2 diffusion (bundle sheath conductance, g_{BS}) varies between different species and individual plants. A useful term to describe this concept, which was coined by Farquhar in the description of carbon isotope discrimination (Farquhar, 1983) is leakiness (Φ), defined as the rate of CO_2 retrodiffusing (leak rate) relative to the PEP carboxylation rate (V_P). Since Rubisco CO_2 fixation (in BS) is complementary to leakage (out of BS), Φ can be used as a proxy for the coordination between the CCM and C_3 assimilatory activity (Bellasio and Griffiths, 2014b; Henderson *et al.*, 1992; Kromdijk *et al.*, 2010; Tazoe *et al.*, 2008; Tazoe *et al.*, 2006; Ubierna *et al.*, 2011; von Caemmerer, 2000).

The CCM has a notable metabolic cost: out of the theoretical minimum of 5 ATP molecules required for the *gross* assimilation of 1 CO_2, 2 ATP are consumed by the CCM (Bellasio and Griffiths, 2014c; Furbank *et al.*, 1990) in the costly regeneration of PEP (Bailey *et al.*, 2007). The common interpretation of C_4 physiology assumes that, at steady state,

leaking CO_2 is entirely refixed by PEP carboxylase (PEPC), hence, anatomical features are tightly bound to biochemical and energy traits. Plants with a higher g_{BS} would have higher rate of CO_2 retro-diffusion, increased CCM cost, and a higher ATP demand for gross assimilation (ATP / *GA*), which is the overall biochemical operating efficiency of C_4 photosynthesis. For this reason, Φ has been used to derive ATP / GA (Tazoe *et al.*, 2008; von Caemmerer, 2000), for instance, plants with higher Φ are considered to have higher ATP / *GA* and, therefore, lower biochemical operating efficiency.

Because of these anatomical, biochemical and energetic complexities, C_4 metabolism is highly sensitive to limiting light intensities [for review: (Ubierna *et al.*, 2011)]. Recently, studies have focussed on characterising the progressive increase in Φ that is usually seen as light intensity decreases at both leaf (Bellasio and Griffiths, 2014b; Kromdijk *et al.*, 2010; Pengelly *et al.*, 2010; Tazoe *et al.*, 2008; Ubierna *et al.*, 2013) and canopy levels (Kromdijk *et al.*, 2008).The theoretical considerations highlighted above have associated this increase in Φ with decreased C_4 efficiency and a potential loss of photosynthetic carbon uptake (Furbank *et al.*, 1990; Kromdijk *et al.*, 2008; Tazoe *et al.*, 2008). Empirical evidence was needed to validate this suggestion and to explore the strategies that mature C_4 leaves deploy to cope with reduced light intensities.

Low light responses are highly relevant for C_4 canopy productivity, since up to 50% of net CO_2 uptake (Baker *et al.*, 1988; Kromdijk *et al.*, 2008; Long, 1993) is fixed by shaded leaves, under a light intensity which is typically 1 / 20 of full sunlight (Shirley, 1929). In a forest canopy, leaves are subjected to a similar degree of exposure throughout the year, whereas in crop canopies, most fully expanded leaves progressively acclimate to shade under newly emerging leaves. This long-term acclimation is accompanied by transitory, short-term responses such as daily shading, or more transient sunflecks. Furthermore, there is a gradient of leaf age down the crop canopy, with younger leaves exposed to full sunlight at the top of the canopy and older leaves subsequently exposed to canopy-filtered light.

Previously, I have studied how long-term acclimation to low light influenced short-term responses to illumination [Chapter 2, (Bellasio and Griffiths, 2014b)]. Plants grown under low light (LL) showed a capacity for maintaining low Φ even under decreasing light intensities, whereas Φ increased in equivalent plants grown under high light (HL). I suggested several mechanisms whereby C_4 leaves adapted throughout growth to low-light

conditions could maintain high photosynthetic conversion efficiency during steady-state photosynthesis.

In this Chapter, I grew maize plants under a light regime representing the acclimation of leaves shaded by an over-growing canopy, consisting of three weeks under high light followed by three weeks under diffuse, low light intensity. The leaf-level ATP production rate (J_{ATP}) was derived from gas exchange measurements under low O_2 in combination with PSII photochemical yield, measured CO_2 assimilation rate and on-line isotopic discrimination during photosynthesis (Δ). A full isotopic discrimination model was used to derive Φ from Δ (Farquhar, 1983; Farquhar and Cernusak, 2012; Ubierna *et al.*, 2011). With the directly derived values for J_{ATP}, the empirical ATP cost of net and gross assimilation (J_{ATP} / GA and J_{ATP} / A) could be calculated and compared with the predicted ATP cost of assimilation (ATP / GA). Mature leaves that had re-acclimated under low light (HLLL) showed very similar traits to plants which had been grown entirely under low light (LL). HLLL plants deployed two strategies to optimise the scarce ATP resources under low light: i) the reduction of respiration in the light (R_{LIGHT}); and ii) the reduction of leakiness (Φ). The comparison of J_{ATP} / GA with ATP / GA estimated with a novel metabolic model, showed that C_4 photosynthetic efficiency was constant in the vicinity of the light compensation point: thus, the predicted decrease in biochemical conversion efficiency based on Φ increase under limiting light does not occur in mature C_4 leaves acclimated to very low light intensities.

4.2 Materials and Methods

4.2.1 Plants

Plants were grown at the Plant Growth Facility located at the University of Cambridge Botanic Garden in controlled environment growth rooms (Conviron Ltd, Winnipeg, Canada) set at 16h day length, temperature of 25 °C / 23 °C (day/night) and 40 % relative humidity. The growth protocol was designed to standardize age and watering conditions throughout the experiment. Two light environments were established: high-intensity direct light (PAR = 600 µE m^{-2} s^{-1}) and low-intensity diffuse light (PAR = 100 µE m^{-2} s^{-1}), obtained using shading to mimic the understory of a canopy. Maize seeds (*Zea mays* L. F1 Hybrid PR31N27, Pioneer Hi-bred, Cremona, Italy) were sown weekly in 1.5 L pots filled with Levington pro M3 pot & bedding compost (Scotts, Godalming, UK). Plants were grown in three conditions: i) HL

plants were grown for 3 weeks under high light (fully expanded 4th leaf stage); ii) LL plants were grown for 4 weeks under low light (fully expanded 4th leaf stage); iii) HLLL plants were grown for 3 weeks under high light, the youngest fully expanded leaf was marked, and then plants were grown for the following 3 weeks under low light. Plants were manually watered daily, with particular care to avoid overwatering. When ready, plants were measured once and then discarded. Measurements were performed on the youngest fully expanded leaf of HL and LL plants, and on marked leaves of HLLL plants.

4.2.2 Gas exchange measurements with concurrent PSI / PSII Yield and on-line carbon isotopic discrimination (Δ)

The experimental setup was previously described in detail [Chapter 2, (Bellasio and Griffiths, 2014b)]. Briefly, an infra-red gas analyser (IRGA, a LI6400XT, Li-cor, USA), was fitted with a 6400-06 PAM2000 adapter, and with a Li-cor 6400-18 RGB light source. RGB light was used because, by providing equal fractions of R, G and B, it is likely to distribute excitation between M and BS with a more similar pattern to natural white light than the conventional 90% R 10% B source. The IRGA was fed with CO_2 ($\delta^{13}C$ = -6 ‰, Isi Soda, Isi, Vienna, A) and either a mixture of 2 % O_2 / N_2 or ambient air. PSI yield and PSII yield (*Y(II)*) were measured using a Dual Pam-F (Heinz Walz GmbH, Effeltrich, D). Pulse intensity was set to 20 mE m^{-2} s^{-1}, enough to saturate *F* and *P* signals (which occurred between 8 and 10 mE m^{-2} s^{-1}, data not shown). The IRGA was connected to a cryogenic H_2O and CO_2 trapping-purification line. Each day, one plant was subject to a RGB-light response curve, under 2 % O_2 and C_a = 600 µmol / mol (to determine the relationship between ETR and J_{ATP}) and a second RGB-light response curve under 21 % O_2 and reference CO_2 set at 400 µmol / mol, during which exhaust gas was trapped to determine Δ. With this procedure each day the $\delta^{13}C$ composition of a total of 12 CO_2 samples and 6 CO_2 references (representing responses to decreasing irradiances of one individual plant) were analysed directly using a VG SIRA dual inlet isotope ratio mass spectrometer (modified and maintained by Pro-Vac Services Ltd, Crewe, UK). Δ was calculated as reported in Table 4.1 (Evans *et al.*, 1986). *Y(II)* was determined at each light level for both light curves. J_{ATP} was calculated individually at each irradiance by multiplying the relationship between ETR and J_{ATP} (determined at low O_2) by the ratio between *Y(II)* at ambient and low O_2 (Table 4.1). Respiration in the light, R_{LIGHT} was

calculated as the *y*-intercept of the linear regression of *A* against $\cdot \mathrm{PAR} \cdot \frac{Y(II)}{3}$ [Table 4.1, (Bellasio and Griffiths, 2014b; Yin *et al.*, 2011b)]. The light compensation point was calculated using dedicated software (Photosyn assistant 1.2, Dundee Scientific, Dundee, UK), followed by repeated measures anova (Genstat). Point estimates were subject to anova and Tukey multiple comparisons as appropriate (Genstat).

4.2.3 Leakiness Φ from isotopic discrimination Δ

Modelling was previously described in detail [Chapter 2, (Bellasio and Griffiths, 2014b)], equations are reported in Table 4.1. Briefly, leakiness, Φ was resolved from Δ using the full model of Farquhar, as recently integrated to take into account the 'ternary' effects, i.e. the effect of water molecules diffusing outward stomata on CO_2 molecules diffusing inwards through still air (Farquhar and Cernusak, 2012). In this model, the weighted individual fractionations of the discriminating processes operating in C_4 photosynthesis are resolved. This model requires the CO_2 concentration in the different cellular compartments (notably M and BS), which were calculated by means of a C_4 model, which was in turn parameterized with the light response data (*A*, *Ci*, *Ca*, J_{ATP}) and respiration in the light (R_{LIGHT}). Bundle sheath conductance, required to parameterize the C_4 model, cannot be measured directly but it can be estimated by fitting the C_4 model to a measured quantity. In the 'Δ / Δ' fitting (Kromdijk *et al.*, 2010; Ubierna *et al.*, 2013), the C_4 model is rearranged to express a modelled isotopic discrimination and fitted to values for Δ. Here, I used the J / J fitting, that I have recently described [Chapter 2, (Bellasio and Griffiths, 2014b)], whereby the C_4 model is rearranged to express a modelled ATP production rate J_{MOD} and fitted to the empirically derived estimate for the leaf level ATP production rate J_{ATP}, described above. This procedure yielded a value for BS conductance (g_{BS}) for each individual plant which was obtained independently from Δ, and did not suffer the circularity of the 'Δ / Δ' fitting, arising from calculating g_{BS} and leakiness from the same values for Δ (Bellasio and Griffiths, 2014b).

4.2.4 Empirical and predicted ATP cost of gross assimilation

I refer to empirical ATP cost of net and gross assimilation as J_{ATP} / *A* and J_{ATP} / *GA*, while I refer to predicted ATP cost of *gross* assimilation as ATP / *GA*.

The empirical ATP cost of net and gross assimilation was calculated from the data obtained during the experiment. Firstly, the apparent leaf-level ATP cost of *net* assimilation

(J_{ATP} / A) was calculated from J_{ATP} and net assimilation, A. The derivation of J_{ATP} was described above (see also Table 4.1). J_{ATP} / A is relevant to net productivity and shows how much ATP the plant has to spend for net gain of a CO_2 molecule. Then, the leaf-level ATP cost of *gross* assimilation (J_{ATP} / GA) was calculated using values for GA, derived by summing A plus respiration in the light, R_{LIGHT} calculated by curve fitting (see above). J_{ATP} / GA is relevant to C_4 biochemistry and shows the empirical conversion efficiency of CO_2 into sugars. It is worth stressing that these values for J_{ATP} / GA are derived with a novel method based on gas exchange under low O_2, (Bellasio and Griffiths, 2014b; Yin *et al.*, 2011a; Yin *et al.*, 2011b), which does not rely on the assumptions used in the traditional derivation based on leaf absorptance and PSII optical section (von Caemmerer, 2000) and should therefore better represent the actual biochemical ATP demand of the portion of leaf subject to ecophysiological characterization. Because of the difficulty to derive J_{ATP} / GA based on leaf absorptance, and the difficulty in capturing the stoichiometry at the electron transport chain, the ATP cost of gross assimilation has often been predicted [e.g. (Tazoe *et al.*, 2008)].

A traditional way to predict ATP / GA uses leakiness as the sole proxy ['Φ' approach, (Furbank *et al.*, 1990; Tazoe *et al.*, 2008; von Caemmerer, 2000)]. The 'Φ' approach relies on the assumption that the ATP cost of the C_3 activity is invariably 3 ATP / CO_2 (photorespiration is neglected) while the ATP cost of the CCM depends solely on Φ. This implies that the CCM is driven solely by the activity of PEPC and that all the retrodiffusing CO_2 is refixed. Under these assumptions the ATP cost of the CCM is calculated by multiplying the ATP cost of PEPC (2 ATP / CO_2) by the ratio of CO_2 overcycling [1 / (1-Φ)]. The total ATP cost of gross assimilation results from summing the cost of the C_3 activity plus the cost of the CCM [Eqn 5 in (Tazoe *et al.*, 2008), or Eqn 4.55 in (von Caemmerer, 2000)]:

$$\frac{ATP}{GA}_{\Phi} = 3 + \frac{2}{1-\Phi} \qquad (4.1)$$

Where the subscript 'Φ' recalls that ATP / GA is derived from leakiness. Eqn 4.1 was solved for the three types of plants (HL, LL and HLLL) and light intensities from 50 to 500 μE $m^{-2}s^{-1}$ using the values of Φ derived from isotopic discrimination shown in Figure 4.3.

I propose a different approach to estimate ATP / GA, whereby the ATP demand of all biochemical processes underpinning assimilation (hence 'B' approach) are summed. The 'B' approach is comprehensive, and requires the quantification of all processes contributing to C_4 photosynthesis. I used the validated C_4 model (von Caemmerer, 2000), as recently integrated to describe the C_4 energetics [Chapter 3, (Bellasio and Griffiths, 2014c)]. The biochemical processes considered are: PGA reduction, carbohydrate synthesis, PEP regeneration, RuBP regeneration, and glycolate recycling while the PGA consumed by mitochondrial respiration is subtracted as likely to be consumed by basal metabolism [for derivation see Chapter 3 (Bellasio and Griffiths, 2014c)]. ATP / GA_B was calculated as:

$$\frac{ATP}{GA}_{\mathrm{B}} = 3V_C + \frac{7}{2}V_O + \frac{1}{6}A + PEPCK + 2PPDK - \frac{1}{3}R_{LIGHT} \quad (4.2)$$

Where the subscript 'B' recalls that all the biochemical processes were summed, V_C is the Rubisco carboxylation rate, V_O is the Rubisco oxygenation rate, A is net assimilation, $PEPCK$ is the PEP carboxykinase rate, $PPDK$ is the pyruvate phosphate dikinase rate, and R_{LIGH} is the respiration in the light. PEPCK was assumed to regenerate 20 % of the PEP required by PEP carboxylase (PEPC), the remainder was regenerated through PPDK. PEPC rate (V_P), V_C, and V_O were calculated with the validated von Caemmerer C_4 model (Table 4.1), in the light-limited form [Chapter 2, (Bellasio and Griffiths, 2014b; von Caemmerer, 2000)]. The model was constrained at each light intensity with the values for A and J_{ATP} shown in Figure 4.1, with the values for C_i / C_a and C_{BS} shown in Figure 4.2, with the values for R_{LIGHT} and g_{BS} reported in Table 4.2, and with the values for Φ shown in Figure 4.3. A parameter, known as x, is required to solve the C_4 model (Table 4.1). x partitions the ATP available between the CCM activity and the C_3 activity (PGA reduction, RuBP regeneration and glycolate recycling). In this calculation I did not assume a value for x to allow fitting to the constraints mentioned above.

Figure 4.1 Maize responses to decreasing light intensities (I)

Plants were grown under high light (HL), low light (LL) or LL following HL (HLLL). **(A)** Net assimilation (*A*). The curves were fitted in order to calculate the light compensation point (Table 4.2). The inset shows a magnification. **(B)** Total ATP production rate (J_{ATP}), measured with the low O_2 - ETR method (See gas exchange measurements). **(C)** On-line isotopic discrimination during photosynthesis (Δ). Error bars represent one standard error. n=6.

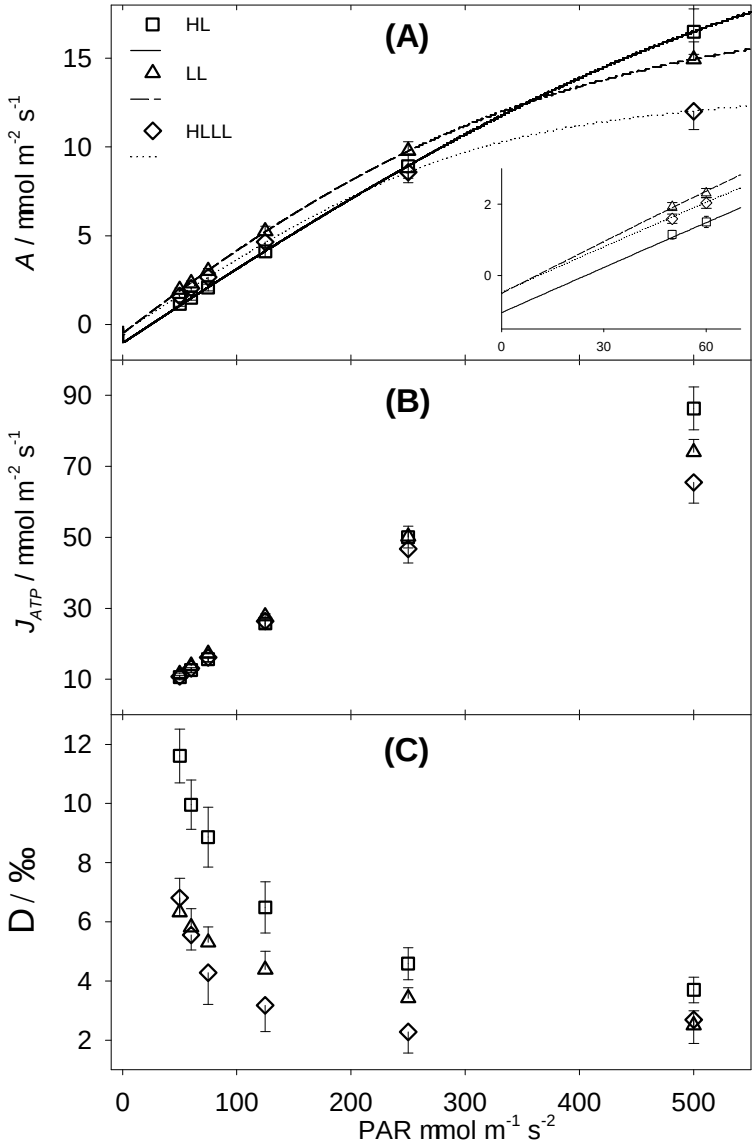

4.3 Results

4.3.1 Physiological response to decreasing light intensities

Figure 4.1 shows the responses of maize plants grown under three different light regimes to decreasing irradiance. Assimilation (*A*) differentiated plant responses (Figure 4.1 A). LL plants had the highest *A* at PAR lower than 500 μE m^{-2} s^{-1}. HL plants had the highest *A* at saturating PAR and the lowest *A* at PAR lower than 250 μE m^{-2} s^{-1}. HLLL plants had the lowest *A* under saturating light, (although these leaves were now 3 weeks older), but as light decreased between PAR (250 and 0) μE m^{-2} s^{-1} the response approached that of LL plants. Consistently, the light compensation point (*LCP*) and respiration in the light (R_{LIGHT}) of HLLL plants were similar to those of LL plants, and clearly lower than those of HL plants (Table 4.2).

The total ATP production rate (J_{ATP}) is shown in Figure 4.1 B. J_{ATP} was derived from gross assimilation under low O_2 and then corrected for photorespiration at ambient O_2 using the ratio of photochemical yield. At high PAR, J_{ATP} tracks the pattern of *A*, however, at low PAR, J_{ATP} of all plants was similar, suggesting that the higher *A* of LL and HLLL plants at limiting PAR (inset in Figure 4.1 A) was achieved through a higher conversion efficiency and lower respiration rate (Table 4.2). Isotopic discrimination during photosynthesis (Δ) is shown in Figure 4.1 C. In HL and HLLL plants Δ increased substantially at PAR lower than 250 μE m^{-2} s^{-1}, although in HLLL plants Δ was, on average, lower than for HL plants. LL plants showed a more gradual increase under decreasing PAR.

Figure 4.2 A shows stomatal conductance (g_s) and Figure 4.2 B shows C_i / C_a. C_i / C_a differentiated clearly between growth conditions, and was lowest in LL plants, highest in HL plants, while HLLL plants had intermediate values at all levels of PAR. C_i / C_a was higher than 0.5 at PAR < 125 μE m^{-2} s^{-1} (LL plants) reflecting the efforts made during the measurements to induce stomatal opening. A high C_i / C_a, was functional in the resolution of the isotopic discrimination model, to maximise the contribution of biochemical processes over the stomatal contribution to total isotopic discrimination [Table 4.1, (Cernusak *et al.*, 2013)]. This was especially important for HL plants which have, under low light, lower assimilation than LL plants [and higher ξ, Table 4.1, Appendix 1, (Evans *et al.*, 1986)]. Figure 4.2 C shows the CO_2 concentration in BS (C_{BS}), which was estimated by fitting a C_4

photosynthesis model, rearranged to express J_{MOD}, to the values for J_{ATP} described above. The difference between conditions was not significant, and was due to a small difference in permeability to CO_2 retrodiffusion out of the BS, (bundle sheath conductance, g_{BS}, Table 4.2).

Figure 4.2. Maize responses to decreasing light intensities (II)

(A) Stomatal conductance and **(B)** *Ci* / *Ca* responses to decreasing light intensity, under different light qualities, for plants grown under high light (HL), low light (LL) or LL following HL (HLLL) measured by gas exchange. **(C)** Response of C_{BS} to decreasing light intensity, under different light qualities, estimated by the C_4 model. Error bars represent one standard error. n=6.

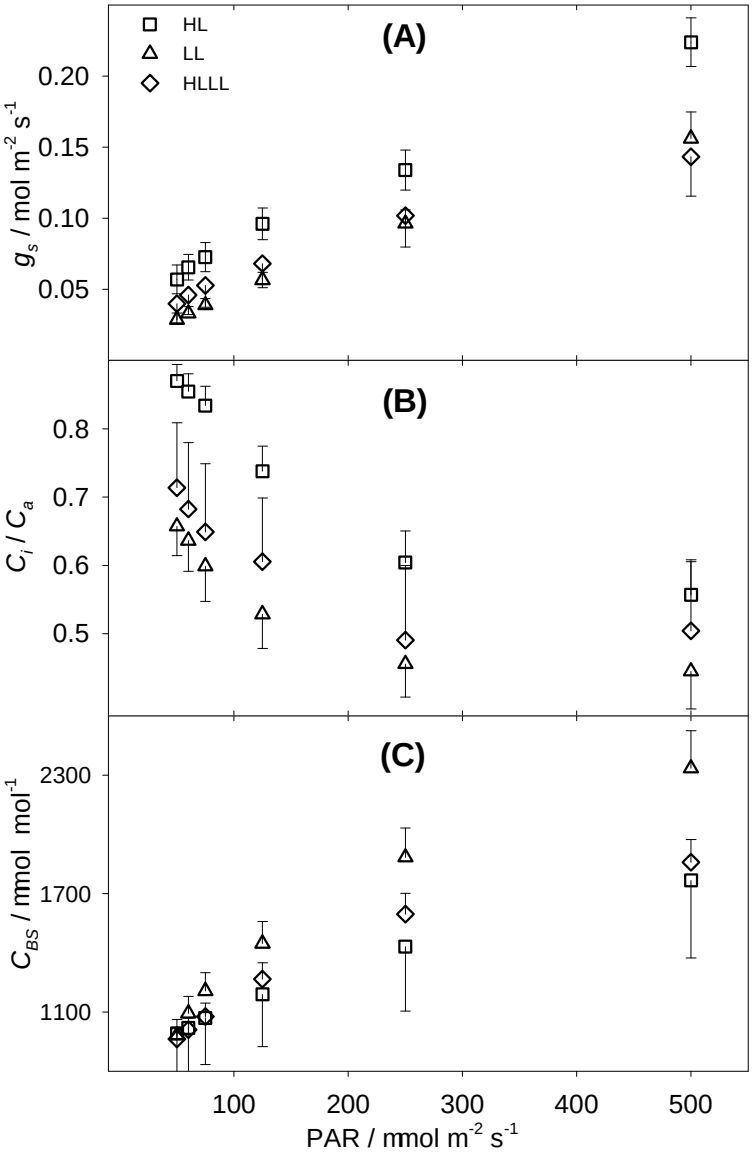

4.3.2 Leakiness

Figure 4.3 shows leakiness, Φ over the experimental range of PAR. These values were derived from real-time carbon isotope discrimination data, Δ, using a full isotopic discrimination model, as recently modified to take into account the ternary effects of gas diffusion across stomata (Farquhar and Cernusak, 2012). This isotopic discrimination model was parameterised using the validated model of C_4 photosynthesis (von Caemmerer, 2000). The C_4 model was fitted to J_{ATP}, using the recently described J / J fitting, which removes the circularity arising with the 'Δ / Δ' fitting whereby the isotopic discrimination model and the C_4 model are both fitted to the values for Δ [Chapter 2, (Bellasio and Griffiths, 2014b)]. HL plants had higher Φ than LL and HLLL under limiting PAR, with Φ increasing from 0.25 to 0.35 under decreasing PAR. HLLL plants had the lowest Φ under light intensities higher than 75 μE m^{-2} s^{-1}, however, at low light intensities, they showed a Φ increase with a similar trend to that of HL plants. In LL plants Φ was close to 0.24 and only marginally affected by light intensity.

Figure 4.3. Leakiness resolved from Δ

Leakiness (Φ) was resolved from on-line isotopic discrimination during photosynthesis (Δ) by means of a full isotopic discrimination model for HL plants (squares), LL plants (triangles) and HLLL plants (diamonds). Error bars represent one standard error. n=6.

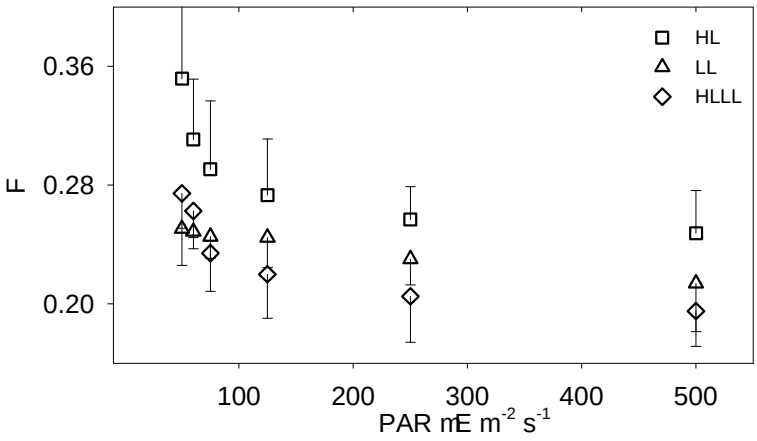

4.3.3 ATP cost of assimilation

Two empirical ATP costs of (net and gross) assimilation were derived. Figure 4.4 shows the empirical ATP cost of net assimilation J_{ATP} / A. This quantity shows the apparent ATP cost involved in the assimilation of CO_2, i.e. how much ATP the plant has to produce to assimilate one CO_2 molecule. Note that, at steady state, ATP production equals ATP consumption Figure 4.4 shows clearly that J_{ATP} / A for HLLL plants was very similar to that of LL plants and significantly lower than that of HL plants. This means that re-acclimation was extremely effective in reducing J_{ATP} / A, particularly in the vicinity of the light compensation point. Figure 4.5 shows the ATP cost of *gross* assimilation J_{ATP} / GA. This quantity is the biochemical conversion efficiency of C_4 assimilation, i.e. how much ATP is needed to convert bicarbonate into stable assimilates. The empirical values for J_{ATP} / GA (Fig. 4.5, symbols in panels A, B, and C) were close to 5.4 and not significantly influenced by light intensity or by the growth light regime. This means that, in contrast to the common interpretation, the biochemical conversion efficiency was not affected by light intensity.

To support this result theoretically, I predicted ATP / GA with two different approaches. These methods are compared in Figure 4.5. A simplified method used Φ as a sole proxy for C_4 operating efficiency ('Φ' approach, solid squares), whereas the complete biochemical method ('B' approach, solid circles) summed the individual ATP demands of processes involved in assimilation. Under low light intensities the 'Φ' approach resulted in a large overestimation of J_{ATP} / GA, especially in HL plants (Fig. 4.5 A), which display the characteristic hyperbolic Φ increase in proximity of the compensation point (Fig. 4.3). Under higher irradiances or when Φ was lower, the 'Φ' approach resulted in an accurate estimation of J_{ATP} / GA. The 'B' approach provided a better estimate of J_{ATP} / GA, across the range of incident light intensities and independent of the values for Φ. It is worth stressing that both these estimates were based on the same dataset shown in Figure 4.3, but, although the 'Φ' approach translated the Φ pattern shown in Figure 4.3 directly into ATP cost, the 'B' approach considered the rates of the underpinning biochemical reactions and summed the ATP costs involved in each individual process.

Figure 4.4. ATP cost of *net* assimilation

Measured ATP cost of *net* assimilation (J_{ATP} / A) for HL plants (squares), LL plants (triangles) and HLLL plants (diamonds). Error bars represent one standard error. n=6.

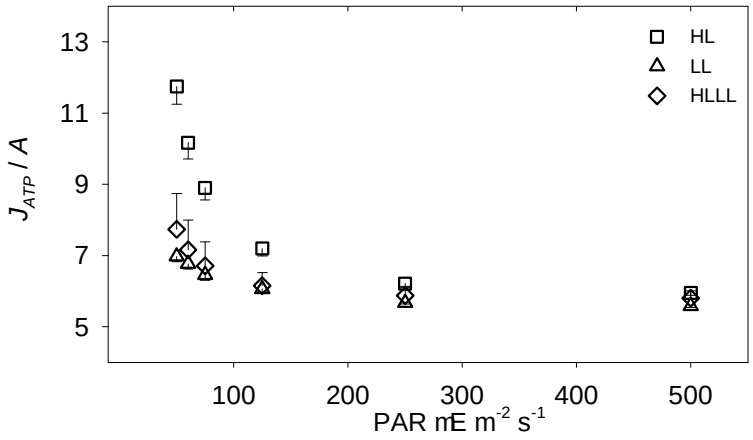

Figure 4.5. ATP cost of *gross* assimilation

ATP cost of *gross* assimilation, representing C_4 biochemical operating efficiency for HL plants (A), LL plants (B) and HLLL plants (C). The empirical values for J_{ATP} / *GA* (empty symbols) were compared to predicted values for ATP / *GA* (solid symbols) calculated with two different approaches. ATP / *GA* was calculated using Φ as the sole proxy for operating efficiency ('Φ' approach, solid squares) or using a comprehensive calculation summing the ATP cost of all processes contributing to assimilation ('B' approach, solid circles). Note that both calculations were based on the same dataset, presented in Figures 4.1, 4.2, 4.3 and Table 4.2. Error bars represent one standard error, n=6 plants per condition.

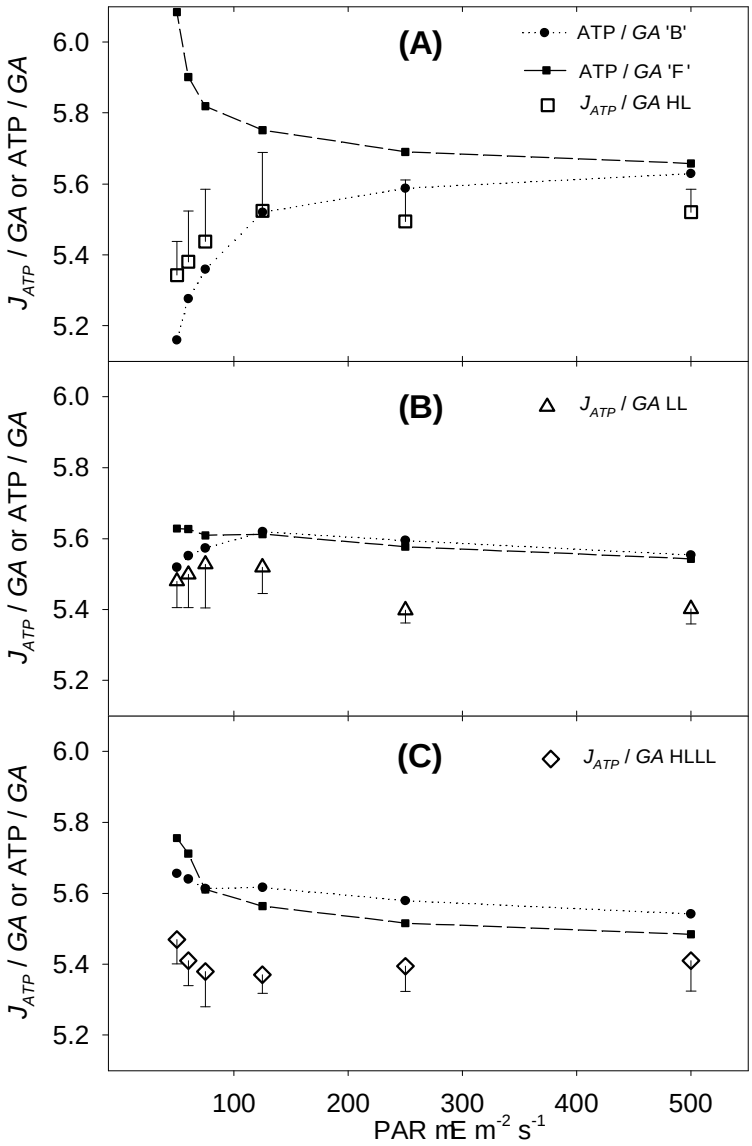

4.4 Discussion

Maize plants were grown under high light, then re-acclimated to diffuse low irradiance, and compared to plants grown either under high light or low light. The particular conditions of re-acclimation were intended to represent the transition from full sunlight to shaded conditions that maize leaves undergo when overgrown by newly emerging leaves at the top of the canopy. This is a natural acclimation process for maize leaves, in fact for the experimental plants all leaves grown under HL were retained throughout the re-acclimation and continued to photosynthesize under low irradiance. The opposite acclimation is not likely to be a physiologically realistic process, and in fact, when LL plants were moved to higher light intensities they promptly shed all leaves grown under low light. The natural re-acclimation to LL brought about substantial physiological changes, which have implications for the energy balance of leaves within a growing canopy.

4.4.1 Acclimation strategies

The three types of plants were subject to concurrent gas exchange, variable fluorescence and isotopic discrimination measurements. Direct estimates for J_{ATP} were derived from a combined low O_2-ETR method, and leakiness was derived from isotopic discrimination. This comprehensive ecophysiological characterization highlighted two main re-acclimation strategies.

A first strategy involved reducing respiration in the light (R_{LIGHT}). This reduction is underpinned by considerable changes at metabolic level that result in reducing the level of basal metabolism. This had a direct effect on the light compensation point (*LCP*) and, for this reason, it had a direct effect on the apparent ATP cost of net assimilation (see below). A second strategy involved the reduction of leakiness (Φ). HLLL plants showed reduced values for Φ as compared to HL plants. However the Φ hyperbolic increase under low irradiance was similar to that of HL plants. In contrast, and in agreement with recent results [Chapter 2, (Bellasio and Griffiths, 2014b; Ubierna *et al.*, 2013)], LL plants showed a linear trend, with Φ values that were only marginally affected by irradiance. Modelling suggested that the general reduction in Φ observed for HLLL plants (Fig. 4.3) could only be partially explain by the very limited reduction observed for g_{BS} (Table 4.2). The observed plasticity in Φ may then involve fine-tuning of biochemical reaction rates and, in particular, the ratio between the

CCM activity and the C_3 activity, or the capacity to accommodate g_{BS} in response to light intensity, as I have recently hypothesized (Bellasio and Griffiths, 2014b). However, the ultimate nature of this fine-tuning is still speculative.

Overall, these strategies were highly effective in reducing the apparent ATP cost of net assimilation J_{ATP} / A, in fact, under PAR = 50 μE m^{-2} s^{-1}, J_{ATP} / A for HLLL plants was 35 % lower than that of HL plants and very similar to that of LL plants (Fig. 4.4). However, this ATP cost reduction was largely associated with the reduced R_{LIGHT}. In fact, when the effect of R_{LIGHT} reduction was isolated and the biochemical operating efficiency (i.e. the ATP cost of gross assimilation J_{ATP} / GA) was considered, only minor energetic differences could be observed between different light treatments. Re-acclimation neither significantly influenced the empirical J_{ATP} / GA (mean of 5.47 for HLLL and 5.45 for HL, as compared to 5.40 for LL) nor the predicted ATP cost of GA (ATP / GA, 'B' approach, mean 5.56 for HLLL and 5.42 for HL, as compared to 5.61 for LL). This shows that if there were any effect of varied Φ on the overall biochemical conversion efficiency, the effect was undetectable using the methods described. On one hand this confirms the difficulties in estimating leakiness from leaf-level energetics (Furbank *et al.*, 1990; Kromdijk, 2010; Kromdijk *et al.*, 2014), on the other it highlights the complexity of the leakiness phenomenon, which depends at the same time on anatomical and biochemical traits. In this study I have specifically addressed the ATP demand, but other aspects are intertwined and may all contribute to Φ dynamics. These could include (Bellasio and Griffiths, 2014c; Furbank, 2011; von Caemmerer and Furbank, 2003), see also Chapter 3: i) regulating the ratio of C_4 dicarboxylic acid versus aminoacid export to BS; ii) regulating reducing power export from M to BS in response to demand; iii) partitioning metabolic work between contrasting cells types (e.g. PGA reduction, carbohydrate synthesis, glycolate recycling, RuBP + PEP regeneration); iv) optimising energy availability in BS and M; at the same time v) maintaining the equilibrium between the CCM and the C_3 activity; and, finally, vi) trading-off at the level of bundle sheath conductance, between the capacity to support very high diffusion (and assimilation) rates and the necessity to limit leakage of CO_2 out of the BS (Sowinski *et al.*, 2008).

4.4.2 Predicting C_4 operating efficiency

The 'conventional' approach to predict C_4 biochemical operating efficiency (i.e. the ATP cost of gross assimilation, ATP / GA) uses leakiness, Φ as the sole proxy (Eqn 4.2, referred

as the '*Φ*' approach). With the '*Φ'* approach the C_3 activity is considered to have an invariable cost of 3 ATP / *GA* (photorespiration is neglected), whereas the CCM is assumed to be supplied solely by PEPC activity, which is assumed to refix entirely the retrodiffused (leaked) CO_2. Our empirical evidence largely confirms the validity of the '*Φ*' approach, which closely predicted the trend and the magnitude of J_{ATP} / *GA* under PAR > 125 μE m^{-2} s^{-1} for LL + HLLL plants, and under PAR ≥ 500 μE m^{-2} s^{-1} for HL plants. However, under low irradiances, the '*Φ*' approach overestimated the trend of J_{ATP} / *GA*, especially for HL plants. This overestimation is dependent on the assumptions of the '*Φ*' approach, which hold only under high irradiances, while under low irradiance they are no longer valid. In fact, PEPC and Rubisco activities proportionally decrease under decreasing irradiance, limited by the decreasing ATP availability. As opposed to that, BS respiration is largely unaffected by light intensity, and, under decreasing light intensities, the BS-respired CO_2 progressively outweighs PEP carboxylation rate (V_P) (Sage, 2014). Hence, *Φ*, i.e. the ratio of retrodiffusing CO_2 over PEP carboxylation rate, becomes progressively higher as light intensity approaches the compensation point. This gives rise to the extensively documented (empirically and theoretically) hyperbolic *Φ* increase [for review see (Ubierna ***et al.***, 2011)], which can be largely supplied by respiration without an additional engagement of PEPC. A constant degree of engagement of PEPC, even under the hyperbolic *Φ* increase is consistent with the observation that both the ratio of PEPC / Rubisco carboxylation rate (V_P / V_C) and the optimal partitioning factor between the CCM activity and the C_3 activity ('*x*') are largely independent of light intensity (Kromdijk ***et al.***, 2010; von Caemmerer, 2000).

These considerations can be better appreciated if the CCM is viewed as complex machinery. The activity of PEPC is only one of the systems which contribute to loading CO_2 into the BS. Recently, it has become increasingly clear how photorespiration may contribute to the CCM, and is the predominant driving force in evolutionally early types of CCM (Sage ***et al.***, 2012; Schulze ***et al.***, 2013). I showed in this Chapter and in previous ones (Bellasio and Griffiths, 2014b) that the CCM can be increasingly supplied by respiration under limiting light conditions, bringing about increased leakiness even without a predicted increase in the activity of PEPC. It is worth noting that the compartmentalization of photochemical water oxidation to M cells, whose degree may vary considerably between subtypes and along the evolutionary line (Furbank, 2011; Meierhoff and Westhoff, 1993; Sage, 2004; Sage ***et al.***,

2011), also contributes to increasing the ratio CO_2 / O_2 at the active site of Rubisco and should also be considered as a component of the complex machinery of the CCM.

In view of this complexity, leakiness, which reflects inherently complex biochemical and anatomical traits, shall only be used to predict the magnitude (and ATP cost) of the CCM under high light. However, I showed that J_{ATP} / GA could be closely predicted using a complete biochemical approach ('B' approach, Eqn 4.2), whereby the ATP cost of all processes contributing to assimilation are summed. I used the equations that I have recently derived [see previous Chapters, (Bellasio and Griffiths, 2014b, c)], which are based on the comprehensive description of the C_4 metabolism outlined by Furbank (2011) and on the validated C_4 model (von Caemmerer, 2000, 2013). Within this approach, the ATP consuming processes considered are: PGA reduction, PEP regeneration (through PPDK and PEPCK) and carbohydrate synthesis. Furthermore the 'B' approach subtracts the PGA used by respiration, which does not need to be reduced (PGA reduction to DHAP consumes 1 ATP and 1 NADPH). With this comprehensive calculation, the empirical data could be closely predicted in the vicinity of the light compensation point. Notably, under decreasing light intensities, the biochemical conversion efficiency did not decrease, regardless of the hyperbolic Φ increase observed in HL and HLLL plants.

4.5 Conclusion

In this study I set out to investigate the strategies deployed by maize plants grown under high light intensities when re-acclimated to low light. I showed that the main re-acclimation drivers were the reduction of respiration and the reduction of leakiness, and these were likely to be accompanied by complex metabolic reorganization. Overall, these strategies were very effective in reducing the ATP cost of *net* assimilation under low light intensities, which, for HLLL plants, decreased by 35 % as compared to HL plants under PAR = 50 μE m^{-2} s^{-1}. This shows clearly that the apparent energy conversion efficiency under limiting light is to a considerable extent ameliorated by the acclimation of mature leaves to low light.

By calculating ATP cost of gross assimilation, I could isolate the contribution of day respiration from the other biochemical effects (which include the reduction of leakiness). The ATP cost of gross assimilation was not significantly different for HLLL plants as compared to HL plants. This showed that re-acclimation did not change the efficiency of C_4

metabolism, even if it considerably reduced leakiness, implying that the effect of reduced leakiness on C_4 energetics was not detectable. Leakiness dynamics may then be associated to other processes occurring at biochemical level such as the regulation between BS versus M metabolic engagement and CCM versus C_3 activity. In addition, I provided compelling theoretical and empirical evidence showing that the hyperbolic leakiness increase, observed under low light intensities (Figure 4.3), is not associated with a loss of energetic efficiency. The well-consolidated idea of C_4 efficiency loss under low light conditions [e.g. (Tazoe *et al.*, 2008; von Caemmerer, 2000)] relies on assumptions that should be reconsidered in view of recent discoveries: the CCM is not uniquely supplied by the ATP-costly PEPC activity, but, under certain conditions, the contribution through respiration and photorespiration may be significant [Chapter 2 (Bellasio and Griffiths, 2014b; Sage, 2014; Sage *et al.*, 2012)]. I proposed a comprehensive biochemical method, derived in Chapter 3 (Bellasio and Griffiths, 2014c), based on the validated C_4 model (von Caemmerer, 2000). The biochemical method, predicts the C_4 conversion efficiency (as ATP cost of gross assimilation), taking into account the active and passive contribution to the CCM.

The implications for loss of productivity at the field scale being specifically associated with increased leakiness (Kromdijk *et al.*, 2008) may be less severe than previously thought. However, here I have shown the potential for acclimation with a somewhat extreme acclimation pattern whereby mature leaves were switched from the full light to deep shade. Realistically, mature leaves will undergo a more gradual transition from full sunlight through a condition characterized by rapid changes in irradiance (daily shading, sunflecks), to complete shade. The actual extent to which leaves optimize energy efficiency, when exposed to such a complex pattern of illumination under field conditions, remains to be addressed.

4.6 Chapter 4 Tables.

Table 4.1. Abbreviations, definitions and units for variables and acronyms described in Chapter 4

Symbol	Definition	Values / Units / References
A	Net assimilation	µmol m^{-2} s^{-1}
a	^{13}C fractionation due to diffusion of CO_2 in air. Due to vigorous ventilation I ignored fractionation at the boundary layer.	4.4 ‰ (Craig, 1953; Kromdijk *et al.*, 2010)
a_d	^{13}C fractionation due to diffusion of CO_2 in water	0.7 ‰ (O'Leary, 1984)
ATP /GA	Predicted ATP demand for gross assimilation, i.e. predicted biochemical operating efficiency	µmol m^{-2} s^{-1}
b_3	^{13}C fractionation during carboxylation by Rubisco including respiration and photorespiration fractionation $b_3 = b_3' - \frac{e\prime \cdot R_{LIGHT} + f \cdot \mathrm{F}}{V_c}$	‰ (Farquhar, 1983; Ubierna *et al.*, 2013).
b_3'	^{13}C fractionation during carboxylation by Rubisco (excluding respiration and photorespiration fractionation)	30 ‰ (Roeske and Oleary, 1984)
b_4	Net fractionation by CO_2 dissolution, hydration and PEPC carboxylation including respiratory fractionation $b_4 = b_4' - \frac{e\prime R_M}{V_P}$	‰ (Farquhar, 1983; Henderson *et al.*, 1992)
b_4'	Net fractionation by CO_2 dissolution, hydration and PEPC carboxylation (excluding respiratory fractionation)	-5.7 ‰ at 25 °C but variable with temperature (Farquhar, 1983; Henderson *et al.*, 1992; Kromdijk *et al.*, 2010).
BS	Bundle sheath	
C_{BS}	CO_2 concentration in the bundle sheath $C_{BS} = \frac{\frac{xJ_{ATP}}{2} - \frac{R_{LIGHT}}{2} - A}{g_{BS}} + C_M$	µmol mol^{-1}
CCM	Carbon concentrating mechanism	
C_i	CO_2 concentration in the intercellular spaces as calculated by the IRGA.	µmol mol^{-1} (Li-cor 6400 manual Eqn 1-18)
C_M	CO_2 concentration in the mesophyll $C_M = C_i - \frac{A}{g_M}$	µmol mol^{-1}
e	^{13}C fractionation during decarboxylation	0 ‰ to -10 ‰, (Barbour *et al.*, 2007; Ghashghaie *et al.*, 2001; Gillon and Griffiths, 1997; Hymus *et al.*, 2005; Igamberdiev *et al.*, 2004; Sun *et al.*, 2012) -6 ‰ in this study (Kromdijk *et al.*, 2010).
e'	^{13}C fractionation during decarboxylation, including the correction for measurement artefacts: $\mathrm{e}' = \mathrm{e} + \delta^{13}C_{measurements} - \delta^{13}C_{growth\ chamber}$	‰ $\delta^{13}C_{measurements}$ = -6.38 ‰; $\delta^{13}C_{growth\ chamber}$ = -8 ‰ (Wingate *et al.*, 2007)
e_s	^{13}C fractionation during internal CO_2 dissolution	1.1 ‰ (Mook *et al.*, 1974; Vogel, 1980; Vogel *et al.*, 1970).
E	Transpiration rate (calculated by the IRGA software, parameter Trmmol)	mmol m^{-2} s^{-1}
ETR	Electron transport rate	µmol m^{-2} s^{-1}
F	Rate of photorespiratory CO_2 evolution $F = 0.5 \cdot V_O$	µmol m^{-2} s^{-1} (Stutz *et al.*, 2014; von Caemmerer, 2013)

f	^{13}C fractionation during photorespiration.	11.6 ‰ (Lanigan *et al.*, 2008).
GA	Gross assimilation $GA = A + R_{LIGHT}$	µmol m^{-2} s^{-1}
g_{ac}	conductance to diffusion of CO_2 in air (calculated by the IRGA software, parameter CndCO2)	mol m^{-2} s^{-1}
g_{BS}	Bundle sheath conductance to CO_2, calculated by fitting J_{MOD} to J_{ATP}	mol m^2 s^{-1} (Bellasio and Griffiths, 2014b)
g_M	Mesophyll conductance to CO_2	1 mol m^2 s^{-1} bar^{-1} (Kromdijk *et al.*, 2010)
g_s	Stomatal conductance to CO_2	mol m^2 s^{-1}
IRGA	Infra-red gas analyzer	
J_{ATP}	ATP production rate $J_{ATP} = \frac{3\,GA_{Low\,O_2}\,Y(II)}{0.59\,Y(II)_{Low\,O_2}}$	µmol m^{-2} s^{-1} (Bellasio and Griffiths, 2014b)
J_{ATP} / *A*	ATP production rate relative to net assimilation	dimensionless
J_{ATP} / *GA*	ATP production rate relative to gross assimilation	dimensionless
J_{MOD}	Modelled ATP production rate $J_{MOD} = \frac{-y+\sqrt{y^2-4wz}}{2w}$ where: $w = \frac{x-x^2}{6A}$; $y = \frac{1-x}{3}\left[\frac{g_{BS}}{A} + \left(C_M - \frac{R_M}{g_{BS}} - \gamma^* O_M\right) - 1 - \frac{\alpha\gamma^*}{0.047}\right] - \frac{x}{2}\left(1 + \frac{R_{LIGHT}}{A}\right)$; $z = \left(1 + \frac{R_{LIGHT}}{A}\right)\left(R_M - g_{BS}C_M - \frac{7\,g_{BS}\gamma^* O_M}{3}\right) + (R_{LIGHT} + A)\left(1 - \frac{7\alpha\gamma^*}{3 \cdot 0.047}\right)$	µmol m^{-2} s^{-1}µm (Bellasio and Griffiths, 2014b; Ubierna *et al.*, 2013; von Caemmerer, 2000)
M	Mesophyll	
O_{BS}	O_2 mol fraction in the bundle sheath cells (in air at equilibrium) $O_{BS} = O_M + \frac{\alpha A}{0.047\,g_{BS}}$	µmol mol^{-1} (von Caemmerer, 2000)
O_M	O_2 mol fraction in the mesophyll cells (in air at equilibrium)	210000 µmol mol^{-1}
PAR	Photosynthetically active radiation	µE m^{-2} s^{-1}
PEP	Phosphoenolpyruvate	
PEPC	Phosphoenolpyruvate carboxylase	
PEPCK	Phosphoenolpyruvate carboxykinase	
PGA	3-phosphoglyceric acid	
PPDK	Pyruvate phosphate dikinase	
PSI	Photosystem I	
PSII	Photosystem II	
RB	Red-Blue	
RGB	Red-Green-Blue	
R_{LIGHT}	Respiration in the light	µmol m^{-2} s^{-1}
R_M	Mesophyll non photorespiratory CO_2 production in the light R_M = 0.5 R_{LIGHT}	µmol m^{-2} s^{-1} (Kromdijk *et al.*, 2010; Ubierna *et al.*, 2013; von Caemmerer, 2000)
RPP	Reductive pentose phosphate	
Rubisco	Ribulose bisphosphate carboxylase oxygenase	
RuBP	Ribulose-1,5-bisphosphate	
s	Fractionation during leakage of CO_2 out of the bundle sheath cells	1.8 ‰ (Henderson *et al.*, 1992).

t	Ternary effects t = $\frac{(1+a)\,E}{2000\,g_{ac}}$	‰ (Farquhar and Cernusak, 2012)
V_C	Rubisco carboxylation rate $V_C = \frac{(A+R_{LIGHT})}{1-\frac{\gamma^* O_{BS}}{C_{BS}}}$	μmol m^{-2} s^{-1} (Ubierna *et al.*, 2011)
V_O	Rubisco oxygenation rate $V_O = \frac{V_C-A-R_{LIGHT}}{0.5}$	μmol m^{-2} s^{-1} (Ubierna *et al.*, 2011)
V_P	PEP Carboxylation rate $V_P = \frac{xJ_{ATP}}{2}$	
x	J_{ATP} partitioning factor between C_4 activity (V_P) and C_3 activity V_C+V_O (RPP pathway and photorespiratory cycle)	0.4 (Kromdijk *et al.*, 2010; Ubierna *et al.*, 2011; Ubierna *et al.*, 2013; von Caemmerer, 2000)
Y(II)	Yield of photosystem II $Y(II) = \frac{F'_m-F_s}{F'_m}$	dimensionless (Genty *et al.*, 1989)
α	Fraction of PSII active in BS cells	0.15 (Edwards and Baker, 1993; Kromdijk *et al.*, 2010; von Caemmerer, 2000).
*γ**	Half of the reciprocal of the Rubisco specificity	0.000193 (von Caemmerer, 2000).
Δ	^{13}C Isotopic discrimination $\Delta = \frac{\xi(\delta_o-\delta_e)}{1+\delta_o-\xi(\delta_o-\delta_e)}$ where: $\xi = \frac{C_e}{C_e-C_o}$ see Chapter 4 Appendix 1; δ_e is the isotopic composition of the reference gas. δ_o is the isotopic composition of the gas leaving the cuvette. C_e and C_o represent the CO_2 mole fraction respectively entering and leaving the cuvette corrected for differing amounts of water vapour according to (von Caemmerer and Farquhar, 1981).	‰ (Evans *et al.*, 1986)
$\delta^{13}C$	^{13}C isotopic composition relative to Pee dee belemnite	‰
Φ	Leakiness defined as the leak rate relative toV_P	dimensionless
Φ	Leakiness estimated with the isotope method including respiratory and photorespiratory fractionation, ternary effects and estimating C_{BS} with the C_4 model $\Phi = \frac{C_{BS}-C_M}{C_M}\frac{b_4 C_M(1+t)+a(C_a-C_i)-C_a\Delta_{OBS}(1-t)}{(1+t)[C_a\Delta_{OBS}(1-t)-a(C_a-C_i)-b_3 C_{BS}+s(C_{BS}-C_M)]}$	dimensionless (Farquhar and Cernusak, 2012)

Table 4.2. Physiological responses for plants grown under high light (HL), low light (LL) or LL following HL (HLLL)

The light compensation point (*LCP*) was determined by fitting light curves with dedicated software; respiration in the light (R_{LIGHT}) was determined by linear regression of *A* against PAR·*Y(II)*/3; bundle sheath conductance (g_{BS}) was determined by fitting a modelled J_{MOD} to the measured J_{ATP} (Fig. 4.3). Different letters identify significant differences across rows at $p<0.05$ in a Tukey multiple comparison test (Genstat). Mean values (± SE), n= 6 per treatment

	Unit	Mean	HL	LL	HLLL
LCP	µE m^{-2} s^{-1}	15.3	24.4(± 1.9)^{a}	10.4(± 0.65)^{b}	11.2(±1.0)^{b}
R_{LIGHT}	µmol O_2 m^{-2} s^{-1}	0.680	1.05(± 0.14)^{a}	0.510(± 0.057)^{b}	0.477(± 0.053)^{b}
g_{BS}	mol m^{-2} s^{-1}	0.000944	0.00136 (± $5.2•10^{-4}$)^{a}	0.000647 (± $9.2•10^{-5}$)^{a}	0.000822 (± $1.9•10^{-4}$)^{a}

5 General conclusion

5.1 Summary of findings

This experimental programme was set out to investigate strategies deployed by C_4 plants to adjust operating efficiency under different conditions of light availability and capture. Firstly, systems deployed to regulate Φ in response to environmental pressures were investigated, under the hypothesis that Φ is not an absolute constraint of C_4 photosynthesis but it has a physiological role which is under metabolic control. Secondly, the models used to describe C_4 physiology were updated, to give a more realistic description of the C_4 energetics under those conditions where disruption or efficiency loss was predicted with a conventional modelling approach.

In the second Chapter Φ was studied in maize plants grown under high light or under low light by isotopic discrimination, gas exchange and photochemistry measurements. Respiration in the light and ATP production rate were measured directly. Data were interpreted using the established approach of fitting Δ to Δ and using a novel approach of fitting J to J that removed the circularity of the Δ / Δ approach. HL plants displayed a characteristic leakiness increase when exposed to decreasing light intensities, a pattern which had been associated with a loss of photosynthetic efficiency (Tazoe *et al.*, 2008). Conversely plants grown in LL showed constant Φ at decreasing light intensities, a response consistent with recent findings (Ubierna *et al.*, 2013). This particular response was not predicted by the C_4 model under common constraints but, by releasing the constraint of equal C_4 / C_3 energy partitioning (x) or equal bundle sheath conductance between light intensities, it was possible to formulate hypotheses to describe the two different acclimation strategies. This response was interpreted as a contrasting strategy deployed by HL and LL plants. HL plants operated efficiently at HL but maintained a high PEPC activity at low light, resulting in high CO_2 overcycling. LL plants under limiting light intensities downregulated PEPC more than proportionally to the C_3 activity, and there was a shift from a PEPC-driven CCM to a respiration-driven CCM, effectively cutting the ATP cost of the CCM when light was limiting. Physiological assimilation rates were maintained either by increasing Rubisco activity or by tuning g_{BS}, effectively trapping the CO_2 resulting from decarboxylation of malate and pyruvate. Overall the second Chapter showed that long term acclimation to low light intensities brought about physiological changes which could potentially increase the operating efficiency under scarce ATP resources.

The third Chapter investigated the influence of light quality on ATP partitioning between contrasting cell types and how this would influence C_4 operating efficiency. Firstly, the ATP imbalance caused by changing light quality was quantified under contrasting light qualities using their projected extinction within the leaf profile simulated with a novel optical model. The rate of ATP synthesis in M and BS compartments was estimated and it was shown that light quality can potentially induce a threefold imbalance in ATP supply between BS and M. Secondly, by measuring gas exchange, variable chlorophyll fluorescence and real-time carbon isotope discrimination, the overall leaf-level operating efficiency could be derived. It was predicted in previous work (Evans ***et al.***, 2007) that the ATP imbalance between BS and M would have caused loss of coordination between BS and M function and, ultimately, a decrease in biochemical conversion efficiency. In contrast to these predictions, plants maintained high biochemical conversion efficiency under different light qualities. In order to explore the underpinning biochemical mechanisms of this plasticity a comprehensive metabolic model was derived and parameterized with the output of validated C_4 model based on leaf-level gas exchange data (von Caemmerer, 2013). It is worth noting that such a data-based parameterization is not necessary and the metabolic model can also be used independently of measured data, to facilitate formulating alternative scenarios of energy and metabolites allocation. Here I investigated whether the maize C_4 system could respond to changing environmental conditions by adjusting the C_4 (amino)acid (MAL or ASP) delivered from M to BS, or by adjusting the proportions of other metabolic reactions shared between both cell types, such as carbohydrate synthesis, PGA reduction and PEP regeneration (Friso ***et al.***, 2010; Furbank, 2011; Majeran ***et al.***, 2010; Spilatro and Preiss, 1987; Walker ***et al.***, 1986; Wingler ***et al.***, 1999). Three scenarios could be depicted, whereby metabolism, although subject to the general constraints imposed by C_4 physiology, was able to take the maximum advantage of environmental conditions by changing the relative engagement of BS and M functions, which were ultimately under environmental control. These results, based on metabolic modelling and empirical measurements, provide definitive evidence for the role of complementarity between BS and M functions, allowing ATP demand to be regulated in response to contrasting environmental conditions. In particular, the two decarboxylase systems in BS of maize, with a variable rate of transamination, allow the regulation of NADPH supply to match demand in BS independently of the delivery of CO_2. The findings

of this Chapter highlight the importance of C_4 metabolic models in helping to explain acclimation and adaptation to changing light intensity for all C_4 subgroups. Furthermore, metabolic plasticity was clearly linked to the capacity to maintain high photosynthetic efficiency under changing environmental conditions.

The fourth Chapter developed the previous lines of research and investigated the strategies deployed by maize plants grown under high light intensities when re-acclimated to low light. Firstly, the hypothesis of whether plants grown under high light can modify their physiology and reach a status of higher operating efficiency when exposed to low light for a suitable acclimation period was tested. Plants were grown under high light and low light for three weeks, then, HL plants were transferred to low light for further three weeks. This re-acclimation was intended to simulate the acclimation of leaves in a crop canopy where younger leaves photosynthesize in full sunlight and older leaves are shaded in a lower position. Re-acclimation was very effective in reducing ATP cost of net assimilation under low light intensities which, for HLLL plants, decreased by 35 % as compared to HL plants under PAR = 50 $\mu E\ m^{-2}\ s^{-1}$. The apparent energy conversion efficiency under limiting light was therefore to a considerable extent ameliorated by the acclimation of mature leaves to low light. The main re-acclimation drivers were the reduction of respiration and the reduction of leakiness, and these were likely to be accompanied by complex metabolic reorganization. By calculating ATP cost of gross assimilation, the contribution of day respiration could be isolated from the other biochemical effects (which include the reduction of leakiness). The ATP cost of gross assimilation was not significantly different for HLLL plants as compared to HL plants. This showed that re-acclimation did not change the efficiency of C_4 metabolism, even if it considerably reduced leakiness. In addition, theoretical and empirical evidence showed that the hyperbolic leakiness increase, observed under low light intensities (Figure 4.3), is not associated with a loss of energetic efficiency. Leakiness dynamics may then be associated to other processes occurring at biochemical level such as the regulation between BS versus M metabolic engagement and CCM versus C_3 activity. Since under low light conditions, respiration and photorespiration may contribute significantly to supplying the CCM (Bellasio and Griffiths, 2014b; Sage, 2014; Sage *et al.*, 2012), and these phenomena do not use light-derived ATP, C_4 operating efficiency can be derived from Φ only under high light intensity. Although, in the vicinity of the compensation point the ATP cost of gross

assimilation could be predicted by newly derived comprehensive biochemical method (Bellasio and Griffiths, 2014c), which takes into account the active and passive contribution to the CCM.

5.2 Wider implications: ecosystem and agroecosystem

As it was recently noted (Sage, 2014) physiologists have long wondered about why the C_4 pathway is maladapted for deep shade environments. An early proposed explanation was that C_4 plants have a lower quantum yield than C_3 species in the relatively cool, low-light conditions of the forest interior (Ehleringer and Pearcy, 1983; Ehleringer, 1978). However, in lower latitudes, temperatures in the forest interiors are not consistently cool enough to favour greater C_3 quantum yields, particularly in the lower CO_2 atmospheres of the recent past (Ehleringer *et al.*, 1997; Pearcy and Calkin, 1983). Later it was hypothesized that, because C_4 plants have a more complex biochemistry, they are slower to exploit sunflecks, which, in forest understories, sunflecks contribute a large fraction of the daily photons a plant may absorb (Pearcy, 1990). This hypothesis was unlikely as examinations of sunfleck use do not reveal any major differences between the photosynthetic pathways. For instance maize has similar efficiency of sunfleck use as C_3 crop species, with the exception of short sunflecks, where maize was slower (Krall and Pearcy, 1993). Insufficient light seem not to explain the limitations either: numerous C_4 grasses are also adapted to the shade of forest interiors (Sage, 2014) and some are successful enough to become severe understory weeds (e.g. *Microstegium vimineum* in forests of the eastern USA). Furthermore, high-light-adapted C_4 grasses can form dense canopies where about half of the leaf area exists in shade (Krall and Pearcy, 1993; Long, 1993). Species forming dense canopies include the three most important C_4 crops in the world (maize, sorghum and sugar cane), the most promising of new bioenergy crops (*Miscanthus*, switchgrass and elephant grass), and dominant pasture and prairie grasses of the warm-temperate to tropical grasslands. In this study I showed that C_4 plants deal with low light conditions and with different light qualities without losing operating efficiency of overall carbon assimilation and the increase in leakiness observed under low light cannot be associated with a decreased C_4 efficiency. The increase in leakiness observed under low light was a leading possibility explaining why the C_4 pathway is maladapted for deep shade environments, hence another possible explanation has now been eliminated. On one hand this

means that the implications for loss of productivity at the field scale being specifically associated with increased leakiness (Kromdijk ***et al.***, 2008) may be less severe than previously thought (Kromdijk ***et al.***, 2014). On the other, it means that the textbook paradigm that the C_4 pathway is maladapted to low light, and an explanation for the failure of C_4 species to succeed as canopy-forming tree has yet to be gained. It has recently be suggested that that there may be no inherent physiological reason for C_4 failure in the shade and we should instead look at non-photosynthetic mechanisms associated with life history, ecological interactions or phylogenetic history to explain the general lack of C_4 forests (Sage, 2014). Probably, though, physiological and phylogenetic traits are intertwined. Maybe only by relating those traits to one another, the question of why most C_4 plants are sun-adapted could be answered.

When the findings of this research are extended to the agroecosystem level, many new factors influencing efficiency come into play. For this reason, although the biochemical efficiency of a C_4 may be at the optimum, the input use efficiency of a C_4 crop canopy may greatly vary. Management techniques will determine how the physiology of the single plant will scale up to the overall performance of the crop. When these are taken into account, the inefficiencies of agroecosystems become apparent. For example, 35 % of water used in agriculture is lost as a result of irrigation techniques (Suat ***et al.***, 2011), or even more strikingly, 50 % of nitrogen applied to agroecosystems is lost as leachate or microbial interconversion (Fageria and Baligar, 2005). This is also because plants have become progressively less efficient during centuries of breeding which have specifically selected plants under optimal availability of resources (soluble nutrients, soft soil, and chemical protection). As a result, modern plants grow faster but require more inputs. Furthermore, the high leaf-level C_4 biochemical conversion efficiency of light into stable assimilates is limited to defined environmental optima (e.g. relatively high temperature and sufficient water supply). Outside these environmental optima, C_4 plant performance is greatly reduced and C_4 plants are generally outperformed by C_3 plants (Ehleringer and Pearcy, 1983; Pearcy and Ehleringer, 1984). For these reasons, although processes may be well optimised at leaf level, at agroecosystem level, both the physiological conversion efficiency and the agroecosystem efficiency have a great potential for improvement.

This potential can be gauged against the inherent high efficiency of spontaneous plants in natural ecosystems (Dawson *et al.*, 2008). The high efficiency of natural ecosystems is associated a high physiological differentiation of the ecosystem, with organisms contributing to supplying, recycling, and recovering resources. For instance, N-fixing microorganisms can supply nitrogen or mycorrhizas can extract nutrients from soil minerals and can contribute to water uptake (Bonfante and Anca, 2009; Humphreys *et al.*, 2010; Read *et al.*, 1989; Taylor *et al.*, 2009). Breeding strategies as well as cropping techniques should therefore be inspired by natural ecosystems, and make use all those resources that maintain high conversion efficiency, with particular regard to physiological diversity. Unfortunately though, technically feasible opportunities are not automatically implementable solutions. Management techniques are influenced by the socio-cultural conditions, by politics and economics, hence possible improvements have to be validated by economic feasibility, i.e. they have to be selected for profitability. In fact, although agriculture is heavily subsidized, the everyday management choices are made by the farmer, who operates towards maximisation of economical return. In this respect the ever more daunting scarcity of resources (and the resulting price dynamics) may turn out to be the most effective drive towards sustainability of our agroecosystems.

In order to improve the efficiency of the agroecosystems, it is of critical importance to consider the inputs (and the outputs) of the ecosystem as a whole. For instance, when evaluating the nitrogen use efficiency, the N required for a certain edible production should be calculated on the basis of the N ***applied*** to the field (Cassman *et al.*, 2002), instead considering the N uptaken by the crop (Schmitt and Edwards, 1981). In this way the runoff, leaching and volatilization losses would be accounted for. Similarly, water use efficiency at field scale should be calculated on the base of water ***applied*** to the field, and not on the base of water evapotranspired by plants (Igbadun *et al.*, 2006). In this way hydraulic efficiency and losses associated to water management would be accounted for (Suat *et al.*, 2011).

5.3 Future perspectives

In the field of light limitations of C_4 photosynthesis many explanations have been proposed and subsequently discarded. As opposed to what recently suggested by R. Sage

(2013), I believe physiological questions have not dried out and the new insights shown here present new challenges and open up new research paths.

Concerning the reasons for the absence of C_4 trees, perhaps shade tolerance is not the key factor in promoting arborescence. If this were true, even if we accept that C_4 plants are not poorer performer in the shade, we would still not be able to explain the lack of C_4 forests. I believe that the reasons for the lack of C_4 trees should be searched in the complex interaction between C_4 biochemistry and hydraulic relations (Griffiths ***et al.***, 2013; Osborne and Sack, 2012; Ripley ***et al.***, 2007; Taylor ***et al.***, 2014). In particular, the key success trait associated with canopy forming trees may not be shade tolerance but drought tolerance instead. The incapacity of putative C_4 tree sapling to succeed may be due to the susceptibility to drought events, key to success in tropical environments (Beerling and Osborne, 2006). This could be due to a causal relationship between leaf water potential and bundle sheath conductance. Were these to be causally linked, drought could constraint metabolite exchange between M and BS, and thus jeopardise assimilation, similarly to what was shown for fluctuating temperature (Bilska and Sowiński, 2010; Sowiński, 2013). To support this hypothesis, many questions need to be answered: To what extent is a tree sapling subject to more extreme fluctuations in leaf water potential than a grass? What is the effect of fluctuating water potentials on leaf turgor? What is the effect of turgor on bundle sheath conductance? What are the constraints on metabolite trafficking between M and BS?

Concerning acclimation to low light intensities, in this experimental programme maize plants showed the potential for acclimation at steady state with a somewhat extreme acclimation pattern, whereby mature leaves were switched from the full light to deep shade and plants were exposed to monochromatic light. Realistically, mature leaves will undergo a more gradual transition from full sunlight through a condition characterized by rapid changes in irradiance (daily shading, sunflecks), to complete shading by the crop canopy. Even in these conditions, light will vary rapidly in quality and in time. The performance of C_4 plants under such variable conditions is still debated. Perhaps C_4 plants have limited capacity to efficiently exploit rapid light transients (Krall and Pearcy, 1993; Sun ***et al.***, 2014), however, the actual extent to which leaves optimize energy efficiency, when exposed to such a complex pattern of illumination under field conditions, remains to be addressed.

Concerning light quality, recently, Sun and colleagues showed that, during steady state photosynthesis under blue (or red) light, a transient exposure to green light induced a transient spike in leakiness (Sun ***et al.***, 2014). In the same experiment, during steady state photosynthesis under green light, a transient exposure to blue light induced a temporary sharp decrease in leakiness. These leakiness transients were explained as a short-term alteration of the equilibrium between the CCM and C_3 activity caused by a change in light quality. Changing light quality from green to blue (which is more rapidly absorbed within the profile, Chapter 3) would have induced a transient ATP starvation in BS, and consequently a reduced RuBP regenerating capacity. This would have limited Rubisco carboxylation, and manifested the leakiness transient. Efficiency eventually recovered after a time lapse dependent on the species (***Miscanthus*** slower than maize). I propose that there is a biochemical rationale underpinning these transients. Those leakiness transients can be associated to another dynamic phenomenon, which has been known for nearly half a century: a light induced CO_2 burst (later LICB). The LICB is a phenomenon whereby dark adapted leaves transiently emit an appreciable amount of CO_2 when exposed to light (Björkman, 1968; Tregunna ***et al.***, 1964). Both the transient leakiness increase and the LICB can be seen as a transient flow of CO_2 out of the bundle sheath. Furthermore they can be both associated to light availability in BS: shifting from blue to green light would increase light availability in BS in the same way of illuminating dark adapted leaves. I propose that the transient leakiness increase and the LICB are of critical importance to supply BS electron transport chain with sources of reductant generated in the stroma. Upon illumination the electron carrier pool is transiently oxidised by the activity of PSI, which rapidly oxidised the electron carrier pool to reduce ferredoxin. In order to maintain a functional BS electron transport chain, plastoquinol and plastocyanin have to be maintained in a reduced state, hence, an additional electron pool has to be rapidly recruited. These electrons cannot be extracted from water because maize BS chloroplasts do not operate water oxidation, but they can be supplied by stromal donors. In this respect, to produce the reducing power needed to supply the electron transport chain, malate decarboxylation could be rapidly activated. This transient malate decarboxylation would have been captured both as the leakiness spike and as LICB. Proving this hypothesis may require a system biology approach, and the dynamic study of electron carrier pools. This may be facilitated by the availability of dynamic models (Wang ***et al.***, 2014a; Wang ***et al.***,

2014b) which could be integrated to the quantitative description of the electron transport chain (Yin and Struik, 2012).

The comparison between my work and the most recent development in this field opens up some interesting questions concerning plasticity in species of the NADP-ME subgroup. Sun and colleagues showed that miscanthus is more susceptible than maize to changing light quality. Is this related to a lower plasticity at biochemical level, and is this lower biochemical plasticity associated to a lower activity of PEPCK in miscanthus (Bräutigam, 2013; Wang *et al.*, 2014a) and thus to a lower capacity to exploit transients? Miscanthus is known to have negligible PSII in BS, whereas maize is known to express appreciable PSII proteins in BS (however maize BS chloroplasts are not capable of splitting water . As I have previously discussed (see Paragraph 3.3.3), the PSII in maize BS may be involved in adjusting the quinone pool reduction state in response to variable light. Is miscanthus susceptibility to light quality associated to the negligible PSII available in BS and to a lower plasticity at the electron transport chain level?

I shall finally highlight that the current description of the C_4 electron transport processes is oversimplified also because the electron transport chain is still considered undivided (Wang *et al.*, 2014b; Yin and Struik, 2012). There is therefore compelling need for a new, mechanistic and realistic mathematical description of the C_4 electron transport processes. This should include all the complexities involved in the exchange of reductants between the stroma and the thylakoids in BS (see references in 3.3.3), the shuttling of reductants between M and BS, and the plasticity mechanisms to supply reductants to BS (see notes to Eqn 3.18 and 3.19).

5.4 Final remarks

Maize, as most of C_4 plants, is a sun-adapted plant that cannot complete its life-cycle in shade. This has traditionally led to the paradigm that the C_4 pathway is maladapted to low light and that this in some ways explains the failure of C_4 species to succeed as shade tolerant species. In the present experimental programme I have eliminated two leading possibilities explaining why the C_4 pathway is maladapted for deep shade: susceptibility to low light and changing spectral quality. Firstly I showed leakiness does not constrain assimilation under low light intensities and maize has efficient mechanisms to acclimate leakiness in response to

irradiance. Secondly I showed that light quality does not constrain assimilation and maize has efficient biochemical mechanisms to take advantage of any light quality.

Bibliography

Allen WA, Richardson AJ. 1968. Interaction of Light with a Plant Canopy. *Journal of the Optical Society of America* **58**, 1023-1028.

Andersson I. 2008. Catalysis and regulation in Rubisco. *Journal of Experimental Botany* **59**, 1555-1568.

Aoyagi K, Nakamoto H. 1985. Pyruvate, Pi Dikinase in Bundle Sheath Strands as Well as in Mesophyll Cells in Maize Leaves. *Plant Physiology* **78**, 661-664.

Bailey KJ, Gray JE, Walker RP, Leegood RC. 2007. Coordinate Regulation of Phosphoenolpyruvate Carboxylase and Phosphoenolpyruvate Carboxykinase by Light and CO2 during C4 Photosynthesis. *Plant Physiology* **144**, 479-486.

Baker NR, Long SP, Ort DR. 1988. Photosynthesis and temperature, with particular reference to effects on quantum yield. In: P LS, I WF, eds. *Plants and temperature: Society for Experimental Biology Symposium No XXXXII*: Company of biologists, 347-375.

Banaś AK, Aggarwal C, Łabuz J, Sztatelman O, Gabryś H. 2012. Blue light signalling in chloroplast movements. *Journal of Experimental Botany* **63**, 1559-1574.

Barbour MM, McDowell NG, Tcherkez G, Bickford CP, Hanson DT. 2007. A new measurement technique reveals rapid post-illumination changes in the carbon isotope composition of leaf-respired CO_2. *Plant Cell and Environment* **30**, 469-482.

Beerling DJ, Berner RA. 2005. Feedbacks and the coevolution of plants and atmospheric CO_2. *Proceedings of the National Academy of Sciences of the United States of America* **102**, 1302-1305.

Beerling DJ, Osborne CP. 2006. The origin of the savanna biome. *Global Change Biology* **12**, 2023-2031.

Bellasio C, Griffiths H. 2014a. Acclimation of C_4 metabolism to low light in mature maize leaves could limit energetic losses during progressive shading in a crop canopy. *Journal of Experimental Botany*.

Bellasio C, Griffiths H. 2014b. Acclimation to Low Light by C_4 maize: Implications for Bundle Sheath Leakiness. *Plant Cell and Environment* **37**, 1046-1058.

Bellasio C, Griffiths H. 2014c. The operation of two decarboxylases (NADPME and PEPCK), transamination and partitioning of C_4 metabolic processes between mesophyll and bundle sheath cells allows light capture to be balanced for the maize C_4 pathway. *Plant Physiology* **164**, 466-480.

Berry JA, Farquhar GD. 1978. The CO_2 concentrating function of C_4 photosynthesis: a biochemical model. In: Hall D, Coombs J, Goodwin T, eds. *Proceedings of the 4th International Congress on Photosynthesis*: Biochemical Society, 119-131.

Bilska A, Sowiński P. 2010. Closure of plasmodesmata in maize (*Zea mays*) at low temperature: a new mechanism for inhibition of photosynthesis. *Annals of Botany* **106**, 675-686.

Björkman O. 1968. Further studies of the effect of oxygen concentration on photosynthetic CO_2 uptake in higher plants. *Annual Report of the Director Department of Plant Biology*, Vol. 1966-1967. Stanford, California: Carnegie Institution.

Boesgaard KS, Mikkelsen TN, Ro-Poulsen H, Ibrom A. 2013. Reduction of molecular gas diffusion through gaskets in leaf gas exchange cuvettes by leaf-mediated pores. *Plant, Cell & Environment* **36**, 1352-1362.

Bonfante P, Anca I-A. 2009. Plants, Mycorrhizal Fungi, and Bacteria: A Network of Interactions. *Annual Review of Microbiology* **63**, 363-383.

BongardPierce DK, Evans MMS, Poethig RS. 1996. Heteroblastic features of leaf anatomy in maize and their genetic regulation. *International Journal of Plant Sciences* **157**, 331-340.

Bowman WD, Hubick KT, von Caemmerer S, Farquhar GD. 1989. Short-term changes in leaf carbon isotope discrimination in salt-and water-stressed C_4 grasses. *Plant Physiology* **90**, 162-166.

Bräutigam A. 2013. A PEP-CK/NAD-ME species derived blueprint of C_4 photosynthesis. *C4 + CAM Plant Biology 2013*. Urbana, IL.

Bräutigam A, Kajala K, Wullenweber J, Sommer M, Gagneul D, Weber KL, Carr KM, Gowik U, Maß J, Lercher MJ, Westhoff P, Hibberd JM, Weber APM. 2011. An mRNA Blueprint for C_4 Photosynthesis Derived from Comparative Transcriptomics of Closely Related C_3 and C_4 Species. *Plant Physiology* **155**, 142-156.

Brodersen CR, Vogelmann TC. 2010. Do changes in light direction affect absorption profiles in leaves? *Functional Plant Biology* **37**, 403-412.

Brown NJ, Newell CA, Stanley S, Chen JE, Perrin AJ, Kajala K, Hibberd JM. 2011. Independent and parallel recruitment of preexisting mechanisms underlying C_4 photosynthesis. *Science* **331**, 1436-1439.

Brown RH. 1999. Agronomic implications of C_4 photosynthesis. In: Sage RF, Monson RK, eds. *C4 Plant Biology*. San Diego, California: Academic Press, 473-507.

Brown RH, Hattersley PW. 1989. Leaf Anatomy of C_3-C_4 Species as Related to Evolution of C4 Photosynthesis. *Plant Physiology* **91**, 1543-1550.

Bukhov N, Carpentier R. 2004. Alternative Photosystem I-driven electron transport routes: mechanisms and functions. *Photosynthesis Research* **82**, 17-33.

Cassman KG, Dobermann A, Walters DT. 2002. Agroecosystems, Nitrogen-Use Efficiency, and Nitrogen Management. *Ambio* **31**, 132-140.

Cernusak LA, Ubierna N, Winter K, Holtum JAM, Marshall JD, Farquhar GD. 2013. Environmental and physiological determinants of carbon isotope discrimination in terrestrial plants. *New Phytologist* **200**, 950-965.

Chapman KSR, Hatch MD. 1981. Aspartate Decarboxylation in Bundle Sheath-Cells of *Zea mays* and its Possible Contribution to C_4 Photosynthesis. *Australian Journal of Plant Physiology* **8**, 237-248.

Chastain CJ. 2011. Structure, function, and post-translational regulation of C_4 pyruvate orthophosphate dikinase. *C_4 Photosynthesis and Related CO_2 Concentrating Mechanisms*: Springer, 301-315.

Christin P-A, Osborne CP, Chatelet DS, Columbus JT, Besnard G, Hodkinson TR, Garrison LM, Vorontsova MS, Edwards EJ. 2013. Anatomical enablers and the evolution of C_4 photosynthesis in grasses. *Proceedings of the National Academy of Sciences* **110**, 1381-1386.

Cousins AB, Badger MR, Von Caemmerer S. 2006. Carbonic anhydrase and its influence on carbon isotope discrimination during C_4 photosynthesis. Insights from antisense RNA in *Flaveria bidentis*. *Plant Physiology* **141**, 232-242.

Cousins AB, Badger MR, von Caemmerer S. 2008. C_4 photosynthetic isotope exchange in NAD-ME- and NADP-ME-type grasses. *Journal of Experimental Botany* **59**, 1695-1703.

Covshoff S, Hibberd JM. 2012. Integrating C_4 photosynthesis into C_3 crops to increase yield potential. *Current Opinion in Biotechnology* **23**, 209-214.

Craig H. 1953. The Geochemistry of the Stable Carbon Isotopes. *Geochimica Et Cosmochimica Acta* **3**, 53-92.

D'Ambrosio N, Arena C, Virzo de Santo A. 2003. Different Relationship Between Electron Transport and CO_2 Assimilation in two Zea mays cultivars as Influenced by Increasing Irradiance. *Photosynthetica* **41**, 489-495.

Dawson JC, Huggins DR, Jones SS. 2008. Characterizing nitrogen use efficiency in natural and agricultural ecosystems to improve the performance of cereal crops in low-input and organic agricultural systems. *Field Crops Research* **107**, 89-101.

Detarsio E, Wheeler MCG, Bermudez VAC, Andreo CS, Drincovich MF. 2003. Maize C_4 NADP-malic enzyme - Expression in *Escherichia coli* and characterization of site-directed mutants at the putative nucleotide-binding sites. *Journal of Biological Chemistry* **278**, 13757-13764.

Dougherty RL, Bradford JA, Coyne PI, Sims PL. 1994. Applying an empirical model of stomatal conductance to three C_4 grasses. *Agricultural and Forest Meteorology* **67**, 269-290.

Downton WJS. 1970. Preferential C_4-dicarboxylic acid synthesis, the postillumination CO_2 burst, carboxyl transfer step, and grana configurations in plants with C_4 photosynthesis. *Canadian Journal of Botany* **48**, 1795-1800.

Drincovich MF, Andreo CS. 1994. Redox Regulation of Maize NADP-Malic Enzyme by Thiol-Disulfide Interchange - Effect of Reduced Thioredoxin on Activity. *Biochimica Et Biophysica Acta-Protein Structure and Molecular Enzymology* **1206**, 10-16.

Driscoll SP, Prins A, Olmos E, Kunert KJ, Foyer CH. 2006. Specification of adaxial and abaxial stomata, epidermal structure and photosynthesis to CO_2 enrichment in maize leaves. *Journal of Experimental Botany* **57**, 381-390.

Edwards GE, Baker NR. 1993. Can CO_2 assimilation in maize leaves be predicted accurately from chlorophyll fluorescence analysis. *Photosynthesis Research* **37**, 89-102.

Egorova EA, Bukhov NG. 2004. Modeling of alternative pathways of electron transport to photosystem I in isolated thylakoids. *Russian Journal of Plant Physiology* **51**, 579-583.

Ehleringer J, Pearcy RW. 1983. Variation in Quantum yield for CO_2 Uptake among C_3 and C_4 Plants. *Plant Physiology* **73**, 555-559.

Ehleringer JR. 1978. Implications of quantum yield differences on distributions of C_3 and C_4 grasses. *Oecologia* **31**, 255-267.

Ehleringer JR, Cerling TE, Helliker BR. 1997. C_4 photosynthesis, atmospheric CO_2, and climate. *Oecologia* **112**, 285-299.

Eprintsev AT, Fedorina OS, Bessmeltseva YS. 2011. Response of the malate dehydrogenase system of maize mesophyll and bundle sheath to salt stress. *Russian Journal of Plant Physiology* **58**, 448-453.

Evans JR, Sharkey TD, Berry JA, Farquhar GD. 1986. Carbon Isotope Discrimination Measured Concurrently with gas exchange to Investigate CO_2 Diffusion in Leaves of Higher-Plants. *Australian Journal of Plant Physiology* **13**, 281-292.

Evans JR, von Caemmerer S, Vogelmann TC. 2007. Balancing light capture with distributed metabolic demand during C_4 photosynthesis. In: J.E. S, P.L. M, B. H, eds. *Charting new pathways to C_4 rice*: IRRI International Rice Research Institute.

Fageria N, Baligar V. 2005. Enhancing nitrogen use efficiency in crop plants. *Advances in agronomy* **88**, 97-185.

FAO. 2012. Fao Statistical division web page, Rome www.fao.org.

Farquhar GD. 1983. On the Nature of Carbon Isotope Discrimination in C_4 Species. *Australian Journal of Plant Physiology* **10**, 205-226.

Farquhar GD, Cernusak LA. 2012. Ternary effects on the gas exchange of isotopologues of carbon dioxide. *Plant Cell and Environment* **35**, 1221-1231.

Farquhar GD, von Caemmerer S, Berry JA. 1980. A biochemical-model of photosynthetic CO_2 assimilation in leaves of C_3 species. *Planta* **149**, 78-90.

Feild TS, Sage TL, Czerniak C, Iles WJD. 2005. Hydathodal leaf teeth of *Chloranthus japonicus* (Chloranthaceae) prevent guttation-induced flooding of the mesophyll. *Plant Cell and Environment* **28**, 1179-1190.

Flexas J, Diaz-Espejo A, Berry JA, Cifre J, Galmes J, Kaidenhoff R, Medrano H, Ribas-Carbo M. 2007. Analysis of leakage in IRGA's leaf chambers of open gas exchange systems:

quantification and its effects in photosynthesis parameterization. *Journal of Experimental Botany* **58**, 1533-1543.

Friso G, Majeran W, Huang MS, Sun Q, van Wijk KJ. 2010. Reconstruction of Metabolic Pathways, Protein Expression, and Homeostasis Machineries across Maize Bundle Sheath and Mesophyll Chloroplasts: Large-Scale Quantitative Proteomics Using the First Maize Genome Assembly. *Plant Physiology* **152**, 1219-1250.

Furbank R, Jenkins C, Hatch M. 1990. C_4 Photosynthesis: Quantum Requirement, C_4 and Overcycling and Q-Cycle Involvement. *Functional Plant Biology* **17**, 1-7.

Furbank RT. 2011. Evolution of the C_4 photosynthetic mechanism: are there really three C_4 acid decarboxylation types? *Journal of Experimental Botany* **62**, 3103-3108.

Furumoto T, Hata S, Izui K. 1999. cDNA cloning and characterization of maize phosphoenolpyruvate carboxykinase, a bundle sheath cell-specific enzyme. *Plant Molecular Biology* **41**, 301-311.

Furumoto T, Hata S, Izui K. 2000. Isolation and characterization of cDNAs for differentially accumulated transcripts between mesophyll cells and bundle sheath strands of maize leaves. *Plant and Cell Physiology* **41**, 1200-1209.

Gandin A, Cousins AB. 2012. The contribution of respiratory fractionation to leaf CO_2 isotope exchange in the C_3 plant Nicotina tabacum. *21st Western Photosynthesis Conference*. Asilomar Conference Grounds Pacific Grove, California, USA.

Gandin A, Koteyeva NK, Voznesenskaya EV, Edwards GE, Cousins AB. 2014. The acclimation of photosynthesis and respiration to temperature in the C_3-C_4 intermediate Salsola divaricata: Induction of high respiratory CO_2 release under low temperature. *Plant, Cell & Environment*, n/a-n/a.

Gates DM. 1980. *Biophysical Ecology*. New York: Springer Verlag.

Genty B, Briantais JM, Baker NR. 1989. The relationship between the quantum yield of photosynthetic electron-transport and quenching of chlorophyll fluorescence. *Biochimica Et Biophysica Acta* **990**, 87-92.

Ghashghaie J, Duranceau M, Badeck FW, Cornic G, Adeline MT, Deleens E. 2001. $\delta^{13}C$ of CO_2 respired in the dark in relation to $\delta^{13}C$ of leaf metabolites: comparison between Nicotiana sylvestris and Helianthus annuus under drought. *Plant Cell and Environment* **24**, 505-515.

Gillon JS, Griffiths H. 1997. The influence of (photo)respiration on carbon isotope discrimination in plants. *Plant Cell and Environment* **20**, 1217-1230.

Gorton HL, Brodersen CR, Williams WE, Vogelmann TC. 2010. Measurement of the Optical Properties of Leaves Under Diffuse Light. *Photochemistry and Photobiology* **86**, 1076-1083.

Gowik U, Bräutigam A, Weber KL, Weber APM, Westhoff P. 2011. Evolution of C_4 Photosynthesis in the Genus Flaveria: How Many and Which Genes Does It Take to Make C_4? *The Plant Cell* **23**, 2087-2105.

Griffiths H. 1998. *Stable Isotopes: The Integration of Biological, Ecological and Geological Processes*. Oxford: BIOS Scientific Publishers.

Griffiths H, Broadmeadow MSJ, Borland AM, Hetherington CS. 1990. Short-Term Changes in Carbon-Isotope Discrimination Identify Transitions between C3 and C4 Carboxylation during Crassulacean Acid Metabolism. *Planta* **181**, 604-610.

Griffiths H, Weller G, Toy LFM, Dennis RJ. 2013. You're so vein: bundle sheath physiology, phylogeny and evolution in C_3 and C_4 plants. *Plant, Cell & Environment* **36**, 249-261.

Gutierrez M, Gracen VE, Edwards GE. 1974. Biochemical and cytological relationships in C4 plants. *Planta* **119**, 279-300.

Han T, Vogelmann TC. 1999. A photoacoustic spectrometer for measuring heat dissipation and oxygen quantum yield at the microscopic level within leaf tissues. *Journal of Photochemistry and Photobiology B: Biology* **48**, 158-165.

Hatch MD. 1971. The C_4 pathway of photosynthesis. Evidence for an intermediate pool of carbon dioxide and the identity of the donor C_4 -dicarboxylic acid. *Biochem. J.* **125**, 425-432.

Hatch MD. 1987. C4 Photosynthesis - a Unique Blend of Modified Biochemistry, Anatomy and Ultrastructure. *Biochimica Et Biophysica Acta* **895**, 81-106.

Hatch MD, Agostino A, Jenkins CLD. 1995. Measurement of the leakage of co2 from bundle-sheath cells of leaves during C_4 photosynthesis. *Plant Physiology* **108**, 173-181.

Hattersley PW. 1984. Characterization of C_4 Type Leaf Anatomy in Grasses (Poaceae), Mesophyll - Bundle Sheath Area Ratios. *Annals of Botany* **53**, 163-179.

Henderson SA, Von Caemmerer S, Farquhar GD. 1992. Short-Term Measurements of Carbon Isotope Discrimination in Several C_4 Species. *Australian Journal of Plant Physiology* **19**, 263-285.

Hertle AP, Blunder T, Wunder T, Pesaresi P, Pribil M, Armbruster U, Leister D. 2013. PGRL1 Is the Elusive Ferredoxin-Plastoquinone Reductase in Photosynthetic Cyclic Electron Flow. *Molecular Cell* **49**, 511-523.

Hibberd JM, Quick WP. 2002. Characteristics of C_4 photosynthesis in stems and petioles of C_3 flowering plants. *Nature* **415**, 451-454.

Humphreys CP, Franks PJ, Rees M, Bidartondo MI, Leake JR, Beerling DJ. 2010. Mutualistic mycorrhiza-like symbiosis in the most ancient group of land plants. *Nature communications* **1**, 103.

Hymus GJ, Maseyk K, Valentini R, Yakir D. 2005. Large daily variation in ^{13}C enrichment of leaf-respired CO_2 in two Quercus forest canopies. *New Phytologist* **167**, 377-384.

Igamberdiev AU, Mikkelsen TN, Ambus P, Bauwe H, Lea PJ, Gardestrom P. 2004. Photorespiration contributes to stomatal regulation and carbon isotope fractionation: a study with barley, potato and Arabidopsis plants deficient in glycine decarboxylase. *Photosynthesis Research* **81**, 139-152.

Igbadun HE, Mahoo HF, Tarimo AK, Salim BA. 2006. Crop water productivity of an irrigated maize crop in Mkoji sub-catchment of the Great Ruaha River Basin, Tanzania. *Agricultural Water Management* **85**, 141-150.

Ivanishchev V, Kurganov B. 1992. Enzymes of Malate Metabolism: Characteristics, Regulation of Activity, and Biological Roles. *Biochemistry* **57**, 441-447.

Ivanov B, Asada K, Edwards GE. 2007. Analysis of donors of electrons to photosystem I and cyclic electron flow by redox kinetics of P700 in chloroplasts of isolated bundle sheath strands of maize. *Photosynthesis Research* **92**, 65-74.

Ivanov B, Asada K, Kramer DM, Edwards G. 2005. Characterization of photosynthetic electron transport in bundle sheath cells of maize. I. Ascorbate effectively stimulates cyclic electron flow around PSI. *Planta* **220**, 572-581.

Ivanov BN, Sacksteder CA, Kramer DM, Edwards GE. 2001. Light-induced ascorbate-dependent electron transport and membrane energization in chloroplasts of bundle sheath cells of the C_4 plant maize. *Archives of Biochemistry and Biophysics* **385**, 145-153.

Jeanneau M, Vidal J, Gousset-Dupont A, Lebouteiller B, Hodges M, Gerentes D, Perez P. 2002. Manipulating PEPC levels in plants. *Journal of Experimental Botany* **53**, 1837-1845.

John CR, Smith-Unna RD, Woodfield H, Hibberd JM. 2014. Evolutionary convergence of cell specific gene expression in independent lineages of C_4 grasses. *Plant Physiology*.

Johnson HS, Hatch MD. 1970. Properties and Regulation of Leaf Nicotinamide-Adenine Dinucleotide Phosphate-Malate Dehydrogenase and Malic Enzyme in Plants with C_4-Dicarboxylic Acid Pathway of Photosynthesis. *Biochemical Journal* **119**, 273-280.

Kajala K, Covshoff S, Karki S, Woodfield H, Tolley BJ, Dionora MJA, Mogul RT, Mabilangan AE, Danila FR, Hibberd JM, Quick WP. 2011. Strategies for engineering a two-celled C_4 photosynthetic pathway into rice. *Journal of Experimental Botany* **62**, 3001-3010.

Kanai R, Edwards GE. 1973. Separation of Mesophyll Protoplasts and Bundle Sheath Cells from Maize Leaves for Photosynthetic Studies. *Plant Physiology* **51**, 1133-1137.

Kanai R, Edwards GE. 1999. The biochemistry of C_4 photosynthesis. In: Sage RF, Monson RK, eds. *C_4 plant biology*. San Diego: Academic Press.

Klughammer C, Schreiber U. 1994. An Improved Method, Using Saturating Light-Pulses, for the Determination of Photosystem-I Quantum Yield Via $P700^+$-Absorbency Changes at 830 Nm. *Planta* **192**, 261-268.

Klughammer C, Schreiber U. 2008. Saturation Pulse method for assessment of energy conversion in PS I. *PAM Application notes* **1**, 3.

Krall JP, Edwards GE. 1990. Quantum yields of photosystem-ii electron-transport and carbon-dioxide fixation in C_4 plants. *Australian Journal of Plant Physiology* **17**, 579-588.

Krall JP, Pearcy RW. 1993. Concurrent Measurements of Oxygen and Carbon-Dioxide Exchange during Lightflecks in Maize (*Zea-Mays* L). *Plant Physiology* **103**, 823-828.

Kramer DM, Evans JR. 2011. The Importance of Energy Balance in Improving Photosynthetic Productivity. *Plant Physiology* **155**, 70-78.

Kromdijk J. 2010. Bundle sheath leakiness in C_4 photosynthesis, University of Cambridge, Cambridge.

Kromdijk J, Griffiths H, Schepers HE. 2010. Can the progressive increase of C_4 bundle sheath leakiness at low PFD be explained by incomplete suppression of photorespiration? *Plant Cell and Environment* **33**, 1935-1948.

Kromdijk J, Schepers HE, Albanito F, Fitton N, Carroll F, Jones MB, Finnan J, Lanigan GJ, Griffiths H. 2008. Bundle Sheath Leakiness and Light Limitation during C_4 Leaf and Canopy CO_2 Uptake. *Plant Physiology* **148**, 2144-2155.

Kromdijk J, Ubierna N, Cousins AB, Griffiths H. 2014. Bundle-sheath leakiness in C_4 photosynthesis: a careful balancing act between CO_2 concentration and assimilation. *Journal of Experimental Botany*.

Kuntz M. 2004. Plastid terminal oxidase and its biological significance. *Planta* **218**, 896-899.

Laisk A, Edwards G. 2009. Leaf C_4 Photosynthesis in silico: The CO_2 Concentrating Mechanism. In: Laisk A, Nedbal L, Govindjee, eds. *Photosynthesis in silico*, Vol. 29: Springer Netherlands, 323-348.

Laisk A, Edwards GE. 2000. A mathematical model of C_4 photosynthesis: The mechanism of concentrating CO_2 in NADP-malic enzyme type species. *Photosynthesis Research* **66**, 199-224.

Laisk A, Talts E, Oja V, Eichelmann H, Peterson RB. 2010. Fast cyclic electron transport around photosystem I in leaves under far-red light: a proton-uncoupled pathway? *Photosynthesis Research* **103**, 79-95.

Lanigan GJ, Betson N, Griffiths H, Seibt U. 2008. Carbon Isotope Fractionation during Photorespiration and Carboxylation in Senecio. *Plant Physiology* **148**, 2013-2020.

Leegood RC. 2008. Roles of the bundle sheath cells in leaves of C_3 plants. *Journal of Experimental Botany* **59**, 1663-1673.

Long SP. 1993. The significance of light-limited photosynthesis to crop canopy carbon gain and productivity - a theoretical analysis. In: Abrol YP, Mohanty P, Govindjee, eds. *Photosynthesis: Photoreactions to Plant Productivity*. New Delhi: Oxford & IBH publishing, 547 - 560.

Long SP, Bernacchi CJ. 2003. Gas exchange measurements, what can they tell us about the underlying limitations to photosynthesis? Procedures and sources of error. *Journal of Experimental Botany* **54**, 2393-2401.

Lundgren MR, Osborne CP, Christin P-A. 2014. Deconstructing Kranz anatomy to understand C_4 evolution. *Journal of Experimental Botany*. DOI: 10.1093/jxb/eru186.

Majeran W, Cai Y, Sun Q, van Wijk KJ. 2005. Functional Differentiation of Bundle Sheath and Mesophyll Maize Chloroplasts Determined by Comparative Proteomics. *The Plant Cell* **17**, 3111-3140.

Majeran W, Friso G, Ponnala L, Connolly B, Huang MS, Reidel E, Zhang CK, Asakura Y, Bhuiyan NH, Sun Q, Turgeon R, van Wijk KJ. 2010. Structural and Metabolic Transitions of C_4 Leaf Development and Differentiation Defined by Microscopy and Quantitative Proteomics in Maize. *The Plant Cell* **22**, 3509-3542.

Majeran W, van Wijk KJ. 2009. Cell-type-specific differentiation of chloroplasts in C_4 plants. *Trends in Plant Science* **14**, 100-109.

Martins SCV, Galmés J, Molins A, DaMatta FM. 2013. Improving the estimation of mesophyll conductance to CO_2: on the role of electron transport rate correction and respiration. *Journal of Experimental Botany*.

Meierhoff K, Westhoff P. 1993. Differential Biogenesis of Photosystem-II in Mesophyll and Bundle-Sheath Cells of Monocotyledonous NADP-Malic Enzyme-Type C_4 Plants - the Nonstoichiometric Abundance of the Subunits of Photosystem-II in the Bundle-Sheath Chloroplasts and the Translational Activity of the Plastome-Encoded Genes. *Planta* **191**, 23-33.

Meister M, Agostino A, Hatch MD. 1996. The roles of malate and aspartate in C_4 photosynthetic metabolism of *Flaveria bidentis* (L). *Planta* **199**, 262-269.

Meyer M, Griffiths H. 2013. Origins and diversity of eukaryotic CO_2-concentrating mechanisms: lessons for the future. *Journal of Experimental Botany* **64**, 769-786.

Miyake C, Miyata M, Shinzaki Y, Tomizawa K-i. 2005. CO_2 Response of Cyclic Electron Flow around PSI (CEF-PSI) in Tobacco Leaves—Relative Electron fluxes through PSI and PSII Determine the Magnitude of Non-photochemical Quenching (NPQ) of Chl Fluorescence. *Plant and Cell Physiology* **46**, 629-637.

Monson RK, Moore Bd. 1989. On the significance of C_3—C_4 intermediate photosynthesis to the evolution of C_4 photosynthesis. *Plant, Cell & Environment* **12**, 689-699.

Monteith JL. 1978. Reassessment of Maximum Growth-Rates for C_3 and C_4 Crops. *Experimental Agriculture* **14**, 1-5.

Mook WG, Bommerso.Jc, Staverma.Wh. 1974. Carbon Isotope Fractionation between Dissolved Bicarbonate and Gaseous Carbon-Dioxide. *Earth and Planetary Science Letters* **22**, 169-176.

Moreno-Sotomayor A, Weiss A, Paparozzi ET, Arkebauer TJ. 2002. Stability of leaf anatomy and light response curves of field grown maize as a function of age and nitrogen status. *Journal of Plant Physiology* **159**, 819-826.

Moroney J, Jungnick N, DiMario R, Longstreth D. 2013. Photorespiration and carbon concentrating mechanisms: two adaptations to high O_2, low CO_2 conditions. *Photosynthesis Research* **117**, 121-131.

Morstadt L, Graber P, de Pascalis L, Kleinig H, Speth V, Beyer P. 2002. Chemiosmotic ATP synthesis in photosynthetically inactive chromoplasts from *Narcissus pseudonarcissus* L. linked to a redox pathway potentially also involved in carotene desaturation. *Planta* **215**, 134-140.

Munekage YN, Eymery F, Rumeau D, Cuine S, Oguri M, Nakamura N, Yokota A, Genty B, Peltier G. 2010. Elevated Expression of PGR5 and NDH-H in Bundle Sheath Chloroplasts in C_4 Flaveria Species. *Plant and Cell Physiology* **51**, 664-668.

Murmu J, Chinthapalli B, Raghavendra AS. 2003. Light activation of NADP malic enzyme in leaves of maize: Marginal increase in activity, but marked change in regulatory properties of enzyme. *Journal of Plant Physiology* **160**, 51-56.

O'Leary MH. 1981. Carbon isotope fractionation in plants. *Phytochemistry* **20**, 553-567.

O'Leary MH. 1984. Measurement of the isotope fractionation associated with diffusion of carbon dioxide in aqueous solution. *The Journal of Physical Chemistry* **88**, 823-825.

Oberhuber W, Dai ZY, Edwards GE. 1993. Light dependence of quantum yields of photosystem-II and CO_2 fixation in C_3 and C_4 plants. *Photosynthesis Research* **35**, 265-274.

Osborne CP, Beerling DJ. 2006. Nature's green revolution: the remarkable evolutionary rise of C_4 plants. *Philosophical Transactions of the Royal Society B-Biological Sciences* **361**, 173-194.

Osborne CP, Sack L. 2012. Evolution of C_4 plants: a new hypothesis for an interaction of CO_2 and water relations mediated by plant hydraulics. *Philosophical Transactions of the Royal Society B-Biological Sciences* **367**, 583-600.

Pantin F, Monnet F, Jannaud D, Costa JM, Renaud J, Muller B, Simonneau T, Genty B. 2013. The dual effect of abscisic acid on stomata. *New Phytologist* **197**, 65-72.

Pearcy R, Calkin H. 1983. Carbon dioxide exchange of C_3 and C_4 tree species in the understory of a Hawaiian forest. *Oecologia* **58**, 26-32.

Pearcy RW. 1990. Sunflecks and Photosynthesis in Plant Canopies. *Annual Review of Plant Physiology and Plant Molecular Biology* **41**, 421-453.

Pearcy RW, Ehleringer J. 1984. Comparative ecophysiology of C_3 and C_4 plants. *Plant, Cell & Environment* **7**, 1-13.

Peisker M. 1982. The effect of CO_2 leakage from bundle sheath-cells on carbon isotope discrimination in C_4 plants. *Photosynthetica* **16**, 533-541.

Peisker M, Henderson SA. 1992. Carbon - terrestrial C_4 plants. *Plant Cell and Environment* **15**, 987-1004.

Peng L, Yamamoto H, Shikanai T. 2011. Structure and biogenesis of the chloroplast NAD(P)H dehydrogenase complex. *Biochimica et Biophysica Acta - Bioenergetics* **1807**, 945-953.

Pengelly JJL, Sirault XRR, Tazoe Y, Evans JR, Furbank RT, von Caemmerer S. 2010. Growth of the C_4 dicot Flaveria bidentis: photosynthetic acclimation to low light through shifts in leaf anatomy and biochemistry. *Journal of Experimental Botany* **61**, 4109-4122.

Petrasovits LA, Zhao LH, McQualter RB, Snell KD, Somleva MN, Patterson NA, Nielsen LK, Brumbley SM. 2012. Enhanced polyhydroxybutyrate production in transgenic sugarcane. *Plant Biotechnology Journal* **10**, 569-578.

Pick TR, Brautigam A, Schluter U, Denton AK, Colmsee C, Scholz U, Fahnenstich H, Pieruschka R, Rascher U, Sonnewald U, Weber APM. 2011. Systems Analysis of a Maize Leaf Developmental Gradient Redefines the Current C_4 Model and Provides Candidates for Regulation. *Plant Cell* **23**, 4208-4220.

Pons TL, Flexas J, von Caemmerer S, Evans JR, Genty B, Ribas-Carbo M, Brugnoli E. 2009. Estimating mesophyll conductance to CO_2: methodology, potential errors, and recommendations. *Journal of Experimental Botany* **60**, 2217-2234.

Prioul JL, Chartier P. 1977. Partitioning of Transfer and Carboxylation Components of Intracellular Resistance to Photosynthetic CO_2 Fixation: A Critical Analysis of the Methods Used. *Annals of Botany* **41**, 789-800.

Rascio N, Colombo PM, Orsenigo M. 1980. The ultrastructural development of plastids in leaves of maize plants exposed to continuous illumination. *Protoplasma* **102**, 131-139.

Rathnam CKM. 1978. Studies with Isolated Bundle Sheath Mitochondria - Evidence for NAD-Malic Enzyme-Catalyzed Decarboxylation of C_4 Acids in Species Representing 3 C_4 Metabolic Subtypes. *Febs Letters* **96**, 367-372.

Rathnam CKM, Edwards GE. 1977. C_4-Dicarboxylic Acid Metabolism in Bundle-Sheath Chloroplasts, Mitochondria and Strands of Eriochloa-Borumensis Hack., a Phosphoenolpyruvate-Carboxykinase Type C4 Species. *Planta* **133**, 135-144.

Rawsthorne S. 1992. C_3–C_4 intermediate photosynthesis: linking physiology to gene expression. *The Plant Journal* **2**, 267-274.

Rawsthorne S, Hylton C, Smith A, Woolhouse H. 1988. Photorespiratory metabolism and immunogold localization of photorespiratory enzymes in leaves of C_3 and C_3-C_4 intermediate species of Moricandia. *Planta* **173**, 298-308.

Read D, Leake J, Langdale A. 1989. The nitrogen nutrition of mycorrhizal fungi and their host plants. *Nitrogen, Phosphorus and Sulphur Utilization by Fungi (Boddy, L., Marchant, R. and Read, DJ, Eds.)*, 181-204.

Ripley BS, Gilbert ME, Ibrahim DG, Osborne CP. 2007. Drought constraints on C_4 photosynthesis: stomatal and metabolic limitations in C_3 and C_4 subspecies of Alloteropsis semialata. *Journal of Experimental Botany* **58**, 1351-1363.

Roeske CA, Oleary MH. 1984. Carbon Isotope Effects on the Enzyme-Catalyzed Carboxylation of Ribulose Bisphosphate. *Biochemistry* **23**, 6275-6284.

Romanowska E, Drozak A, Pokorska B, Shiell BJ, Michalski WP. 2006. Organization and activity of photosystems in the mesophyll and bundle sheath chloroplasts of maize. *Journal of Plant Physiology* **163**, 607-618.

Sage RF. 2002. Variation in the kcat of Rubisco in C_3 and C_4 plants and some implications for photosynthetic performance at high and low temperature. *Journal of Experimental Botany* **53**, 609-620.

Sage RF. 2004. The evolution of C_4 photosynthesis. *New Phytologist* **161**, 341-370.

Sage RF. 2014. Stopping the leaks: New insights into C_4 photosynthesis at low light. *Plant, Cell & Environment* **37**, 1037-1041.

Sage RF, Christin P-A, Edwards EJ. 2011. The C_4 plant lineages of planet Earth. *Journal of Experimental Botany* **62**, 3155-3169.

Sage RF, Khoshravesh R, Sage TL. 2014. From proto-Kranz to C_4 Kranz: building the bridge to C_4 photosynthesis. *Journal of Experimental Botany*. **doi/10.1093/jxb/eru180**.

Sage RF, Peixoto MM, Sage TL. 2013. Photosynthesis in Sugarcane. *Sugarcane: Physiology, Biochemistry, and Functional Biology*: John Wiley & Sons Ltd, 121-154.

Sage RF, Sage TL, Kocacinar F. 2012. Photorespiration and the evolution of C_4 photosynthesis. *Annual review of plant biology* **63**, 19-47.

Saliendra NZ, Meinzer FC, Perry M, Thom M. 1996. Associations between partitioning of carboxylase activity and bundle sheath leakiness to CO_2, carbon isotope discrimination, photosynthesis, and growth in sugarcane. *Journal of Experimental Botany* **47**, 907-914.

Schmitt MR, Edwards GE. 1981. Photosynthetic Capacity and Nitrogen Use Efficiency of Maize, Wheat, and Rice: A Comparison Between C_3 and C_4 Photosynthesis. *Journal of Experimental Botany* **32**, 459-466.

Schulze S, Mallmann J, Burscheidt J, Koczor M, Streubel M, Bauwe H, Gowik U, Westhoff P. 2013. Evolution of C_4 Photosynthesis in the Genus Flaveria: Establishment of a Photorespiratory CO_2 Pump. *Plant Cell* **25**, 2522-2535.

Sharkey TD. 1988. Estimating the rate of photorespiration in leaves. *Physiologia Plantarum* **73**, 147-152.

Sheehy JE, ed. 2007. *Charting New Pathways to C_4 Rice*. Singapore: World Scientific Publishing.

Shirley HL. 1929. The Influence of Light Intensity and Light Quality Upon the Growth of Plants. *American Journal of Botany* **16**, 354-390.

Smith AM, Woolhouse HW. 1983. Metabolism of Phosphoenolpyruvate in the C_4 Cycle during Photosynthesis in the Phosphoenolpyruvate-Carboxykinase C_4 Grass Spartina-Anglica Hubb. *Planta* **159**, 570-578.

Smith H. 1982. Light Quality, Photoperception, and Plant Strategy. *Annual Review of Plant Physiology* **33**, 481-518.

Snaydon RW. 1991. The Productivity of C_3 and C_4 Plants - a Reassessment. *Functional Ecology* **5**, 321-330.

Sowiński P. 2013. Characteristics of Symplasmic Transport. In: Sokołowska K, Sowiński P, eds. *Symplasmic Transport in Vascular Plants*: Springer New York, 1-39.

Sowinski P, Szczepanik J, Minchin PEH. 2008. On the mechanism of C_4 photosynthesis intermediate exchange between Kranz mesophyll and bundle sheath cells in grasses. *Journal of Experimental Botany* **59**, 1137-1147.

Spilatro SR, Preiss J. 1987. Regulation of starch synthesis in the bundle sheath and mesophyll of *Zea mays* L. Intercellular compartmentalization of enzymes of starch metabolism and the properties of the ADPglucose pyrophosphorylases. *Plant Physiology* **83**, 621-627.

Stutz SS, Edwards GE, Cousins AB. 2014. Single-cell C_4 photosynthesis: efficiency and acclimation of Bienertia sinuspersici to growth under low light. *New Phytologist* **202**, 220-232.

Suat I, Odhiambo LO, Eisenhauer DE. 2011. Irrigation Efficiency and Uniformity, and Crop Water Use Efficiency. *University of Nebraska - Extension*, Vol. EC732. Lincoln: University of Nebraska.

Sun W, Ubierna N, Ma J-Y, Walker B, Kramer D, Cousins AB. 2014. The coordination of C_4 photosynthesis and the CO_2 concentrating mechanism in *Zea mays* and *Miscanthus* × *giganteus* in response to transient changes in light quality. *Plant Physiology*.

Sun WEI, Ubierna N, Ma J-Y, Cousins AB. 2012. The influence of light quality on C_4 photosynthesis under steady-state conditions in *Zea mays* and *Miscanthus* × *giganteus*: changes in rates of photosynthesis but not the efficiency of the CO_2 concentrating mechanism. *Plant, Cell & Environment* **35**, 982-993.

Takabayashi A, Kishine M, Asada K, Endo T, Sato F. 2005. Differential use of two cyclic electron flows around photosystem I for driving CO_2-concentration mechanism in C_4 photosynthesis. *Proceedings of the National Academy of Sciences of the United States of America* **102**, 16898-16903.

Taylor L, Leake J, Quirk J, Hardy K, Banwart S, Beerling D. 2009. Biological weathering and the long-term carbon cycle: integrating mycorrhizal evolution and function into the current paradigm. *Geobiology* **7**, 171-191.

Taylor SH, Ripley BS, Martin T, De-Wet L-A, Woodward FI, Osborne CP. 2014. Physiological advantages of C_4 grasses in the field: a comparative experiment demonstrating the importance of drought. *Global Change Biology* **20**, 1992-2003.

Tazoe Y, Hanba YT, Furumoto T, Noguchi K, Terashima I. 2008. Relationships between quantum yield for CO_2 assimilation, activity of key enzymes and CO_2 leakiness in Amaranthus cruentus, a C_4 dicot, grown in high or low light. *Plant and Cell Physiology* **49**, 19-29.

Tazoe Y, Noguchi K, Terashima I. 2006. Effects of growth light and nitrogen nutrition on the organization of the photosynthetic apparatus in leaves of a C_4 plant, Amaranthus cruentus. *Plant Cell and Environment* **29**, 691-700.

Tcherkez G, Bligny R, Gout E, Mahé A, Hodges M, Cornic G. 2008. Respiratory metabolism of illuminated leaves depends on CO_2 and O_2 conditions. *Proceedings of the National Academy of Sciences* **105**, 797-802.

Terashima I, Fujita T, Inoue T, Chow WS, Oguchi R. 2009. Green Light Drives Leaf Photosynthesis More Efficiently than Red Light in Strong White Light: Revisiting the Enigmatic Question of Why Leaves are Green. *Plant and Cell Physiology* **50**, 684-697.

Tregunna EB, Krotkov G, Nelson CD. 1964. Further evidence on the effects of light on respiration during photosynthesis. *Canadian Journal of Botany* **42**, 989-997.

Trost P, Fermani S, Marri L, Zaffagnini M, Falini G, Scagliarini S, Pupillo P, Sparla F. 2006. Thioredoxin-dependent regulation of photosynthetic glyceraldehyde-3-phosphate dehydrogenase: autonomous vs. CP12-dependent mechanisms. *Photosynthesis Research* **89**, 263-275.

Ubierna N, Sun W, Cousins AB. 2011. The efficiency of C_4 photosynthesis under low light conditions: assumptions and calculations with CO_2 isotope discrimination. *Journal of Experimental Botany* **62**, 3119-3134.

Ubierna N, Sun W, Kramer DM, Cousins AB. 2013. The Efficiency Of C_4 Photosynthesis Under Low Light Conditions In Zea mays, Miscanthus X giganteus And Flaveria bidentis. *Plant, Cell & Environment* **36**, 365-381.

Usuda H. 1985. Changes in Levels of Intermediates of the C_4 Cycle and Reductive Pentose-Phosphate Pathway during Induction of Photosynthesis in Maize Leaves. *Plant Physiology* **78**, 859-864.

Vogel JC. 1980. *Fractionation of the carbon isotopes during photosynthesis*. Berlin and New york: Springer.

Vogel JC, Grootes PM, Mook WG. 1970. Isotopic Fractionation between Gaseous and Dissolved Carbon Dioxide. *Zeitschrift Fur Physik* **230**, 225-238.

Vogelmann TC. 1989. Penetration of light into plants. *Photochemistry and Photobiology* **50**, 895-902.

Vogelmann TC, Evans JR. 2002. Profiles of light absorption and chlorophyll within spinach leaves from chlorophyll fluorescence. *Plant, Cell & Environment* **25**, 1313-1323.

Vogelmann TC, Nishio JN, Smith WK. 1996. Leaves and light capture: Light propagation and gradients of carbon fixation within leaves. *Trends in Plant Science* **1**, 65-70.

von Caemmerer S. 2000. *Biochemical models of leaf Photosynthesis*. Collingwood: CSIRO Publishing.

von Caemmerer S. 2013. Steady-state models of photosynthesis. *Plant, Cell & Environment* **36**, 1617-1630.

von Caemmerer S, Farquhar GD. 1981. Some Relationships between the Biochemistry of Photosynthesis and the Gas-Exchange of Leaves. *Planta* **153**, 376-387.

von Caemmerer S, Furbank RT. 2003. The C_4 pathway: an efficient CO_2 pump. *Photosynthesis Research* **77**, 191-207.

von Caemmerer S, Ghannoum O, Pengelly JJL, Cousins AB. 2014. Carbon isotope discrimination as a tool to explore C_4 photosynthesis. *Journal of Experimental Botany*.

Wada M. 2013. Chloroplast movement. *Plant Science* **210**, 177-182.

Walker GH, Izawa S. 1979. Photosynthetic Electron-Transport in Isolated Maize Bundle Sheath-Cells. *Plant Physiology* **63**, 133-138.

Walker GH, Ku MSB, Edwards GE. 1986. Activity of Maize Leaf Phosphoenolpyruvate Carboxylase in Relation to Tautomerization and Nonenzymatic Decarboxylation of Oxaloacetate. *Archives of Biochemistry and Biophysics* **248**, 489-501.

Wang L, Peterson RB, Brutnell TP. 2011. Regulatory mechanisms underlying C_4 photosynthesis. *New Phytologist* **190**, 9-20.

Wang Y, Bräutigam A, Weber APM, Zhu X-G. 2014a. Three distinct biochemical subtypes of C_4 photosynthesis? A modelling analysis. *Journal of Experimental Botany*.

Wang Y, Long SP, Zhu X-G. 2014b. Elements Required for an Efficient NADP-Malic Enzyme Type C_4 Photosynthesis. *Plant Physiology* **164**, 2231-2246.

Weiner H, Burnell JN, Woodrow IE, Heldt HW, Hatch MD. 1988. Metabolite Diffusion into Bundle Sheath-Cells from C_4 Plants - Relation to C_4 Photosynthesis and Plasmodesmatal Function. *Plant Physiology* **88**, 815-822.

Wingate L, Seibt U, Moncrieff JB, Jarvis PG, Lloyd J. 2007. Variations in ^{13}C discrimination during CO_2 exchange by Picea sitchensis branches in the field. *Plant Cell and Environment* **30**, 600-616.

Wingler A, Walker RP, Chen ZH, Leegood RC. 1999. Phosphoenolpyruvate carboxykinase is involved in the decarboxylation of aspartate in the bundle sheath of maize. *Plant Physiology* **120**, 539-545.

Woolley JT. 1971. Reflectance and Transmittance of Light by Leaves. *Plant Physiology* **47**, 656-662.

Yin X, Struik PC. 2009. C_3 and C_4 photosynthesis models: An overview from the perspective of crop modelling. *Njas-Wageningen Journal of Life Sciences* **57**, 27-38.

Yin X, Struik PC. 2010. Modelling the crop: from system dynamics to systems biology. *Journal of Experimental Botany* **61**, 2171-2183.

Yin X, Sun Z, Struik PC, Gu J. 2011a. Evaluating a new method to estimate the rate of leaf respiration in the light by analysis of combined gas exchange and chlorophyll fluorescence measurements. *Journal of Experimental Botany* **62**, 3489-3499.

Yin X, Van Oijen M, Schapendonk A. 2004. Extension of a biochemical model for the generalized stoichiometry of electron transport limited C_3 photosynthesis. *Plant, Cell & Environment* **27**, 1211-1222.

Yin XY, Struik PC. 2012. Mathematical review of the energy transduction stoichiometries of C_4 leaf photosynthesis under limiting light. *Plant Cell and Environment* **35**, 1299-1312.

Yin XY, Sun ZP, Struik PC, Van der Putten PEL, Van Ieperen W, Harbinson J. 2011b. Using a biochemical C_4 photosynthesis model and combined gas exchange and chlorophyll fluorescence measurements to estimate bundle-sheath conductance of maize leaves differing in age and nitrogen content. *Plant Cell and Environment* **34**, 2183-2199.

Yoshimura Y, Kubota F, Ueno O. 2004. Structural and biochemical bases of photorespiration in C_4 plants: quantification of organelles and glycine decarboxylase. *Planta* **220**, 307-317.

Zhu X-G, Long SP, Ort DR. 2010. Improving photosynthetic efficiency for greater yield. *Annual review of plant biology* **61**, 235-261.

Appendix

Chapter 2 Appendix 1. Derivation of Eqn 2.1 and 2.2

Assimilation can be described by the equation (Yin and Struik, 2009; Yin *et al.*, 2011b):

$$A_{Low\ O2} = s' \frac{PAR\ Y(II)_{Low\ O2}}{3} - R_{LIGHT} \quad (2.12)$$

Where *s'* is a dummy variable that represents the light conversion efficiency into assimilation. For the definition of Gross Assimilation $GA = A + R_{LIGHT}$, Eqn 2.12 can be written as:

$$s' = \frac{3\ GA_{Low\ O2}}{PAR\ Y(II)_{Low\ O2}} \quad (2.13)$$

J_{ATP} at any O_2 concentration can be calculated as (Yin *et al.*, 2011b):

$$J_{ATP} = \frac{s'\ PAR\ Y(II)}{0.59} \quad (2.14)$$

Substituting Eqn 2.14 into Eqn 2.13:

$$J_{ATP} = \frac{3}{0.59}\ GA_{Low\ O2} \frac{PAR\ Y(II)}{PAR\ Y(II)_{Low\ O2}} \quad (2.15)$$

At low O_2 Eqn 2.15 simplifies to Eqn 2.1. Eqn 2.2 is obtained substituting Eqn 2.1 into Eqn 2.15.

ξ values for Eqn 2.16

	ξ	
PAR	**LL**	**HL**
500	5.13 ± 0.14	3.81 ± 0.32
250	7.81 ± 0.16	6.91 ± 0.25
125	10.6 ± 0.088	11.4 ± 0.15
75	14.1 ± 0.71	15.7 ± 0.21
50	15.4 ± 0.82	18.3 ± 0.22
30	28.7 ± 0.22	46.1 ± 1.2

Chapter 2 Appendix 2. Calculation of isotopic discrimination during photosynthesis Δ

Δ was calculated as (Evans *et al.*, 1986)

$$\Delta_{OBS} = \frac{\xi(\delta_o - \delta_e)}{1 + \delta_o - \xi(\delta_o - \delta_e)} \quad (16)$$

Where; $\xi = \frac{C_e}{C_e - C_o}$; δ_e is the isotopic composition of the reference gas. δ_o is the isotopic composition of the gas leaving the cuvette. C_e and C_o represent the CO_2 mole fraction respectively entering and leaving the cuvette.

Chapter 4 Appendix 1. ξ values for the calculation of Δ (see also Table 4.1).

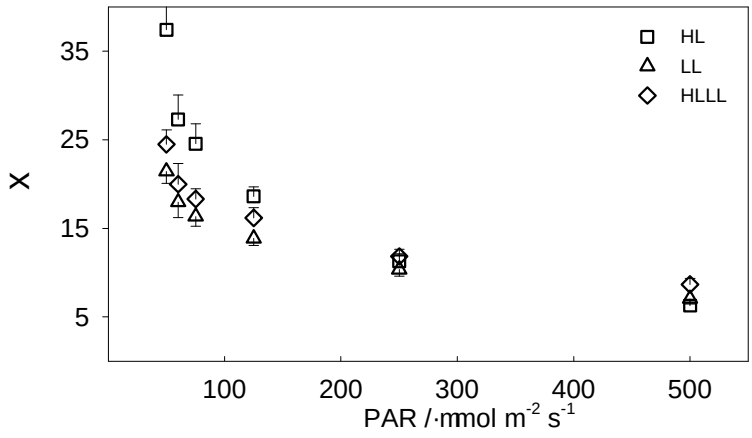

Acknowledgements

I would like to thank my supervisor, Howard Griffiths. Howard believed in me even when there was no apparent reason for doing so. He trusted my word when it was the only thing I had to offer, and he made available the tools, including economic support, to make this project possible.

I am grateful to EU FP7 Marie curie ITN, grant n° 238017 which funded this research and the Cambridge Philosophical Society which supported the completion of the project. I wish to thank my consortium, Harvest, which offered administrative assistance and contributed to raising my professional profile by providing top level, state of the art training (biophysics, proteomics, molecular biology, science-to society interactions, and grant administration).

I am grateful to the University, the Department, the school of Biological Sciences, the College, and in particular the Board of Graduate Studies, the Graduate Education Committee, the Degree Committee, for the administrative and educational support, which ultimately made possible my PhD.

Thank you to Jessica Royles, Nick Owen, Madeline Mitchell, Glyn Jones, Richard Jeffrey, Del Hawtin, Johannes Kromdijk, Xinyou Yin, Jeremy Harbinson, Asaph Cousins, Bernard Genty, Joe Berry, Davide Gusberti, Paul Langley, Nigel Boulding, for their invaluable contribution, in terms of hospitality, ideas, and time, dedicated to this research programme.